# DISTILLATION ASSISTED PURIFICATION, TRANSPORT AND DELIVERY OF LIQUIFIED NATURAL GAS

A Dissertation
Presented to
The Academic Faculty

by

Veera Manek

In Partial Fulfillment
of the Requirements for the Degree
Doctor of Philosophy in the
The George W. Woodruff School of Mechanical Engineering

Georgia Institute of Technology
December 2019

**DISTILLATION ASSISTED PURIFICATION, TRANSPORT AND DELIVERY OF LIQUEFIED NATURAL GAS**

Approved by:


Dr. S. Mostafa Ghiaasiaan, Advisor
The George W. School of
Mechanical Engineering
*Georgia Institute of Technology*

Dr. Sheldon M. Jeter
The George W. School of
Mechanical Engineering
*Georgia Institute of Technology*

Dr. Mitchell L. R. Walker
Daniel Guggenheim School of
Aerospace Engineering
*Georgia Institute of Technology*

Dr. Rhett Mayor
The George W. School of
Mechanical Engineering
*Georgia Institute of Technology*

Dr. Comas Haynes
Georgia Tech Research Institute
*Georgia Institute of Technology*


Date Approved: October 31 2019

To my parents, Barnali and Vinay Manek

And my baby sister, Murgi

## ACKNOWLEDGEMENTS

First and foremost, I would like to thank my adviser, Dr. S. Mostafa Ghiaasiaan for his guidance and constant support throughout my PhD. here at Georgia Tech. He has constantly mentored me through every stage of my research, and his expertise and advice will be invaluable to me for the rest of my career.

I am grateful to our industrial sponsors and collaborators, Chart Industries Inc., for their generous financial and material support. More specifically, I would like to thank Mr. Jeff Patelczyk for providing the opportunity to work on multiple interesting projects throughout the years. He was very involved and supportive of my research since I started here at the Georgia Tech Cryo Lab, and his vast technical knowledge and industrial vision have helped shape the course of my dissertation as well as my career.

I would like to thank my dissertation committee members Dr. Mitchell L. R. Walker, Dr. Rhett Mayor, Dr. Sheldon M. Jeter and Dr. Comas Haynes, for taking the time to serve on my committee and for their insightful comments and critiques.

I also want to thank past and present members of the GT Cryo Lab, especially Tao Fang, Michael Baldwin, Ali Ghavami and Matthew Perrella, for stimulating discussions and technical assistance and support.

Last but not least, I would like to express my deepest gratitude to my parents, sister and friends. This dissertation would not have been possible without their inspiration, unyielding patience, and endless support.

# TABLE OF CONTENTS

## LIST OF TABLES

## LIST OF FIGURES

# LIST OF SYMBOLS AND ABBREVIATIONS

| | |
|---|---|
| A | Flow area ($m^2$) |
| a | half of the major axis of an ellipse |
| b | half of the minor axis of an ellipse |
| $C_3$ | Propane |
| $iC_4$ | Iso-butane, 2-methylpropane |
| $nC_4$ | Normal-butane, butane |
| $iC_5$ | Iso-pentane, 2-methy butane |
| $nC_5$ | Normal-pentane, pentane |
| $C_p$ | Constant-pressure specific heat (J/kg·K) |
| D | Demethanizer column, Diameter (m); Distillate flow |
| $D_a$ | Major axis of ellipsoid |
| $D_b$ | Minor axis of ellipsoid |
| E | Extractive column |
| f | Darcy friction factor |
| G | Mass flux ($kg/m^2 \cdot s$) |
| g | Gravitational constant ($m/s^2$) |
| h | Specific enthalpy (J/kg) |
| j | Superficial velocity (m/s) |
| K | Loss coefficient |
| $k_\omega$ | Thermal conductivity (W/m·K) |
| L | Length (m); reflux flow |
| LNG | Liquefied Natural Gas |
| NG | Natural Gas |
| P | Pressure ($N/m^2$) |
| p | Perimeter (m) |
| q" | Heat flux ($W/m^2$) |
| R | Recovery column; Reflux ratio |
| Re | Reynolds number |
| T | Temperature (K) |
| t | Time (s) |
| x | Quality |

## Greek Characters

| | |
|---|---|
| $\theta$ | Angle of inclination with respect to the horizontal plane (rad or degrees) |
| $\phi^2$ | Two-phase pressure multiplier |
| $\rho$ | Density ($kg/m^3$) |

## Subscripts

| | |
|---|---|
| fr | Frictional |
| g | Hydrostatic |
| i | Inside |
| o | Outside |
| sa | Spatial acceleration |
| ta | Temporal acceleration |
| L | Liquid |
| G | Gas |

## SUMMARY

The removal of dissolved $CO_2$ from natural gas is essential for the safe and reliable operation of liquefied natural gas (LNG) systems. The purification of natural gas (NG) from CO2 down to a concentration of 50 ppm by multi-stage distillation is theoretically investigated. A three-column distillation system is proposed that can purify NG to lower than 50 ppm concentration of $CO_2$, while avoiding $CO_2$ freezeout. The columns include a 30-stage *Demethanizer*, in which high purity methane is obtained in the distillate by separating the impurities from natural gas including $CO_2$; a 50-stage extractive column where the azeotrope between $CO_2$ and ethane is broken; and a 50-stage solvent recovery column that recovers a mixture of heavy hydrocarbons suitable for recycling as a solvent back into the extractive column. The proposed system avoids $CO_2$ freezeout by utilizing a multi-component feed of some heavier hydrocarbons added to natural gas; propane, butane and pentane additives are injected into stage 20 of the *Demethanizer* column alongside the raw feed. Furthermore, arrangements are made to break the $CO_2$-ethane azeotrope, which may occur in the bottoms stream of the *Demethanizer* by administering a solvent stream in the extractive column. The proposed system can operate in a closed-loop arrangement where the bottoms stream that leaves the recovery column can be recycled and injected into the extractive column for azeotrope prevention.

Hydrodynamic and heat transfer characteristics of a double helically coiled tube confined in a cylindrical shell is experimentally studied using an instrumented test loop that represents a prototypical LNG fuel delivery system for natural gas-burning IC engines. The test loop comprises of a heat exchanger consisting of a double-helically coiled tube that carries liquid nitrogen (liquefied natural gas (LNG) in the real system), placed in a shell-confined secondary side through

which a secondary coolant (a mixture of propylene glycol and water in the experiments, and engine oil in the prototype) flows. Experiments addressing liquid (water) and gas (nitrogen) single-phase flows, as well as two-phase flows (air-water), are performed. CFD simulations are carried out, and empirical correlations are developed for the frictional pressure losses and two-phase pressure multiplier for the double helically coiled heat exchanger.

# CHAPTER 1. INTRODUCTION

## 1.1 Cryogenic distillation for removal of $CO_2$ from natural gas

The removal of $CO_2$ from natural gas (NG) can be a challenging and expensive process. $CO_2$ is naturally present in NG, in amounts usually varying from 0.1 to 15% volume range [1, 2]. The current global energy demands dictate that we tap into new natural gas reservoirs to meet our energy requirements. These new natural gas reservoirs contain higher levels of contamination and were previously ignored owing to high extraction costs. This has led to the re-evaluation of extraction technologies aimed at developing better contamination removal methods and technology. Natural gas can be obtained from different sources, and in this particular work, we are using pipeline natural gas for our simulations.

$CO_2$ needs to be removed from NG for various reasons. $CO_2$ provides no heating value, and its removal improves the heating value of NG. The most important reason for $CO_2$ removal from NG, however, is to avoid the solidification of $CO_2$ during the transport and delivery of liquefied natural gas (LNG). $CO_2$ has a high freezing temperature (-56.6 $^oC$; equivalent to -69.8 $^oF$; and 5.18 bar triple point pressure), and $CO_2$ freeze out in LNG transport and delivery operations can lead to plugged equipment and other operational problems. Furthermore, $CO_2$ and other acid gases, including $H_2S$ and $SO_2$, in the presence of water can corrode the pipelines as well as other equipment.

Separation of impurities from NG can be accomplished based on differences in molecular, thermodynamic or transport properties of the components in the mixture. Some molecular properties that can help in separation are kinetic diameter, polarizability and molecule moments.

Thermodynamic and transport properties that can be exploited are vapor pressure, boiling points, solubility, diffusivity and adsorption capacities. One of the most common industrial processes is absorption which uses chemical or physical solvents.

Currently, the most widely used technique for $CO_2$ removal from natural gas is by chemical absorption using amines, where the -$NH_2$ functional group of the amine provides a weak organic base to react with weak acids. An exothermic reaction follows and the amines act as a solvent that removes the acid gases. The literature dealing with amine processes in great detail is extensive and includes [3-8]. Processes that are based on using hot carbonate or alkali salts such as potassium carbonate ($K_2CO_3$) and sodium carbonate ($NaCO_3$) are also popular chemical absorption technologies.

While the techniques of absorption using amines [3-8] commonly adopted in industries work well for very large plants, for medium-sized plants (37.85 $m^3/s$, equivalent to 10,000 gallons/day of LNG) they may not be economic. This is due to the large amounts of energy required for the regeneration of the amine. In addition amines have a relatively low $CO_2$ loading capacity which required high solvent circulation rates. Amine solutions are corrosive and induce high equipment corrosion rates, which leads to high maintenance and replacement costs. Co-absorption of hydrocarbon compounds such as benzene, toluene, ethylbenzene and xylene are emitted with $CO_2$. To obtain $CO_2$ as a side product that can be used in alternate applications, these impurities must be removed separately, which adds to the cost of separation. A significant drawback of using amines is that it exposes the employees of the sweetening plant to health hazards. Another drawback of using amines (and also membranes) for removal of acid gases from natural gas is that it generates $CO_2$ as a low-pressure gaseous product. Revenue and resources need to be further invested to convert this low-pressure gaseous $CO_2$ to liquefied or compressed $CO_2$, which can be used for other

industrial applications. Other absorption processes like aqueous ammonia and hot carbonate processes are also associated with most of the disadvantages of using amines listed above.

With the rising LNG demand in various applications, smaller plants that feed relatively small markets and distribution centers are upcoming. A promising alternative method for mid-size plants which overcomes the above-mentioned drawbacks, is multi-stage fractional distillation. Distillation produces high pressure or liquefied $CO_2$, generates other hydrocarbons as side products, and most importantly generates liquefied natural gas at high pressures. Distillation utilizes the difference in volatilities of mixture components for separation. Species in the feed mixture undergo partial condensation or partial vaporization, and higher volatility species are preferentially boiled out. If the volatility differences are not large they cannot be separated in a single contact stage, and multiple vapor-liquid contact stages are required for adequate separation, and this is the basis for multistage distillation.

Thus, an objective of this investigation is to demonstrate the feasibility of the purification of natural gas (NG) from $CO_2$ down to a concentration of 50 ppm by multi-stage distillation.

## 1.2 Hydrodynamic characteristics of a prototypical Liquefied Natural Gas fuel delivery System

Once LNG has been purified of its impurities, it is ready to be stored, transported and distributed. As a liquid, its specific volume is about 600 times smaller than its gaseous counterpart, which makes its storage and transportation process feasible and economical. While natural gas is usually transported by pipelines (which can pose problems like being produced or consumed in

regions not connected to pipelines, or adequate pipeline facilities being unavailable, or being transported across the ocean), the easiest way to transport LNG over long distances is, like oil, in supertankers. LNG is used in a wide variety of applications, including as a fuel in internal combustion (IC) engines of large vehicles, such as buses and long-haul tractor-trailers. These trucks operate over long distances (usually cross country), and are equipped with heat exchangers to heat and evaporate LNG before it is injected into the IC engine chamber. Cars and especially large long-distance trucks that run on LNG are gaining popularity since natural gas is far cheaper than gasoline, and natural gas is being made more readily available across the country. In the United States, public LNG fueling capability is gradually becoming more popular and shows potential for becoming a mainstream fuel for transportation needs. The US Departments of Energy (Energy Efficiency and Renewable Energy) reported 74 LNG fueling stations across the country in 2018 [9, 10], thus making cross country trips viable.

An objective of this investigation is to examine the hydrodynamic characteristics of a double helicoidally coiled tube. Due to the advantages of accommodating large heat transfer areas, high heat transfer coefficients, small residence times and compactness of space helical tube coils are extensively used in the auto industry. An instrumented test loop is used for this purpose, which represents a prototypical fuel delivery system in large vehicles. The test loop in this investigation comprises of a double-helically coiled tube heat exchanger that carries LNG placed in a shell-confined secondary side through which the engine coolant flows. The engine coolant is recycled from the test section back into the heat exchanger and is thus referred to as “coolant” even though it is the hotter fluid. Due to practical and safety concerns, instead of LNG, liquid nitrogen (LN2) is used as fuel in the experiments. A mixture of propylene glycol and water is used as a coolant in the secondary side. Even though safety issues do not permit the use of LNG to run experiments at

the lab, experiments with LN2 provide fundamental information that are likely to apply to LNG as well. For example, the influence of flow passage curvature, in comparison with a similar straight flow passage, is likely to be similar in LN2 and LNG. The data with LN2, furthermore, can be used for validation/adjustment of empirical or numerical models. Such numerical models, again, are likely to apply to LNG as well. Ultimately similar experiments may be needed with LNG for understanding the performance of a real system. But, experience with LN2 provides valuable information that can at least provide scoping information about the phenomena expected with LNG.

Thus, the objective of this study is to completely characterize the double helicoidally coiled heat exchanger for hydrodynamics properties. Experiments are performed to determine the friction factor of a double helicoidally-coiled heat exchanger that carries a single-phase flow of nitrogen and water. Laminar, transition and turbulent flows are captured and the complete range of the flow regimes is characterized. Furthermore, pressure drop in the aforementioned double-helicoidally coiled heat exchangers when they carry two-phase flows consisting of air and water mixtures is also investigated and the two-phase pressure drop multiplier correlations are proposed.

# CHAPTER 2. BACKGROUND

## 2.1 Distillation principles and literature review

### 2.1.1 Principles of multistage distillation

Distillation as a method for separation and purification is an ancient technique. It was an art during its early years of use, which encompassed about 3500 to 4000 years. It emerged as a technique for separation over a comparatively short period of 300 years. The earliest use of distillation from historical alchemy descriptions is believed to be sometime around 1000-2000 B.C. At the time it was believed to be an exotic technique for making essential oils, perfumes, medicines, beverages, etc. The earliest traceable written description of bath description is believed to be in Cleopatra's time in Egypt around 50 B.C according to many historians [11-13]. Records of fresh-water being produced by distillation of sea-water by using a sponge as a condenser date back to around 300 A.D. and in the 11th century the first record of alcohol by distillation was made. The first record of distillation equipment is from the 4th century, and it consists of a long tube exposed to the air and leading to the receiver. Distillation principles were first used for large scale industrial applications for the production of beverage alcohol during the period between 11th and 14th centuries. In order to obtain products with high enough alcohol content to be profitable a number of techniques used in modern-day distillation procedures were devised, such as sealing the joints in the still and developing a water-cooled condenser. The earliest books on distillation theories record back to the 16th century [14-18]. Hausbrand [19] and Sorel [20] introduced the elementary quantitative and mathematical methods as could be applied to distillation in the late 19th century. This included relations to the fractional separation of binary mixtures, variable boil

up and overflow, molal enthalpy, heat losses, heat balances, compositions, rate, reflux, and pressure effects. Modern-day distillation design calculations are extensions and modifications of these original methods developed in the late 19th century by these two pioneers.

In the process of distillation, the separation of a mixture of two or more substances to obtain one or more desired products is achieved by the selection of conditions of temperature and pressure. This must be done such that at least a vapor and liquid phase coexist, and a difference in relative concentration of the materials to be separated in the two phases is attained. The maximum relative difference in the concentration of the substances in the phases is at physical equilibrium, thereby maximum separation occurs when the mixture constituents are in a state of physical equilibrium. Therefore, attainment of equilibrium conditions is desirable in the distillation process, and most design techniques use equilibrium as one of the boundary conditions for quantitative calculations. Therefore a good understanding of the Gibbs phase rule, ideal mixtures, non-ideal gas mixtures, non-ideal liquid mixtures, phase diagrams and effect of pressure on phase equilibrium is essential in understanding distillation theory. Most modern-day, practical situations encounter distillation systems that are multicomponent and not binary. A multi-component system is defined as a system composed of more than two identifiable compounds or pseudo compounds or constituent to which physical properties can be reasonably assigned. Multi-component systems composed of mixtures of hydrocarbons, mixtures of isomeric compounds, or mixtures of homologous compounds may approximate ideal behavior in both vapor and liquid states. On the other hand, mixtures which have highly dissimilar nature or are in conditions of severe pressure and temperatures, experience extreme non-ideal behavior. The third type of system called complex system, is defined as one composed of such a large number of components that it is not feasible to identify them or to determine the composition of the mixture in terms of the individual

components. Individual component properties cannot be used in quantitative analysis of the system properties and in distillation calculations for such systems. This type of mixture is represented primarily by petroleum mixtures, or mixtures prevalent in chemical industries. Because these mixtures cannot be represented by a series of true components having specific compound properties, it is necessary to characterize them in some indirect manner by empirically determined and average properties. This work will not be dealing with complex system vapor-liquid equilibrium mixtures. The current work deals with multi-component system composed of a mixture of hydrocarbons that exhibit ideal behavior in both vapor and liquid states.

Distillation may also be classified according to the type of separation as equilibrium or equilibrium flash; differential or fractionating. In equilibrium distillation, it is assumed that all the components in the mixture existing in the liquid phase also exist in the vapor phase and equilibrium is achieved. Equilibrium condition makes it necessary for the temperature and pressure in both liquid and vapor phases to be same while they are in contact. True equilibrium can never be achieved because this would require either infinite contact time or infinite area of contact between the phases. However, equilibrium is closely approximated by proper adjustment of pressure and temperature conditions in the distillation equipment. The drawback of using equilibrium flash distillation method is that conditions of distillation must be selected such that both vapor and liquid phases exist. The conditions for the two-phase region lie between the bubble-point temperature and pressure and the dew-point temperature and pressure. The bubbles-point temperature is defined as the temperature at which the first bubble of vapor is formed on heating the liquid at constant pressure. The bubble-point pressure is the pressure at which first bubble of vapor is formed on lowering the pressure of the liquid at a constant temperature. The dew-point temperature is the temperature at which the first droplet of liquid is formed as the vapor mixture is cold at

constant pressure. The dew-point pressure is defined as the pressure at which the first droplet of liquid is formed as the pressure is decreased on the vapor at constant temperature. For equilibrium flash method the composition and conditions of the feed must be known, and the quantity and quality of the vapor and liquid is determined based on temperature and pressure that is selected lying in the two-phase region mentioned above. Differential vaporization is a batch operation in which the constituents of the mixture that need to be separated are charged in a still pot and the potting mixture is heated to the bubble point. At the bubble point, boiling starts and continues as the distillate is continuously removed as a vapor and condensed to a liquid product externally from the mixture part. As the lower boiling components are distilled off, a gradual increase in boiling temperature of the liquid takes place until the desired quantity of distillate is obtained. This method is usually used in laboratory and pilot plant work to concentrate desirable material in the distillate or residue. In differential distillation, the vapor evolving from the mixture part at any instant from the boiling liquid mixture is assumed to be in equilibrium with it. Thus, as the composition of the liquid changes continuously throughout the distillation process, the boiling temperature changes, the composition of the differential element of the vapor also changes continuously, but it is assumed to be equilibrium at any instant with the liquid composition remaining in the still.

Furthermore, they may be designated as a batch or continuous. This classification is fairly simple. As the name suggests, continuous distillation is done as a continuous process of incoming feed and the batch distillation is done in a batch-wise manner. The biggest advantage of batch processing is that it provides a large amount of flexibility. A single system will handle a wide variety of chemicals and varying compositions. A single column can separate multiple chemicals with each going to its own receiver tank. Depending on the chemicals used a batch can be run daily for a week and then changed out for another completely different batch quickly and

efficiently. In most cases, two or three receiver tanks and one column with a still pot is needed as setup equipment. Although batch processing comes with a high level of flexibility, it also comes with the risk of contamination when the composition of distillation mixture is changed between distillation batches. The main advantages of a continuous process are efficiency and quantity. Continuous distillation is not limited by the physical size of the pot or batch. A higher level of efficiency is inherent in continuous distillation once the process has been set up and is operational in the lack of needing to continually clean and adjust the system. A continuous distillation process is usually more expensive than a batch system. The number of columns required is N-1 where N is the number of components to be separated. Therefore, a multicomponent feed will require multiple columns, each with its own reboiler, condenser and reflux system. Installation cost and capital investments are high for continuous distillation processes. However operational costs tend to be lower as compared to batch distillation.

Often when distillation is used as a method of separation for industrial purposes, there are certain specifications that must be met to satisfy sales criteria. This may include purity of the material, or boiling range, and sometimes the tolerance for impurity in the distillate or residue can be in parts per million (ppm). Although it is possible to obtain specified materials by boiling over a temperature range by equilibrium or flash equilibrium distillation, it is impossible to obtain the maximum yield of such materials by these methods. The economic considerations of obtaining such properties and specific characteristics has resulted in the development of the process of fractional distillation. This may be of stage type or differential type. In the current work, stage type fractional distillation is used.

Stage fractional distillation can be explained in a simplified manner as a process in which a series of flash equilibrium vaporization stages are arranged in a series adjacent to each other.

Products (both vapor and liquid) from each stage are fed to the adjacent stages as feed. The vapor produced in a particular stage is fed to the stage above and the liquid from that stage is fed to the stage below. Following a similar fashion, this particular stage receives the liquid from the state above and the vapor from the stage below as its feed material. Evidently the concentration of the lower boiling or less volatile component or components is being increased in the vapor produced in each stage in the direction of vapor flow. Similarly, the higher boiling constituent or less volatile component is being decreased in the liquid in the direction of the liquid flow. As the lighter boiling constituents are increasing in the vapor from each successive stage moving up along the distillation column, the temperature decreases from states to stage while moving up the column and reaches the minimum as the final vapor is produced from the topmost stage. Similarly, the reverse concentration change has the opposite effect on temperature moving down the column, and the temperature increases along the direction of flow of the liquid, and the maximum temperature is reached at the bottommost stage where the liquid product is withdrawn. Heat energy is necessary for the distillation process. Heat energy is required to maintain the temperature differential so that equilibrium distillation can take place in series at every stage. In addition to that, energy equivalent to the latent heat of vaporization evolved from the last/bottommost stage with respect to vapor flow must be supplied. The energy or work may be supplied in the feed, in the last stage from which the liquid product is drawn or in both places.

An evident flaw in the successive-stage distillation column described above, is that there is no liquid returned to stage one or the topmost stage. If there is no liquid returned to stage one (or the topmost stage) there can be no condensation of vapor in stage 2 (or second from the top stage) to supply liquid leaving stage 1. The vapor leaving stage 1 then would be the same quantity and composition of the vapor leaving stage 2, and the vapor leaving stage 2 would be the same quantity

and composition of the vapor leaving stage 3, etc, all the way to the bottom of the distillation column. This defeats the purpose of having a fractional column as this begins to mimic equilibrium distillation physics. For the fractional distillation to function as is intended, it is necessary to supply a liquid stream to the topmost stage or stage 1. In this stage of final vapor production (stage1) it is necessary to remove all or part of the latent heat contained in the vapor. The liquid stream introduced by removing the latent heat of vapor is called reflux. The reflux is produced by condensing all or part of the vapor leaving stage 1 and then returning some of the liquid to stage 1. The liquid reflux further aids the efficiency of fractional distillation by serving as an absorbing liquid for the heavier components in the vapor, thereby concentrating the light component in the vapor and the heavier components in the liquid. The ratio of the mass in kgs or moles of liquid returned to the column to the mass in kgs or moles of the liquid or vapor product is called operating reflux ratio. It is the ratio of reflux flow (L) to distillate flow (D). It is a measure of how much of the material going up the top of the column is returned back to the column as reflux, $R = L/D$. The ratio of the mass of liquid flowing from any stage to the next lower stage to the mass of vaporizing in the stage is called the internal reflux ratio of that stage. If the column has N stages and the topmost stage is stage 1 and the bottom stage is N, internal reflux ratio is $L_1/V_2$, $L_2/V_3$, etc. Each contact stage in series can be called a plate or tray (or stage).

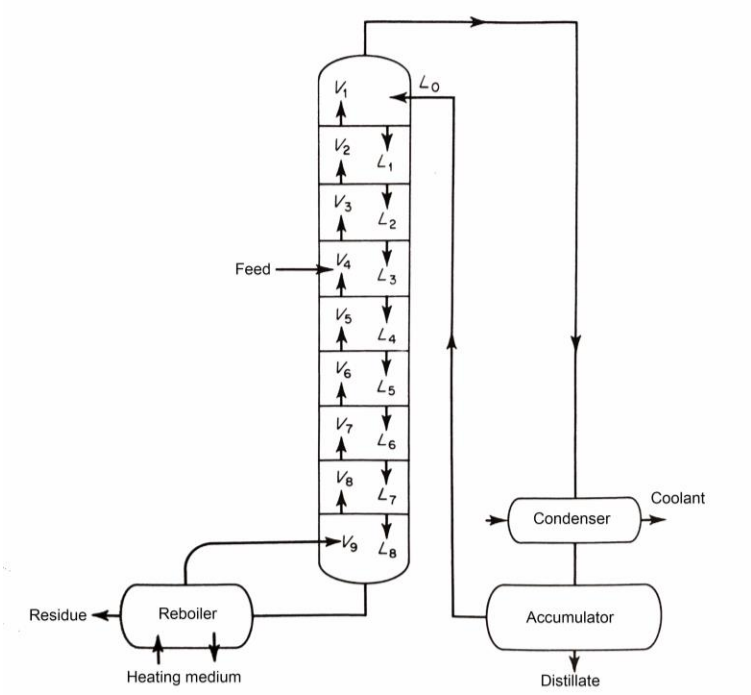


**Figure 1 Schematic representation of a conventional fractionating column**

A conventional fractionating distillation column is shown schematically in Figure 1. The most common components of a fractionating distillation tower are:

1. Feed stream
2. Distillate product stream (D)
3. Residual liquid product stream
4. Contact stages that serve as equilibrium vaporization stages
5. Heat energy source like reboiler
6. Heat removal source to produce reflux such as reflux condenser
7. Liquid and vapor flow path in between stages (conduits)

Because of the relative densities of vapor and liquid, at each stage there is a natural flow of the liquid down the column and the vapor up the column. Each tray or stage has two

conduits, one on each side, called downcomers. Liquid falls through the downcomers by gravity from one tray to the one below it. Being lighter, vapor flows up the column and is forced to pass through the liquid, via the openings on each tray. The area allowed for the passage of vapor on each tray is called the active tray area. In addition, there are weirs on each stage that ensure liquid holdup of suitable height. In practice, a pressure differential can be artificially maintained to boost the natural flow rate and create an artificially induced relative counterflow rate of liquid and vapor. Maintaining the pressure differential however, adds to operational costs.

Ideally, the liquid and vapor in the contact stage (or trays or plates) are in equilibrium. A schematic representation of a contact stage is shown in Figure 2.

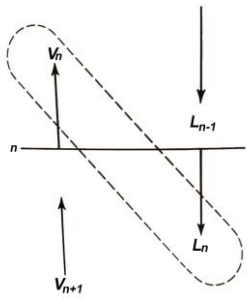


**Figure 2 Single plate of the contact stage in the distillation tower**

The vapor $V_{n+1}$ rising to the plate $n$ from plate $n+1$ and the liquid $L_{n-1}$ falling from plate $n-1$ to plate $n$ are intimately contacted by mixing so that the vapor $V_n$ and liquid $L_n$ approach a state of equilibrium in both composition and temperature. If such an ideal situation existed where they were able to achieve equilibrium at stage $n$ the efficiency of the contact stage would be 100% and it would truly be an equilibrium stage or an equilibrium flash stage. It is theoretically impossible for equilibrium to be achieved since equilibrium is a function of the rate operations of mass and

heat transfer. Thus, it is also theoretically impossible for the stage to be 100% efficient. This would require infinite area, or infinite time of contact of vapor and liquid at the contact stage, or both. Also, the rate of transfer decreases as equilibrium approaches because the driving forces, both temperature difference and concentration difference approach zero. Even though true equilibrium for the contact stage is not possible in conventional methods, the stages can be assumed to be in equilibrium, because under optimum conditions of pressure and temperature near-equilibrium conditions can be achieved.

In order to understand a fractionating distillation column for multicomponent systems like the present work, concepts of separation quality in a single fractionating tower must be understood. For example, if an 8 component (current work) mixture were to be fractionated, separations in any single distillation tower can be made between any two components. The separated components are designated *light key* and *lighter than light key components* and *heavy key* and *heavier than heavy key components*. This depends on where on the relative volatility spectrum the two components lie. Components that lie in the intermediate boiling region between the designated light and heavy key being separated are known as *intermediate* or *distributed keys*. For example, if components 3 and 5 were being separated then component 4 would be the *distributed key,* components 1 and 2 would be *lighter than light keys,* and components 6, 7, and 8 would be the *heavier than heavy keys*. The *light key* and *lighter than lights keys* would appear in the distillate, and the *heavy key* and *heavier than heavy keys* would be in the bottoms product. The distributed key could be present in both places or in either one place. Evidently in a binary system there are only 2 keys: *light key* and *heavy key* which show up in the distillate and bottoms product respectively.

The operating pressure of a distillation column is based on several considerations. As pressure increases, the equilibrium concentrations of vapor and liquid approach each other. At

critical pressure the mole fraction of component in liquid and vapor are equal and only one phase exists. That's as pressure increases separation becomes more difficult and for a given separation quality and comparable efficiency, more equilibrium stages are required to make the separation. Conversely as pressure decreases the difference between equilibrium vapor and liquid concentration increases, thus the ease of separation increases an fewer stages are required for the same given quality of separation. As is the case in almost all industrial operations the deciding factor in the selection of operating pressure is economics. As pressure decreases, ease of separation increases, but vapor volume increases. This means that larger diameter columns are required to handle the increase in vapor volume, and thus the initial installation costs and investments increase. As the pressure increases, the ease of separation decreases, thus number of stages increases and the height increases. Increasing the pressure also increases the wall thickness to withstand the high pressures. This means an increase in installation costs and also an increase in operating costs. Another factor to consider in selecting the operating pressure is the boiling point of light hydrocarbons. As pressure decreases, boiling points decrease, and in some cases refrigeration costs of lighter hydrocarbon gaseous mixtures to attain temperatures low enough to condense the overhead vapor and supply liquid reflux also increase. An optimum pressure must be determined for the best economic situation for a particular mixture distillation. The operating pressure is also controlled by the bubble-point pressure of the reflux and the type of coolant used in the condensers. Another factor influencing the operating pressure is the thermal stability of the components in the distilling mixture. It must be ensured that at all times all components of the distilling mixture do not decompose, polymerize, condense, or interact with one another when the temperature reaches some critical value corresponding to the operating pressure. In the current work, the pressure is

determined and restricted by the phase equilibrium diagram more than economic factors, as will be discussed later.

The relationship between reflux liquid and the number of plates in the distillation column have been studied in great detail by many researchers. The reflux may be the bubble-point liquid resulting from partial condensation of vapor from stage 1, or it could be liquid condensate cooled below the bubble point of the liquid. In some instances, additional reflux is supplied by cooling some of the liquid from lower stages of the column, externally cooling it further and then supplying it at the top with usual condensed reflux liquid. The reflux ratio calculation has been researched, and many different approaches have been proposed for its calculation.

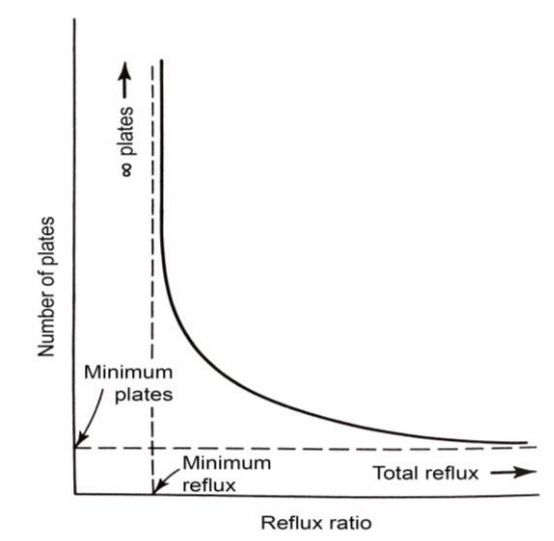


**Figure 3 Schematic relationship between reflux ratio and number of plates or stages**

Figure 3 shows a schematic representing the relationship between the reflux ratio and the number of plates or stages. It has been established that the distillation tower must operate between the limits of minimum reflux and total reflux. The economic evaluation must be done for the range of reflux ratios to determine the best operating conditions. It must be noted that the common

graphical methods used are only applicable to binary systems and cannot be extended to multi-component distillation systems. Some shortcut methods that have been popularized are Colburn [21], Underwood [22], Brown and Martin [23], Gilliland [24], Mayfield and May [25] who modified Underwood's method, Shiras et al. [26], Bachelor [27], May [28]. Several other methods for minimum and total reflux ratio have been reviewed by Holland [29].

Binary fractional distillation is simpler to analyze, and many graphical methods have been developed to study the reflux ratio and plates required for such processes. Some notable works to calculate stages, minimum reflux or total reflux include the methods of Sorel [20], Lewis [30], McCabe-Thiele [31], Ponchon [32], Savarit [33]. Some of the mentioned works are proposed empirical equations, graphical methods or distillation charts/diagrams.

In industrial applications, true binary and ternary systems are almost never encountered. As mentioned earlier N-1 columns are required for fractional distillation of a N-component system. Multicomponent systems are more complex than binary and ternary systems and considerably more effort goes into designing the fractionating towers for such systems. Distribution of key components (light, heavy, intermediate, etc.) needs to be decided based on purity and yield specifications and requirements. Calculations are usually started with the distillate and continued down the column to the feed plate. Simultaneous calculations are started with the bottoms composition, quantity, and temperature, and continued up the column, plate by plate, to the feed plate. Trial and error is used until the composition ratios calculated from both directions match within designated limits in the vicinity of the feed location. These calculations involve using mass balance, heat balance and equilibrium equations to obtain results. The correct number of stages is determined when feed temperature composition and condition from both sets of calculations match. The exact matching can rarely be accomplished, and a large number of trials are needed to

get a reasonable match. Other methods include matching qualities in composition of the plate resulting from plate to plate calculations from the top and bottom of the column without attempting to match the feed composition or even temperature and its thermal condition. Another approach involves the assumption of reflux ratio, number of equilibrium plates, and temperature profile. Then assuming a fixed known feed composition, calculations are carried out plate to plate for the assumed number of stages to the rectifying section. The calculation proceeds in a similar manner for the number of stages specified in the stripping section to obtain bubble point or dew point of the vapor and liquid at each stage. A major problem associated with the multi-component system is that the feed stage location is unknown and cannot be determined as in the case for binary systems. This introduces an additional unknown to the above described method and further adds complexity to the multicomponent fractionation system design. For both of the methods described above, if the first trial does not converge, a different number of plates reflux ratio or temperature profile is assumed and the calculation is repeated. As evident, this method is very tedious and takes a long time, and sometimes convergence cannot be achieved easily and on occasion the right "guesses" for convergence cannot be determined.

Studies to calculate compositions, feed stage location, equilibrium stages, etc., in the field of multicomponent distillation research have been done by many researchers. Some of the prominent ones are Gilliland [24], Kirkbride [34], Sorel [20], Lewis-Matheson [35], who devised a simplified method based on Sorel's works, Thiele-Geddes [36] and Hummel [37]. Shortcut methods used for binary distillation calculations, though not very accurate, may be used to approximate plates or reflux ratio, before doing extensive and expensive calculations. With the advent of high-speed computing, tedious trial-and-error plate to plate calculations have been made possible. The same assumptions and approximations of the earlier referenced methods can now be

coded into computer programs and much more accurate calculations are produced. The ability of the computer to solve complex trial-and-error iterative calculations (which is the nature of most solution methods due to the complexity of such systems) in a short period of time has advanced the field of distillation column design. Using computer programs the reflux ratio, the number of theoretical equilibrium stages, feed stage location, component distribution ratios in the distillate and bottoms product, for a given set of operating conditions, feed rate, temperature, and pressure can now be easily determined. Before the advancement of complex computer software and programs this level of accuracy in a short time frame used to be extremely difficult to achieve with reasonable accuracy, if not impossible. Computationally compatible methods for distillation design include methods developed by Lewis-Matheson [35], Bonner [38, 39], Newman [40], Holland et al. [29], Mills [41], Greenstadt et al. [42], Rose et al. [43, 44], Amundson et al. [45-47], Baer et al. [48], O'Brien and Franks [49], Waterman and Frazier [50], Gerster [51] and Hansen et al. [52]. Substantial research has been done in developing graphical methods for ternary systems, which provide quick approximate solutions but they will not be referred or mentioned here.

The current work focusses on the removal of $CO_2$ from natural gas using distillation techniques. In such a multi-component distillation system there are two major technical challenges in the distillation-based removal of $CO_2$ from natural gas. The first problem is that the CO2 freezes out in the *Demethanizer distillation column*. The second problem is the formation of azeotropic mixtures. These problems and methods for avoiding them are explained in the forthcoming sections.

*2.1.2 Freezeout of carbon dioxide*

CO2 exists primarily as vapor-solid phase at typical Demethanizer conditions. Significant research has been done on the CO2-CH4 phase equilibrium [53-56]. The phase diagram of $CO_2$-$CH_4$ shows why $CO_2$ freeze out poses a problem. The right side boundary in the phase diagram shown in Figure 4 [57] is the $CO_2$ vapor-liquid equilibrium while the left boundary is methane vapor-liquid equilibrium line. The unshaded region in between these lines represents the co-existence of equilibrium vapor-liquid phases of $CO_2$-$CH_4$. The shaded inner corner is the region of vapor-solid $CO_2$ equilibrium. To avoid freeze out we avoid clear of this shaded region. The critical pressure of $CH_4$ is 4.64 MPa (673 psia) [54], and is thus lower than the peak pressure of the solid region of $CO_2$, thereby making it impossible to get pure methane at a constant pressure without $CO_2$ freezeout as we will have to pass the solid region of $CO_2$, if substantial $CO_2$ is present in the mixture. Ryan and Holmes [57] altered the solubility characteristics of the $CO_2$-methane system by adding $C_{3+}$ hydrocarbons to the distillation column thereby circumventing the freeze out problem. They ran experiments with various concentrations of $C_4$ and other heavier hydrocarbons to study the operation of distillation away from freezeout zones. A similar approach is adopted in this work where a multicomponent feed containing heavier hydrocarbons is used in the demethanizer column.

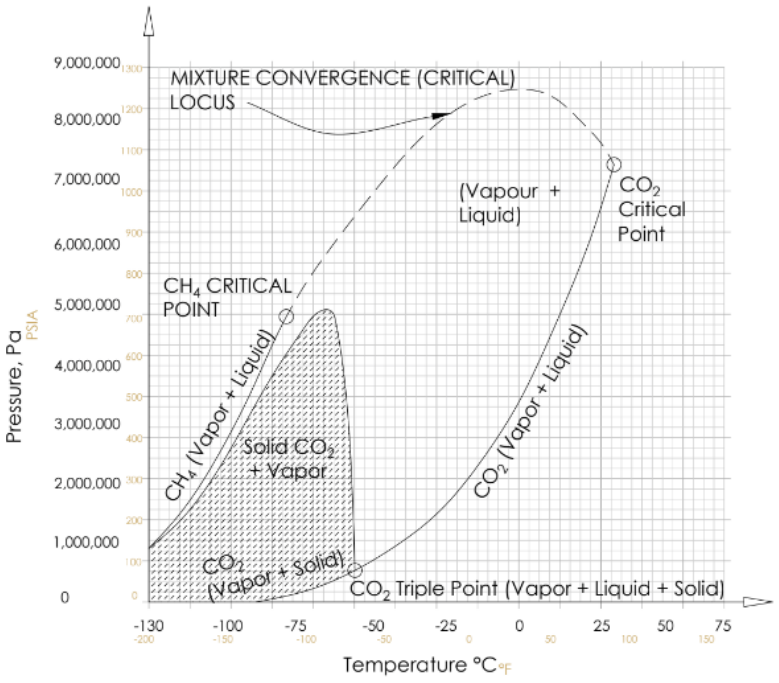


**Figure 4 Phase diagram of $CO_2$-$CH_4$ (after [57]).**

*2.1.3 Azeotropic or Extractive Distillation*

The second major problem associated with distillation-based removal of CO2 from NG is that $CO_2$ and ethane, the second largest constituents of NG after methane, form an azeotrope in the bottom streams of the *Demethanizer Column* of the distillation system. This azeotrope must be broken.

Fractional distillation or simple distillation discussed in the earlier section is a great separation tool but can only be applied in certain situations. However, simple distillation techniques cannot be used in the following situations:

- The components do not have appreciable differences in volatility or the relative volatility of the components to be separated is less than 1.05
- There is azeotrope formation.
- The components react with each other under fractionating conditions
- The components decompose or polymerize at distillation conditions.
- Close boiling compounds whose vapor pressure curves cross or which have somewhat different slopes. In such cases, the components are not capable of vaporization at practical temperatures and pressures for achievable operating conditions of the fractionating columns.

An azeotrope is a constant boiling point mixture or a mixture of two or more liquids whose proportions cannot be altered or changed by simple distillation. This happens because when an azeotrope is boiled, the vapor has the same proportions of constituents as the liquid mixture or the vapor and liquid are of the same composition.

Systems containing compounds which form azeotropes cannot be separated by simple distillation techniques. The exception to this is an azeotrope composition which is pressure sensitive and varies over a change of total pressure, in which case it is possible to use two column fractionating schemes to separate such a pressure-sensitive azeotropic mixture.

Thus, when the mixture consists of species where relative volatilities are at or near unity separation cannot occur by fractional distillation. Extractive distillation and azeotropic distillation methods are then used where a component called solvent or entrainer is used to alter the relative volatilities of the key components. Entrainer and solvent are used for azeotropic and extractive distillations respectively. The principal difference between azeotropic distillation and extractive

distillation is that the entrainer is recovered in the distillate in azeotropic distillation, whereas the solvent is recovered in the bottoms in extractive distillation [58]. The optimum point of addition of the entrainer or the solvent to the *Extractive Column* is different for the two types of processes. For azeotropic distillation processes, the entrainer is introduced into the distillation column towards the bottom of the column, whereas in extractive distillation processes the solvent is introduced to the distillation column towards the top stages of the column.

The entrainer or solvent is used to modify the relative volatility of the key components to some value greater or less than unity which will enable them to be separated. Solvents present a physical-chemical solution to alter the relative volatility. A solvent is a component that forms a complex or hydrogen bond with component i but not with component j. The complex reduces effective vapor pressure of i and thereby reducing $\alpha_{ij.}$ This is a commonly used physical-chemical method in extractive distillation. Alternately in azeotropic distillation methods a component is added that can break the complexes between i molecules, or break the H-bonds of i molecules. This increases the effective vapor pressure of component i, thereby increasing $\alpha_{ij.}$ The exact mechanism of the relative volatility change is not entirely known. There are many theories and hypotheses regarding how the entrainer and solvents help break the azeotrope. A common belief is that the entrainer in azeotropic distillation forms a minimum boiling or azeotrope with one of the key components and not with the other, and this new is azeotrope has composition and properties very different from the azeotrope between the key components of distillation. This assumption of combination between the entrainer and one of the key components resulting in a larger complex molecule, however, cannot explain the increased volatility of the composition under consideration, since a larger molecule would mean lower volatility and the entrainer is one of the light key components. However, a theory was proposed to explain this. If the entrainer has

a higher boiling point than the component with is associates in the distillate, then it must have higher volatility. The associated component must have originally existed in more complex state as a pure liquid than it does as a complex molecule after entrainer addition. Thus adding the entrainer to the mixture reduces the size of the original larger molecule complexes so the new molecular species volatility is greater than that when the material existed alone [58]. A different theory assumes that one or more of the original components in the distillation mixture exists in a loosely bound complex form with other molecules in the mixture. The theory of hydrogen bonding suggests that when the entrainer is added it breaks the hydrogen bond or destroys the original complexes of like or unlike molecules in the original solution. As a result of breaking this hydrogen bond or breaking the complex, the new molecular species or the new smaller complex has a lower molecular weight. Thus the new complex has greater volatility, and the relative volatility of the key components of distillation becomes further away from unity and separation can be achieved [58]. The same theories discussed in this section can be used to explain how the solvent can form heavier and less volatile complexes with one or more key components and leave the column at the bottom.

A minimum amount of solvent is required to break the $CO_2 – C_2H_6$ azeotropic point. The azeotropic line is represented by the straight line x = y in Figure 5 [59]. The amount of $C_5$ solvent required for an azeotropic feed is dictated by the vapor-liquid equilibrium of the column and is also a function of operating parameters like pressure, temperature, feed inlet stage, and solvent inlet stage [59]. Figure 5 shows the phase diagram of $CO_2 – C_2H_6$ mixture and solvent quantity, $C_5$ dependence on phase equilibrium of $CO_2 – C_2H_6$.

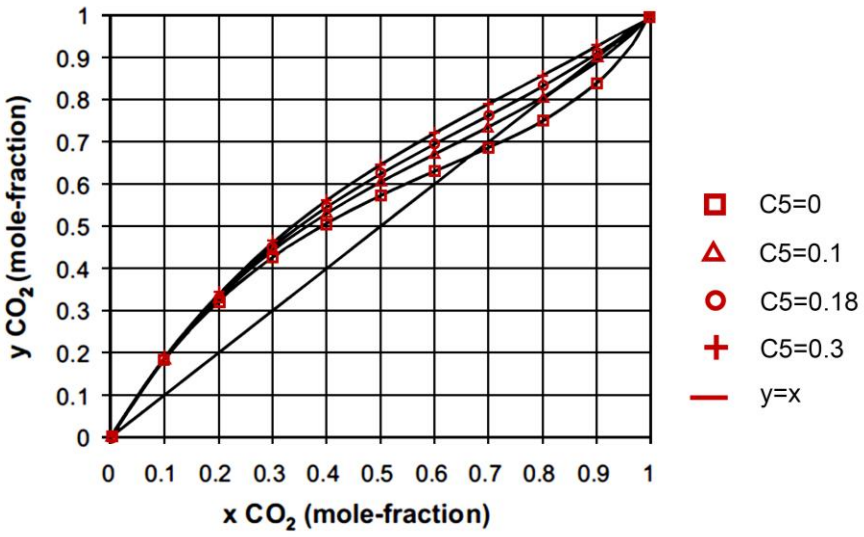


**Figure 5 Phase diagram of carbon dioxide-ethane mixture as a function of nC5 additive [59]**

The choice of an entrainer or solvent must be made carefully, and some characteristics of the compound must be taken into consideration. Apart from the obvious quality of changing the relative volatility of the key components, it must have a low latent heat so it can be vaporized easily (entrained), must be thermally stable, nonreactive, inexpensive, noncorrosive, nontoxic, and must be easily separable from the distillate or bottoms components after separation has taken place.

The ease of separation by distillation is closely related to relative volatility, which is a measure of the effective vapor pressure ratio of the key components of distillation that need to be separated.

$$\alpha_{ij} = \frac{y_i / x_i}{y_j / x_j} = \frac{\gamma_i P_i \nu_j}{\gamma_j P_j \nu_i} \qquad (1)$$

where $\alpha_{ij}$ is the relative volatility of components designated by i and j, $x_i$ and $x_j$ denote the mole fractions in the liquid phase, $y_i$ and $y_j$ denote the mole fractions in the vapor phase, $P_i$ and $P_j$ are the vapor pressures, $\gamma_i$ and $\gamma_j$ are the activity coefficients, and $\nu_i$ and $\nu_i$ are the fugacity coefficients of components i and j, respectively. The activity coefficient and fugacity coefficient are important parameters to define the relative volatilities of a non-ideal system for vapor-liquid equilibria calculations. The activity coefficient is the extent of deviation from the ideality of components in liquid mixtures. The fugacity coefficient relates partial pressure exerted by an actual gas to that which it would exert if it behaved ideally. The fugacity coefficients are usually unity at distillation operating pressures.

The number of stages required for distillation varies according to [60]:

$$N = 4/\left(\alpha_{ij} - 1\right) \tag{2}$$

Evidently the number of stages and therefore the capital cost can be very high if the relative volatility is close to unity, as is the case for an azeotrope. Keeping into account the capital investment and operating costs, relative volatility values greatly different from unity are desired. The ratio of vapor pressures cannot be changed appreciably by altering operating conditions. The only term in Equation (1) that can change the relative volatility is the activity coefficient. However, it has been found that doing so by changing operating conditions, though possible, is very expensive.

The operating costs are also closely related to the reflux ratio, defined as the ratio of the liquid returned to a column to the liquid removed from the column as a distillate product. As reflux ratio increases the operating costs increases because more liquid is to be handled (pump power,

cooling capacity, etc). On the other hand, as the reflux ratio increases the capital costs decrease since the number of stages decreases. Thus an optimum reflux ratio and stages must be selected such that the total cost of installation and operation is at a minimum.

A recent study by Pellegrini [61, 62] shows an innovative new approach for $CO_2$ removal process that is based on dual pressure distillation. De Guiodo et al. [63] studied the effect of hydrocarbons heavier than methane on the dual pressure low-temperature distillation process. An energy and exergy analysis by M. Baccanelli et al. [64] examined the differences in low-temperature distillation, anti-sublimation and hybrid configuration purification techniques.

An objective of this investigation is to examine the feasibility of designing a multi-stage distillation based $CO_2$ removal system for LNG, where freezeout of $CO_2$ and azeotropes are avoided, and to develop and theoretically demonstrate a self-sustaining, multi-tower pseudo-closed loop distillation system with solvent recovery which can be recycled back into the system. This is a more traditional approach that involves fewer distillation towers but at the same time, faces azeotrope formation challenges. Furthermore, operating pressures in this investigation are lower than most pressures found in the literatureand are consistent with current industry needs.

## 2.2 Hydrodynamics of helicoidally coiled flow passages

### 2.2.1 General remarks

Many applications and industries use coiled flow passages. Almost all piping systems, blood vessels in the human body, automobiles, have curves and bends. Thus studying the effect of curvature is an important branch of fluid mechanics with many applications.

Flow in curved conduits is more complex than straight conduits and has attracted attention as early as1876 [65-70]. The first scientific record of effects of curvature were made by Thomson in 1876 and 1877 [65, 66]. He studied the effects of curvature in an open channel flow. Amongst the early works on coiled flow passages are Grindley and Gibson [71] who studied the effect of curvature on the viscosity of air flowing through a coiled pipe. Williams et al. [67] noted that the location of the maximum axial velocity of a curved pipe shifts toward the outer wall instead of being in the center as observed in straight pipes. The important concept of secondary flow in curved passages was discovered by Eustice [69, 70] by conducting experiments with injection of ink in water flowing through a coiled pipe.

Dean [72, 73] was the first to study the secondary flow in a helical enclosures and explain the physics behind the formation of the secondary vortices. He found that in a helical pipe, a secondary flow normal to the direction of the primary or main flow is created due to the unbalanced centrifugal forces between the fluid elements at the inner and outer radial locations within the tube. As prevalent in straight pipes, the maximum velocity at the center of the pipe is shifted by the centrifugal force gradient towards the outer wall. Though the velocity profile remains parabolic, it is no longer symmetric. The slower moving fluid elements near the inner wall and the faster moving fluid elements near the outer wall create vortices that are symmetrical about a horizontal plane through the center of the tube. Dean used theoretical analysis to study the centrifugal effect and proposed a concentric toroidal co-ordinate system to study the flow in a curved pipe. An important dimensionless number, the Deans number, Dn, is defined as

$$Dn = \mathrm{Re}_D \left( R_i / R_{cl} \right)^{0.5} \tag{3}$$

As Dn increases, the strength of the secondary flow and the intensity of mixing increases. Numerous authors subsequently utilized Dean's co-ordinates to investigate the various aspects of the flow in a toroidal pipe. The critical Reynolds number for laminar-turbulent transition for curved tubes is generally higher than straight tubes and can be as high as 6000-8000 [74] as compared to ~2100 for straight tubes, as the secondary flow stabilizes the laminar flow. A widely used correlation for critical Reynolds number proposed by Schmidt [75] for simple helicoidal tubes is

$$\mathrm{Re}_{critical} = 2300\left(1+8.6\left(R_i \diagup R_{cl}\right)^{0.45}\right) \tag{4}$$

Another popular and accurate correlation for critical Reynolds number for laminar-turbulent transitional was proposed by Srinivasan et al. [76]

$$\mathrm{Re}_{critical} = 2100\left(1+12\left(R_i \diagup R_{cl}\right)^{0.5}\right) \tag{5}$$

The transition from laminar to turbulent flow in helical coiled tubes is, of course, gradual, and fully developed turbulent flow occurs at high values of the Reynolds number. Critical Reynolds number for the establishment of fully turbulent flow has been  was proposed by Mori and Nakayama [77]. As a fluid flows in contact with any surface, some of the energy is lost as friction between the walls and the fluid.

The friction factor, as a dimensionless parameter that relates pressure loss to average velocity, is an important hydrodynamic parameter. It depends on geometry, thermophysical properties of the fluid and the velocity or kinetic energy of the fluid. The friction factor of a curved tube is generally higher than the same tube when the tube is straight. Dean [73] observed that the

presence of a secondary flow in curved/helical tubes dissipates additional kinetic energy and increases wall shear stress or resistance to flow. Thus the pressure drop for the same flow volume in a curved tube is sometimes several times higher than that in a straight tube.

The pressure drop of turbulent flows in helical tubes is a function of Reynolds number and curvature ratio. The friction factor in helically-coiled tubes has been investigated by a number of researchers. Some notable studies include White [78], Ito [74], Srinivasan et al [76, 79], Mishra and Gupta [80], Manlapaz and Churchill [81], Gnielinski [82], Hart et al. [83], Ali [84], Downing and Kojasoy [85] and Coronel [86] who studied the friction factor of curved or coiled tubes. Investigations dealing with the flow phenomenology in helicoidally coiled flow passages are numerous, and in what follows, some important studies will be briefly reviewed.

Tarbell and Samuels [87] investigate the flow in helically coiled tubes with circular cross-sections and were the first to solve the momentum and energy equations and studied the flow characteristics by using the alternating direction-implicit numerical technique. Wang [88] studied the effect of torsion and curvature on flow characteristics. A non-orthogonal helical coordinate system was proposed and used to study the effects of curvature and torsion in low Reynolds number flows. His results showed that when the Deans number was greater than 20, the effect of curvature was noticeable on the flow rate, and the effect of torsion was mostly observed on the secondary flow. He also observed that at Reynolds number less than 20, the two recirculating cells of the secondary flow become asymmetric. Huttl and Friedrich [89, 90] performed numerical analysis on helically coiled pipes by using a second-order finite volume method for solving the incompressible Navier–Stokes equations and reported the effects of curvature and torsion on turbulent flow in helically coiled pipes. They used an orthogonal helical coordinate system. Yamamoto et al. [91, 92] performed experiments with three different dimensionless curvatures

and seven different torsional parameters to independently study the effect of torsion and curvatures in a helical tube. They correlated the onset of turbulence or the critical Reynolds number with torsional parameters and performed stability analysis in helical circular tubes. Yamamoto et al. [93] also performed numerical studies on helical pipes to elucidate the combined effects of rotation, torsion, and curvature on incompressible viscous steady flow.

Grundman [94] presented a friction diagram of the helically coiled tube which accounts for the effect of diameter ratios. Their work was based on the correlations proposed by Mishra and Gupta [95, 96]. Hart et al. [83] presented a tube friction chart for laminar and turbulent flow for single-phase and two-phase flow through helically coiled tubes. Bolinder and Sunden [97] performed experiments in a helical square duct and observed the flow pattern visually using Laser-Doppler Velocimetry techniques. Their velocity profiles were in good agreement with published numerical calculations using finite-volume method of a fully developed flow. Ujhidy et al. [98] performed experiments in coils and tubes containing twisted tapes and helical static elements using laser technique for visualization of the laminar flow of water. The secondary flow was studied in detail.

Many other researchers have studied the hydrodynamic phenomena in helicoidally-coiled flow passages. Some of these investigations were primarily interested in two-phase flow, but their investigations addressed single-phase flow as well. In what follows, some important investigations will be reviewed only briefly.

Xin et al. [99] performed experimental studies on the effects of coil geometry and the flow rates of on pressure drop in vertical and horizontal helicoidally coiled pipes with annular cross-sections. The single-phase working fluid was either water or air. They used test sections with three

different diameters of inner and outer tubes. They concluded that for single-phase flow transition from laminar to turbulent flows can occur over a wide range of Reynolds numbers. Ju et al [100] evaluated the hydraulic performance of small bending radius helical pipe using a HTR-10 steam generator. They also showed that the critical Reynolds number for a helical pipe is much larger than a straight pipe. Guo et al. [101] studied frictional pressure drops and the effect of four different helix axial inclination angles in single-phase water flow in two helically coiled tubes. They showed that the helix axial angles have insignificant effects on the single-phase frictional pressure drop. Ali [102] studied steady isothermal flow of Newtonian fluids in helically coiled pipes and proposed a pressure drop correlation in terms of Euler number, Reynolds number, and geometrical group. Test sections with eight different geometrical parameters were tested, and it was concluded that the Reynolds number and the defined geometrical number/group affected the friction factor. Downing and Kojasoy [85] studied the effect of curvature on the pressure drop of R-134a flowing through miniature helical channels using eight different curvatures and channel sizes over a wide range of flow conditions. Their data were consistent with Hart's [83] data.

The secondary flow in helical coils enhances heat transfer and temperature uniformity due to increased mixing. Pioneering work on heat transfer in helically coiled pipes was done Kirpikov [103], Seban et al. [104] and comprehensive analysis by Rogers and Mayhew [105] for turbulent flows. Schmidt [75] derived widely-used heat transfer correlations for helically coiled tubes over a large parameter range. Among other notable works for heat transfer are Pratt [106], Orlov and Tselishchev [107], Yang and Ebadian [108], Lin and Ebadian [109], Prabhanjan et al. [110], Jayakumar [111], Di Piazza and Ciofalo [112].

### *2.2.1 Pressure drop in Two-Phase Flows*

Compared to single-phase flow, two-phase flow characteristics and frictional pressure drop are more complex, and are important for engineering practice. Two-phase flow of gas-liquid mixtures occurs in numerous industrial and natural processes. The hydrodynamics of two-phase flows are very complicated and difficult to model and analyze. The fundamental conservation equations governing two-phase flows are the same as singlephase but cannot be solved easily due to various factors. Discontinuities are present in the flow due to the gas-liquid interphase. This interphase is deformable and unsteady, in other words, the shape and position of the discontinuity can change with time. The two phases in the flow often have different properties and can respond to external forces very differently. The gas-liquid two-phase flow is characterized by complicated spatial and temporal fluctuations.

For analyzing the hydrodynamics of two-phase flows, in particular the pressure drop, the concept of two-phase multipliers has been introduced. Two-phase multipliers is a way for correlating the two-phase frictional pressure losses in terms of the pressure losses in the same flow passage if the flow was single-phase. This concept was first introduced by Lockhart and Martinelli in 1949 [113], and was derived from their analysis of idealized annular flow. However, the concept of two-phase multipliers is universal and has been extended by numerous researchers to characterize all other flow regimes and many two-phase flow and boiling/condensation processes. The studies of the two-phase flow pressure drop in helically coiled tubes mostly use the correlations based on the Lockhart–Martinelli parameter.

The two-phase pressure drop multipliers can be used for two-phase flow pressure drop calculations in four different but equivalent ways:

$$\left(-\frac{\partial P}{\partial z}\right)_{fr} = \Phi_{L0}^2 \left(-\frac{\partial P}{\partial z}\right)_{fr,L0} \tag{6}$$

$$\left(-\frac{\partial P}{\partial z}\right)_{fr} = \Phi_{G0}^2 \left(-\frac{\partial P}{\partial z}\right)_{fr,G0} \tag{7}$$

$$\left(-\frac{\partial P}{\partial z}\right)_{fr} = \Phi_{L}^2 \left(-\frac{\partial P}{\partial z}\right)_{fr,L} \tag{8}$$

$$\left(-\frac{\partial P}{\partial z}\right)_{fr} = \Phi_{G}^2 \left(-\frac{\partial P}{\partial z}\right)_{fr,G} \tag{9}$$

where the left-hand side terms in all four equations, namely $(-\partial P/\partial z)_{fr}$, is the two-phase pressure drop due to frictional losses. The pressure loss terms on the right-hand side represent frictional pressure losses in single-phase flows. The subscripts L0 and G0 correspond to frictional pressure gradients when all the mixture is liquid and gas, respectively. The subscript L represents the frictional pressure gradient when only pure liquid at a mass flux of G(1-x) flows in the channel, and subscript G represents the case when pure gas at mass flux Gx flows in the channel. The parameters $\Phi^2_{L0}$, $\Phi^2_{G0}$, $\Phi^2_{L}$ and $\Phi^2_{G}$ are two-phase multipliers. The derivation of these equations and a detailed discussion can be found in Ghiaasiaan [114]. The two-phase pressure multipliers for homogenous flows can also be derived by analysis in the following forms:

$$\Phi_{L0}^2 = \left[1 + x\frac{\mu_L - \mu_G}{\mu_G}\right]^{-1/4}\left[1 + x\left(\frac{\rho_L}{\rho_G} - 1\right)\right] \tag{10}$$

$$\Phi_G^2 = \left[1 + \frac{\rho_G}{\rho_G}(1-x)\right]x^{-7/4}\left[x + \frac{\mu_G}{\mu_G}(1-x)\right]^{-1/4} \tag{11}$$

$$\Phi_{G0}^2 = \left[x + \frac{\rho_G}{\rho_G}(1-x)\right]\left[x + \frac{\mu_G}{\mu_G}(1-x)\right]^{-1/4} \tag{12}$$

$$\Phi_L^2 = \left[1 + x\frac{\mu_L - \mu_G}{\mu_G}\right]^{-1/4}\left[1 + x\left(\frac{\rho_L}{\rho_G} - 1\right)\right](1-x)^{-7/4} \tag{13}$$

The homogeneous mixture (HM) model, however, is inaccurate for most practical cases. As a result often empirical methods are used for two-phase pressure drop calculations, many of which are based on the two-phase multiplier concept. The Lockhart-Martinelli method [113] is one of the oldest methods for analyzing two-phase flows. Even though this method is famous and known universally, it is based on a simple but inaccurate model. Most recent works use the Martinelli parameter, X defined as:

$$X^2 = \frac{\Phi_G^2}{\Phi_L^2} = \frac{\left(-\frac{\partial P}{\partial z}\right)_{fr,L}}{\left(-\frac{\partial P}{\partial z}\right)_{fr,G}} \tag{14}$$

The Martinelli parameter for turbulent flows can be shown to be:

$$X_{tt}^2 = \left(\frac{\mu_L}{\mu_G}\right)^{0.25} \left(\frac{1-x}{x}\right)^{1.75} \frac{\rho_G}{\rho_L} \tag{15}$$

Or, equivalently,

$$X_{tt} = \left(\frac{\rho_G}{\rho_L}\right)^{0.5} \left(\frac{\mu_L}{\mu_G}\right)^{0.1} \left(\frac{1-x}{x}\right)^{0.9} \tag{16}$$

Extensive literature exists and a large number of correlations are available for calculating the two-phase frictional pressure drop. The method of Chisholm and Laird [115], which is an extension of the Lochhart-Martinelli method, was found to predict some two-phase flow experimental data on vertically coiled tubes including Rippel et al. [116], Boyce et al. [117], Banerjee et al. [118], Kasturi and Stepanek [119, 120]. They proposed a simple algebraic approach based on the following expressions

$$\Phi_L^2 = 1 + \frac{C}{X} + \frac{1}{X^2} \tag{17}$$

$$\Phi_G^2 = 1 + CX + X^2 \tag{18}$$

where the values of C depend on whether the liquid and gas, when each flows alone in the flow passage, are in turbulent or viscous regimes.

Kasturi and Stepanek [119] determined pressure drop and void fraction for the two-phase co-current flow of gas-liquid in a helical coil. Air–water, air–corn-sugar–water, air–glycerol–water, and air–butanol–water were used as working fluids. Their experiments were compared to the results from the Lockhart–Martinelli correlation [113], Duckler correlation [121] and Hughmark correlation [122]. They published a second paper [120] where they proposed new correlations for void fraction and pressure drop once again but this time in terms of new parameters. They claimed that the advantage of functional dependence of these new parameters was that it accounted for the complex behavior of the two-phase flow on a more fundamental level than the simple correlation in terms of Lockhart–Martinelli parameters. Rangacharyulu and Davies [123] used water, glycerol, and isobutyl alcohol as the liquid in their air-liquid experiments to study pressure drop and holdup for co-current upwards flow of air-liquid in helical coils. They also proposed a modified Lockhart–Martinelli parameter and a new correlation for the two-phase frictional pressure drop.

However, more recent investigations have shown that the methods of Chisholm and Laird do not always predict experimental results accurately and the pressure drop correlations need to be modified. This is particularly true for miniature flow passages, as well as curved flow passages. Xin et al. [124] performed experiments with air-water two-phase flows on helically coiled tubes of two different diameters, coiled around cylinders of two different diameters. They derived the following expressions. When, $F_d \le 0.1$,

$$\frac{\phi_L^2}{\left(1+\frac{20}{X_{tt}}+\frac{1}{X_{tt}^2}\right)} = \left(1+\frac{X_{tt}}{65.45F_d^{0.6}}\right)^2 \tag{19}$$

When, $F_d > 0.1$, then

$$\frac{\phi_L^2}{\left(1+\frac{20}{X_{tt}}+\frac{1}{X_{tt}^2}\right)} = \left(1+\frac{X_{tt}}{434.8F_d^{1.7}}\right)^2 \tag{20}$$

where, $F_d$ is defined as $F_d = \frac{j_{L0}^2}{2R_i g}\left(R_i \diagup R_{cl}\right)^{0.5}\left(1+\tan\theta\right)^{0.2}$ (21)

Awaad et al. [125, 126] performed similar experiments as Xin et al. [124] using two-phase flow mixtures of air and water but instead of using vertical helicoidal tubes they used horizontally oriented helicoidal tubes. They proposed the following correlation

$$\phi_L = \left(1+\frac{X_{tt}}{C\left[F_d\right]^n}\right)\left(1+\frac{12}{X_{tt}}+\frac{1}{X_{tt}^2}\right)^{\frac{1}{2}} \tag{22}$$

where, $F_d$ is defined as $F_d = Fr\left(R_i \diagup R_{cl}\right)^{0.1} = \frac{j_{L0}^2}{R_i g}\left(R_i \diagup R_{cl}\right)^{0.1}$ (23)

When $F_d \le 0.3$, $C = 7.79$ and $n = 0.576$

When $F_d > 0.3$, $C = 13.56$ and $n = 1.3$

Ruffell [127] was interested in the performance of steam generators used in Advanced Gas cooled Reactors (AGR) and performed experiments with three different coil curvatures over a parameter range at high pressures. Guo et al. [101], Unal et al. [128] and Zhao et al. [129] were also interested in the parameter ranges relevant to steam generators in nuclear reactors and proposed relations for the two-phase pressure multiplier based on experiments relevant to such steam generators. Guo et al. [101] studied the pressure drops of steam–water two-phase flows in two helical coiled tubes with four different helix axial inclinations. The results showed that the system pressure and mass quality both had significant effects on the two-phase pressure drop.

Downing and Kojasoy [85] used Chisholm and Laird's equation with modifications to the constant C for their experimental data with R-134a in miniature helically coiled tubes

$$C = 3.598X^{-0.012} \tag{24}$$

Colorado et al. [130] performed numerical 1-Dimensional analysis on helically coiled steam generators using boiling water. Colorado et al. used the experimental data of Santini et al. [131] in conjunction with their numerical model, to propose a modified Lockhart Martinelli correlation as follows:

$$\phi_L^2 = 1 + \frac{3.2789}{X_{tt}} + \frac{0.37}{X_{tt}^{2.0822}} \tag{25}$$

Chen and Guo [132] carried out an experimental study on three-phase flows. The flow patterns and pressure drops of oil–air–water three-phase flows in helically coiled plexiglass tubes with two different coil diameters were studied. The effects of flow rates and liquid properties on

the pressure drop were investigated. They showed that flow characteristics can be classified into more than four flow patterns, and some flow regime maps were presented.

Compared with the numerous investigations of single-phase flow and gas–liquid two-phase flow through the helical coil tubes, very little research on the gas-solid two-phase flow is available in literature. Weinberger and Shu [133] determined the pressure drop of gas-solid mixtures in helically coiled flow passages with two different helix diameters. They showed that the variations of the pressure drop depends on solids flow rate, helix radius, and loading ratios. They published a second paper [134] on gas-solids flows where they presented the transition velocities as a function of bend or helix radius and solids flow rate. They proposed a modified horizontal flow correlation for velocities and found that transition velocities decreased with increasing bend radius and solid flow rate.

The above brief review shows that the literature dealing with single and two-phase flow hydrodynamics in helicoidally coiled flow passages is extensive. However, this study is novel in three aspects. First, a double helically-coiled tube will be studied, which has not been investigated in the past. Second, single and two-phase flows of a cryogen (LN2) is investigated, which has also not been studied in the past. Furthermore, it is planned to investigate heat transfer associated with a non-boiling gas-liquid two-phase flow in the future, which has also not been investigated in the past. The heat exchanger studied in this investigation is manufactured on a large scale by employing methods of extrusion, and consequently, the tube cross-section is not perfectly circular but is rather elliptical. This provides the opportunity to analyze how flows in an elliptical cross-section compare to circular flows widely found in literature.

# CHAPTER 3. METHODOLOGY

## 3.1 Distillation based $CO_2$ removal from Natural Gas

The design of a multi-column distillation system is to a great extent an art, and often requires extensive iterations. These systems are typically designed in steps. In the first step, the first column is designed and fully characterized, with output parameters set at pre-determined nominal design levels. Using these design parameters of the first column, the design of the second column is then attempted. Because there is one- and two-way coupling between the two columns, extensive iterations are often needed as a result of which the design details of both columns need to be modified and adjusted. The third column is then added to the system, and the iterative adjustment of all three columns is resumed until the three columns operate in unison, and so on. In this investigation, a three-column system is proposed.

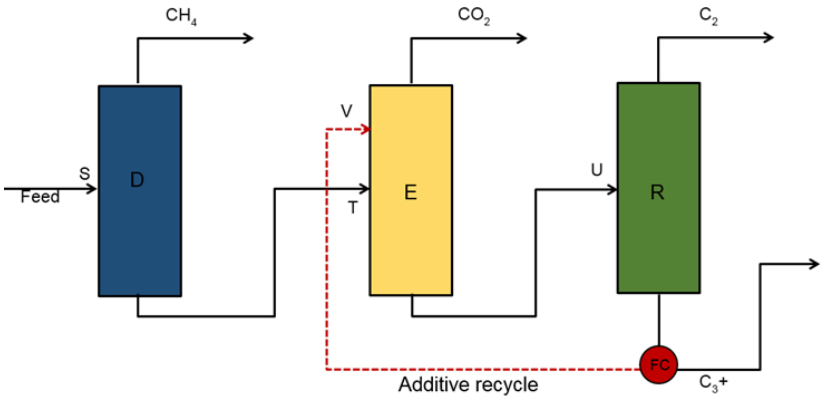


**Figure 6 Schematic of a three column distillation system used in current work**

Figure 6 is a schematic of the three-column distillation system. A serious complicating factor for distillation-based purification of LNG is $CO_2$ freezeout. (In fact, a major reason for removal of $CO_2$ from LNG is to avoid $CO_2$ freezeout in transport and processing equipment). In our case, $CO_2$ freezeout is a major design restriction in the first column. The aforementioned iterative design of the first column must thus consider, and avoid freezeout everywhere in the column. A further serious concern, which primarily applies to the second column is the formation of a $CO_2$-ethane azeotrope which, if unresolved, prevents the purification of ethane from $CO_2$. This azeotrope can be broken by using heavier hydrocarbon additives.

Aspen Plus Version 9 [135] is used as the primary design and analysis tool. Aspen Plus is a process modeling tool for the design, optimization and performance monitoring in various applications including physical chemistry, mass-energy balance, thermodynamics, heat transfer, fluid mechanics, process design and control. It has been used in similar distillation studies extensively [59, 136-138].

Aspen Plus requires an initial setup where some of the methods used in the simulation are specified. The main flowsheet window is where the flowsheet is graphically created and is the basis of the simulation environment. The model palette is used to select the unit operations in the main flowsheet window. Aspen used different models and options for for heat balance calculations, and for calculating the component molecular weight from atomic formula. Each convergence pass uses the results from the previous convergence or trial. The convergence tolerance in all blocks is set to E-04.

The unit operation models for distillation columns in Aspen are DSTWU, Distl, RadFrac, Extract, MultiFrac, SCFrac, PetroFrac, and ConSep.

As a preliminary analysis was attempted to simulate a basic and easy distillation model that could use some of the graphical methods in this field. The goal was to set up an easy simple model and then extend the work to a more realistic computational model. The DSTWU distillation model was employed, that performs shortcut design calculations for single-feed, two-product distillation columns with a partial or total condenser. The graphical/shortcut methods implemented were Winn- Underwood – Gililand for calculation of minimum number of stages, minimum reflux ratio and required reflux ratio for a specified number of stages or the required number of stages for a specified reflux ratio. Unfortunately these simple two component methods do not perform well because a two component system of $CH_4$ and $CO_2$ gives will freezeout and inaccurate results (because of the nature of the $CH_2 – CO_2$ phase equilibrium diagram). Thus a simpler analysis for verification of a more realistic model was not possible.

The separation block for the distillation method being used in this work is RadFrac. RadFrac is a rigorous model for simulating all types of multistage vapor-liquid fractionation operations like ordinary distillation, absorption, reboiled absorption, stripping, reboiled stripping, extractive, and azeotropic distillation.

Ordinary distillation and extractive/azeotropic distillation are used in the current work. This block can perform simulation, sizing, and rating of tray and packed columns. The model specification, requires complete specifications of column configuration, specifications, feeds, products, pressure, and any side streams. RadFrac possesses other impressive abilities like three-phase distillation, very narrow or wide-ranged boiling systems, strong liquid non-ideality, reacting distillation, salt precipitation, etc, which have not been employed here. The number of specifications required depends on the degrees of freedom available and can be based on the distillate or bottom rates, the reflux or boilup ratio, the condenser or heat duties, the distillate or

bottoms ratio to the feed, or any combination of the above. Pressure can be input as a constant, fixed pressure drop, or a pressure profile. RadFrac distillation columns can be used in series and are a good tool to emulate multiple distillation towers as is usually the case in industrial settings. The condenser and reboiler can also be configured. The method of equilibrium type distillation is selected in the Radfrac models. In equilibrium separation processes, two or more coexisting zones are created with the preferential distribution of the different components involved in the process in each zone. For example, in distillation liquid and vapor zones are created and the components are separated in different proportions between these zones. This means that the temperature, pressure, and phase compositions are all in thermodynamic equilibrium. Thus, while all separation processes are essentially mass transfer processes, the equilibrium assumption cancels out the need for dealing with transfer rates and focuses only on the transfer amounts. Usual distillation tower designs and architecture discussed earlier make the equilibrium separation process feasible. Equilibrium separation processes are usually operated in a counter-current configuration in which the two zones are made to flow opposite to each other in a closed vessel (or column). Equilibrium separation required adequate contact surfaces which are available in distillation towers in the form of stages or trays. Each stage proceeds to a different stage where it is contacted again to leave at equilibrium, and so on. The counter-current configuration provides better driving force for transfer than co-current configuration. This is why most equilibrium distillation columns are designed with counter flowing vapor and liquid. Since each separation stage is assumed to be an equilibrium system, it is possible to treat a distillation column using thermodynamic phase equilibrium relations. The validity of this assumption depends on the ability of each stage to achieve temperature, pressure, and phase equilibrium. Achieving equilibrium could take infinite time or infinite contact area. To impose a practical considerations, a tray efficiency is imposed which is

used to express the deviation from theoretical equilibrium. A theoretical stage is one that achieves equilibrium between the phases, while the actual stage represents an actual tray in the column.

The RadFrac algorithm has two parts: Initialization and convergence. The maximum number of iterations for the RadFrac model is set to 25. In a RadFrac equilibrium simulation the first trial or iteration starts with a guess solution. Consecutive trials or iterations use the previous solution as the initialization. Convergence limit is set and the guess is refined until it does not change from iteration to iteration. RadFrac determines P, T, x, y, V and L on every stage. It performs flash calculations based on bubble and dew points to obtain results of each iteration.

Four blocks are used in the simulation, including three distillation blocks called RadFrac and one stream splitter block called FSplit.

Streams connect unit operation models and transfer material or energy flow. Streams can also connect different sections of the same unit operation model. Streams feed material or energy to the flowsheet, transfer material or energy between unit operation models (blocks), transfer products from unit operation models, and can also represent the internal flows of a unit operation model. Most streams used in this simulation are material streams of the *mixed* type. Conditions including composition and molar flow rates are specified at input.

The Peng-Robinson equation of state [139] is used in this work. Peng-Robinson is the most useful and commonly applied equation of state in both industrial and academic applications. This cubic equation of state was developed specifically for a project on natural gas systems. Their equation of state was a modification of the Redlich-Kwong model [140], while preserving the cubic form and simplicity of this model. They overcame limitations for heavy hydrocarbons where deviations increased near the vicinity of the critical point [141]. The Peng-Robinson equation of

state can predict phase equilibrium in natural gas systems with high accuracy, is accurate for liquid density calculations and for predicting other properties near the critical point. Even though the Peng-Robinson equation of state was developed for natural gas systems it is a universal equation of state. Given that the current system is for natural gas and heavy hydrocarbons this equation of state is perfect for the current work and can be used with high reliability in the Aspen simulations.

The Peng-Robinson option for equation of state uses the standard Peng-Robinson cubic equation of state for all thermodynamic properties except liquid molar volume. By default, this property method uses the literature version [142] of the alpha function and mixing rules. The use of this method is recommended for nonpolar or mildly polar mixtures. Some examples are hydrocarbons and light gases, such as carbon dioxide, hydrogen sulfide, and hydrogen. The results can be expected to be reasonable at all temperatures and pressures.

A property set is a collection of thermodynamic, transport, and other properties. Property sets are used in this simulation to analyze, report and calculate parameters at different stages in distillation columns. User-defined property sets can be defined and a property set called TFREEZ is built. This property set helps calculate the freezeout temperature of the composition at the given conditions and can be used based on necessity. An analysis tool for analyzing the results of the corresponding property set is also built.

### *3.1.1 Column I: Demethanizer Column, D*

The first column primarily aims to separate the $CO_2$ from methane, producing a stream of pure industrial grade methane, and thus is commonly called the *Demethanizer Column,* denoted by *D*. Being the lighter component, methane is obtained as the distillate product at the top, and the heavier components, including $CO_2$ are obtained as the bottoms product. A feed comprising of

heavier hydrocarbons is used in the *Demethanizer Column* to alter the phase characteristics of the mixture and prevent freezeout. The freezeout problem in this work is particularly challenging because the *Demethanizer Column* is highly susceptible to $CO_2$ freezeout at the operating conditions at which distillation of methane and $CO_2$ is usually carried out.

As discussed in Section 2.1 the freeze out problem is particularly challenging because the demethanizer column is susceptible to $CO_2$ freezeout at the operating conditions at which distillation of methane and $CO_2$ is usually carried out because of the nature of the carbon dioxide-methane phase equilibrium diagram. Operating conditions above the freeze out temperature and at the lowest possible pressure, while keeping in mind operational cost, are desired. Comprehensive freeze-out analysis simulations were conducted in a different setup under identical conditions of temperature and pressure. It was found that, with the composition of the mixture kept constant, as pressure increases the freezeout temperature or the tendency of $CO_2$ to freeze out also increases. At constant pressure, as the concentration of $CO_2$ increases, the freezeout temperature also increases. Moving down the column stages, the operating temperatures increase giving the illusion that freeze out would occur at the top or the coldest regions of the column. However, the concentration of $CO_2$ also increases as we go down the column. This makes it necessary to perform a freezeout analysis at every stage in the column. We adopted the concept of pseudo streams at each stage and performed freezeout analysis to ensure that no freezeout takes places anywhere in the system. Pseudo streams duplicate column internal streams and pump around as external streams without actually drawing material from the column. A pseudo stream is a representative side product stream having zero velocity.

To ascertain the reliability of the freezeout utility function (TFREEZ), the utility function was tested separately and compared to the work of [143] which deals with similar mixture

components. The freezeout utility function performed well and was able to match their results. In certain instances, the freezeout utility function produced results that were conservative by a few degrees.

### *3.1.2 Column II: Extractive Column, E*

The bottoms product of the *Demethanizer Column* comprises of $CO_2$, ethane, propane, n-butane, i-butane, n-pentane and i-pentane, i.e., all the components of the feed natural gas except methane that has been extracted in the distillate of the *Demethanizer*. These bottoms product components are all valuable and ideally should not be wasted. By-products of distillation find many uses in the distillation plant/industry for different applications. Separating these components requires additional distillation towers and units. The second technical problem associated with this system is encountered while trying to obtain by-products. An azeotrope between $CO_2$ and ethane forms in this bottoms mixture. The formation of $CO_2$ –ethane, as mentioned earlier, is a major challenge. Past investigations have shown that the azeotrope can be broken by adding heavier hydrocarbons [59, 136-138]. The second distillation or the *Extractive Column*, denoted by E, is added to perform extractive distillation and break the azeotrope between $CO_2$ and ethane so the components can be further separated by using a solvent stream. A solvent stream consisting of heavier hydrocarbons inspired by [57, 136, 137, 144] is used in this *Extractive Column*. The solvent stream must be injected near the top of the extractive column for the best results. This approach works well, the azeotrope is broken and a very high percentage of $CO_2$ is extracted in the distillate. The bottoms product of the extractive column consists of ethane, propane, butane, and pentane.

### *3.1.3 Column III: Recovery Column, R*

Once $CO_2$ has been obtained there is the opportunity to further extract side products using a similar approach as used in the *extractive column, E* or the second column for $CO_2$ extraction. Additional distillation columns may be added and all the components in the bottoms product of the *extractive column, E* can be extracted individually. As mentioned earlier, a total of *N-1* fractional towers would be needed to extract each component of the feed mixture. While extraction of side products has advantages, in this particular work due to the nature of the azeotrope a different route is taken which satisfies the solvent production needs in the current fractionating system.

The *extractive column, E* requires a solvent stream consisting of a mixture of heavy hydrocarbons. A third column, referred to as the *Solvent Recovery Column,* denoted by *R*, can be added to obtain a mixture of heavier hydrocarbons that works well as a solvent for breaking the $CO_2$ - ethane azeotrope. Ethane is obtained as a distillate or light key component of distillation in the *Recovery Column*. Heavier hydrocarbons like propane, butane and pentane are obtained as the bottoms product or heavy key component of distillation.

### *3.1.4 Self-sustained System and Solvent Recycle*

A self-sustainable system where bye-products of distillation can be recycled back into the system as a solvent to the extractive column has aspired. The final step is solvent recycle implementation using the heavy component of the solvent recovery column. A stream splitter is fitted to the bottoms product of the solvent recovery column to control the fluid flow rate back into the extractive column because more solvent is produced in the extractive column than is needed. The stream is split and the ideal mass flow rate is recycled back to the *Extractive Column* at the desired solvent stage.

## 3.2 Hydrodynamic characteristics of a prototypical Liquefied Natural Gas (LNG) fuel delivery system

An experimental set up for studying the hydrodynamics of single-phase and two-phase flow in the double helicoidally coiled heat exchanger was developed. The heat exchanger test section, the experimental set up for single-phase flow analysis and the experimental set up for two-phase flow analysis are discussed in this section.

### *3.2.1 Test section or the double helically coiled heat exchanger*

Figure 7 shows a schematic diagram of the double helically coiled tube. The helicoidally coiled tube is made of 301 Stainless Steel and has a horizontal axis. Two coils are used in the experiments, one (Coil 1) with 0.64 m (25.5 in) length, and the other (Coil 2) with 0.60 m (23.62 in) length. The coil radius is 0.043 m (1.687 in). The total flow lengths of the two coils are 4.09 m (161.02 in) and 4.08 m (160.78 in), respectively. Except for their lengths, the two coils are identical in all geometric dimensions and flow boundary condition aspects. The helical angle is $9.1^{o}$ and the pitch is 4.3 cm (1.7 in).

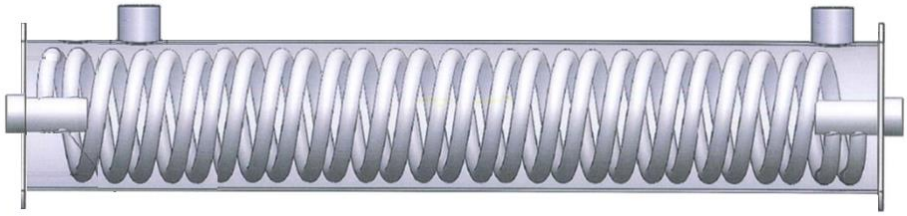

**Figure 7 Schematic of double helically coiled heat exchanger test section**

The tube, before it is coiled, is circular with inner and outer radii equal to 1.02 cm (0.402 in) and 1.27 cm (0.5 in), respectively. The cross-section of the tubes becomes slightly distorted into an ellipsoid during coiling, however, once it is coiled. The distortion, it must be emphasized, is slight and the cross-section remains near-circular. Figure 8 shows a picture of the double helicoidal test section by itself and with the second outer shell. The elliptical shape of the cross-section is not apparent to the naked eye or in the pictures indicating that the deviation from a perfectly circular shape is very slight. Samples were tested, and the typical maximum values of the major and minor axes of the ellipsoidal cross-sections were 1.171 and 0.811 cm, respectively. The equivalent circular diameter of the ellipsoidal cross-section is 0.874 cm.

**Figure 8 Picture of the double helically coiled heat exchanger without and with the secondary coolant shell**

### *3.2.2 Single-phase flow experimental set up*

Figure 9 depicts a picture of the test apparatus. A simplified schematic of the apparatus for single-phase experiments is shown in Figure 10.


**Figure 9 Lab setup to test the double helical heat exchanger using Liquefied Nitrogen Gas (LN2)**

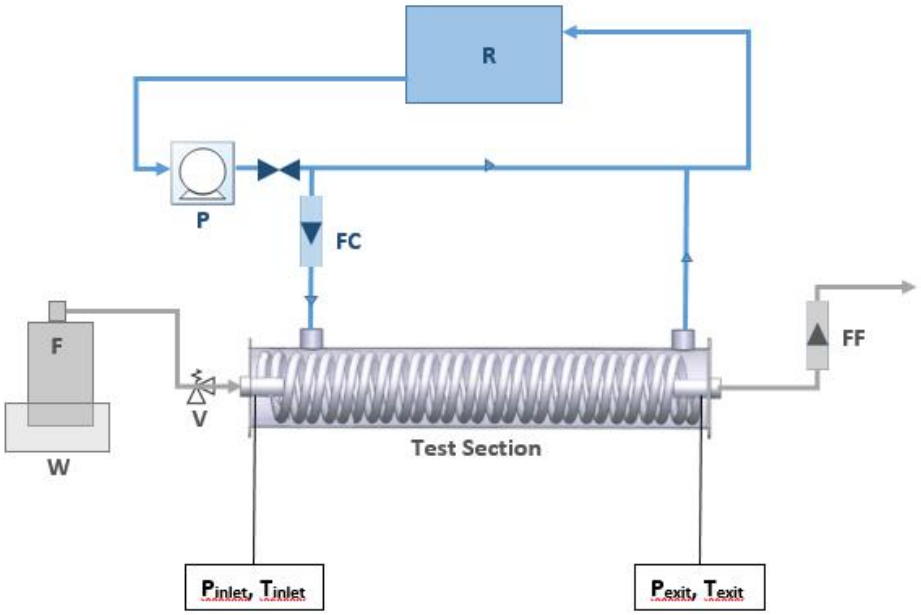


**Figure 10 Schematic representation of prototypical fuel delivery system heat exchanger**

The system consists of two main lines: the fuel flow (shown in grey), which flows inside the helically-coiled tubes, and the coolant flow loop (shown in blue), which flows through the secondary side of the heat exchanger. The fuel in a prototype system is LNG, however, for safety reasons LN2 is used in the experiments instead. The cylinder (for single-phase flow experiments with gas) or dewar (for LN2 tests) F supplies the fuel. The cylinder or dewar is placed on a weighing scale, W, to calculate the average mass flow rate in an experiment by measuring the slope of the curve representing the variation of the cylinder's or dewar's weight against time. A vacuum jacket insulated hose connects the dewar to the inlet of the heat exchanger. A safety valve, V is placed in the fuel line, right before the fuel enters the heat exchanger. The fuel flows through the double helicoidally coiled tube of the heat exchanger, and from there into an analog flowmeter, FF that reports the volumetric flow to the Data Acquisition System (DAS). This analog flow meter provides an approximate on-line mass flow rate during the experiments. Upon leaving the test section, the fuel is discharged into the surroundings. On the secondary side a large reservoir, R,

contains a 50:50 mixture by volume of Propylene glycol and water. A pump (AMT 2853-95), P, is used to pump the coolant in the outer shell of the heat exchanger. The coolant mixture is heated to about 180 F (82.2$^{o}$C) in the reservoir and is then pumped into the secondary side (outer shell) of the heat exchanger. A bypass valve controls the coolant flow rate. A flowmeter, FC, measures the coolant flow line. The coolant exiting the heat exchanger shell is recycled back into the reservoir. Thermocouples and pressure sensors are placed at the inlet and outlet of the helical coils and outer shell of the heat exchanger. The outer shell is covered by two layers of insulation. The experimental set up is equipped with an oxygen sensor to monitor $O_2$ levels since $N_2$ gas is being released continuously. (Note that the secondary side does not affect experiments that address hydrodynamics of the coiled tubes.)

The uncertainty and errors in these experimental tests are based on the measuring devices discussed above and are discussed in detail in Section 4.2.1

### *3.2.3 Two-phase flow experimental set up*

Figure 11 shows the experimental set up used for experiments that deal with hydrodynamic characteristic of a two-phase flow comprising of a mixture of air and water. The experimental system consists of an air/water flow loop, the test section, and associated instrumentation. A schematic representation of the experimental system is shown in Figure 12.

The setup mostly remains the same as the single-phase flow setup described in Section 3.2.2, except that a mixing section is now added to mix the air and water before they are injected into the primary side of the heat exchanger.


**Figure 11 Lab setup to test the hydrodynamic characteristics of a gas-liquid two-phase flow using air and water**

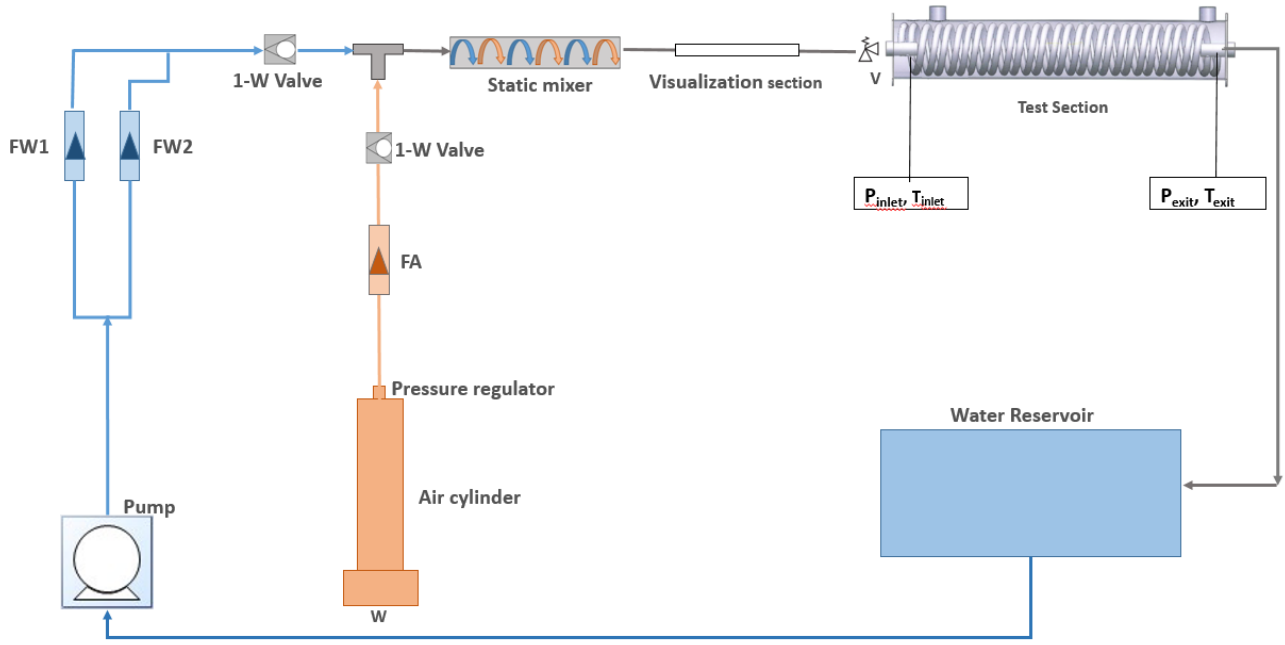


**Figure 12 A simplified schematic representation of the air-water two-phase flow experimental setup**

The experimental setup consists of an air supply system; a water supply system that recycles the water; a mixing section where the air and water are well mixed without any back flow in either circuit; the double helicoidally coiled test section and control and measuring systems for the flow rate, pressure drop, and other accessories.

The orange line in Figure 12 represents the air supply system. It consists of an air cylinder which supplies a synthetic blend of oxygen and nitrogen. The air cylinder is placed on a weighing scale, denoted by W, to calculate the average mass flow rate by measuring the slope of the curve representing the variation of weight against time. It is fitted with a pressure regulator to reduce the air supply pressure below 14.75 bars (200 psig) since the test section is built to a maximum pressure rating of 200 psig. The flow rate of air is also measured and mainly controlled using an air flowmeter, denoted by FA, which is fitted with a flow controlling valve.

The blue lines or the water supply section feeds water from a reservoir or tank to the test section, by means of a centrifugal pump that is designed for continuous duty high flow and high pressure applications. An AMT 553B-98 (American Machine and Tool Company, Chicago, Illinois) straight centrifugal pump is used. It is a 1.5 HP, 3 phase, 250 V pump that operates at 30 Amps to provide a maximum flow 156 gpm at 0 ft head and 0 gpm flow at 130 ft head. This pump was selected to overcome the high-pressure head that is present on the airside and is transmitted back into the water supply. Trials showed that a less powerful pump could not overcome the back pressure and could cause back flow of water into the pump and thereby cause damage to the pump. Two flowmeters, denoted by FW1 and FW2, with different flow ranges are installed. Depending on the required flow rate either one flow meter can be used to control and measure the water flow rate.

Both the water and air line are fitted with one-way flow valves or backflow prevention valves. These valves open to allow flow in one direction and close when flow stops or reverses. This provides a safety feature since water can flow back into the mixing section in some tests subsequently no air can flow back into the water supply section. Since the air is supplied at a higher pressure than the water side, there is usually a likelihood for air back flow to occur. Similarly the one-way flow valve or backflow prevention valves on the air side guarantees that only air can flow into the mixing section and there can be no backflow of water into the air cylinder (even though this is not very common). This ensures that the water pump or air cylinder are not damaged in anyway. The one-way flow vales play a dual role by providing a strong localized pressure drop in order to avoid any eventual dynamic instability (pressure drop-flow rate oscillations [114] for both the water line and the air line.

The gas-liquid mixing section consists of a T-section, with water and air coming in and a mixture of air and water flowing out. The T-section does not ensure good mixing of the two-phases, therefore a PVC inline static mixer is used to mix the air and water. These static mixers are installed in pipes and mix liquid and gas as the two-phases pass over fixed spiral blades. They have no moving parts and require no external power source. The total number of blades required is calculated by the range of Reynolds number. For the current experiments a six-blade mixture is used for homogenous mixing of air and water.

**Figure 13 T-section and inline static mixture use to mix the air and water**

A visualization section is present downstream of the mixing section and upstream from the test section. It provides a visual monitor or check to see the two-phase flow before it enters the test section. The pressures and temperatures are measured at the inlet and outlet of the double helical coil using pressure transducers and thermocouples installed on the inside of the primary coil. The pressures and temperatures are recorded at intervals of one second.

The outlet of the test section leads into the water reservoir which is open to the air. The air escapes into the atmosphere and the water is stored in the reservoir to be pumped back into the water supply lines by a centrifugal pump.

# CHAPTER 4. RESULTS AND DISCUSSION

## 4.1 Three column distillation system for purification of Liquefied Natural Gas

### *4.1.1 Feed and System Conditions*

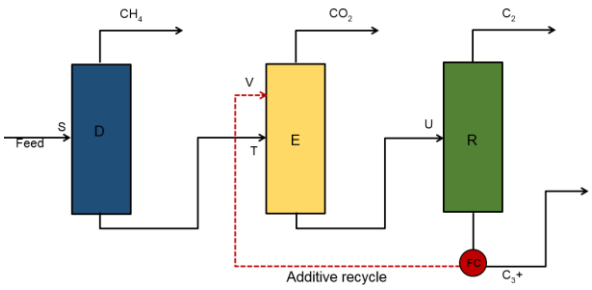


Figure 14 Schematic of a three column distillation systemFigure 14 displays the schematic of a three column system that meets the aforementioned objectives of this investigation. The first column denoted by *D* represents the *Demethanizer column*, which essentially removes all the methane from the mixture. The feed (natural gas) comprises of a multicomponent mixture of hydrocarbons like $C_3$, $iC_4$, $nC_4$, $iC_5$ and $nC_5$, as shown in Table 1. Natural gas can have vastly different compositions depending on where it is extracted. The main constituents are methane and ethane, however, and the methane content typically varies in the 60 to 90% range, and contains other hydrocarbons and carbon dioxide occurring naturally in most reserves [145]. The feed natural gas is assumed to be 85% methane in this study and the remainder is assumed to be a mixture of heavier hydrocarbons and carbon dioxide occurring naturally in most reserves. The feed is preconditioned to a temperature of -80$^{o}$C and a pressure of 40 bars. To fulfill typical LNG demands of a small-sized plant, the feed flow rate can be estimated to be 10,000 kmol/hr.

Components must be listed before every simulation. A component ID is assigned to every component in Aspen. This is a nine components system comprising of methane ($CH_4$), carbon dioxide ($CO_2$), ethane ($C_2H_6$), propane ($C_3H_8$), n-butane (n-$C_4H_{10}$), iso-butane (i-$C_4H_{10}$), n-pentane (n-$C_5H_{12}$) and iso-pentane (i-$C_5H_{12}$). Main flowsheet is created using operation blocks and streams to connect the blocks. Stream types must also be specified for the entire flowsheet using the model palette.

**Table 1 Feed composition to *Demethanizer* column**

| **Feed composition to *Demethanizer*** | |
|---|---|
| Component | Mole fraction |
| $CH_4$ | 0.85 |
| $CO_2$ | 0.03 |
| $C_2H_6$ | 0.04 |
| $C_3H_8$ | 0.02 |
| n-$C_4H_{10}$ | 0.02 |
| i-$C_4H_{10}$ | 0.01 |
| n-$C_5H_{12}$ | 0.02 |
| i-$C_5H_{12}$ | 0.01 |

Equilibrium or Equilibrium Flash type separation is used inall the distillation blocks. This type of separation process treats the system as a mass transfer process but rates are not accounted for because of the equilibrium assumption. In reality, it is hard to achieve true equilibrium despite enforcing “equilibrium conditions”. Thus at each tray or stage a tray efficiency is defined to take into account deviation from actual tray conditions or actual equilibrium conditions.

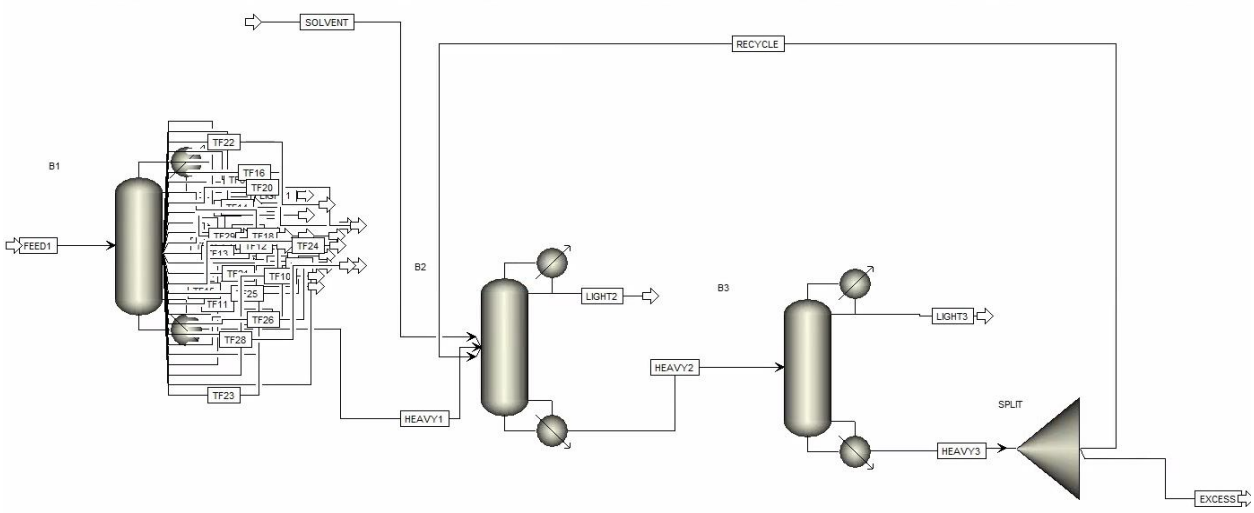


**Figure 15 Three column distillation simulation of Demthenaizer Column, Extractive Column and Solvent Recovery Column with solvent recycle implemetation in Aspen Plus**

The total number of stages in *Demethanizer* is 30 and the feed is introduced at stage 20. The distillation is more effective for these constituents when the feed stage is below the middle point or the center stage of the column. As discussed earlier, freezeout analysis is done at every stage to ensure smooth operation and thus 28 pseudo streams in between the top and bottom "real" streams are employed. Condenser type is *total.* This means that the liquid distillate will be at bubble point. The reboiler type is *kettle*. In *kettle* type reboiler, liquid flows from the column into a shell in which there is a horizontal tube bundle, and boiling takes place from the outside this bundle. The flux of vapor generated is passed back to feed the distillation column. The reflux ratio in the *Demthanizer* is 2 and the distillate to feed ratio is 0.85. The pressure is selected based on the phase equilibrium diagram of the feed mixture composition to circumvent freezeout problem and have quality separation. The pressure is selected to be 35 bar for this distillation column. The Peng-Robinson equation of state is used in the *Demthanizer* block.

The second column denoted by E in Figure 14 is the *Extractive column*. The bottoms azeotropic mixture from *D* is injected at T and the solvent is injected at V. The feed composition to *E* (heavy stream distillation obtained from column *D*) is shown in Table 4. Unlike the *Demethanizer column* there are no pseudo-streams in this column since there is no threat of any of the components freezing out. Thus, there is no need to monitor the conditions at each stage in this column. The number of streams associated with this column are fewer and comprise of feed stream (which is the heavy bottoms stream from the *Demethanizer column),* the solvent stream and the light and heavy component products streams.

The total number of stages is 50, feed is injected at stage 26 and the solvent at stage 3. In this particular extraction case, the solvent injected at the top of the column is more effective in breaking the $CO_2$ – $C_2H_6$ azeotrope. Equilibrium or Flash equilibrium is used in the *Extractive column* like it was used in the *Demethanizer Column.* Similarly, the condenser type and reboiler type are unchanged from the *Demethanizer Column.* The *Extractive column* can be operated at a considerably lower pressure than *D* since all the methane has been separated from $CO_2$ and there is no risk of $CO_2$ freezeout or separation quality issues at lower pressures. The pressure in this column is at 24 bar. The reflux ratio in the *Extractive column* is 4 and the distillate to feed ratio is 0.1.

The formation of $CO_2$ –ethane azeotrope, as mentioned earlier, is a major challenge. Past investigations have shown that the azeotrope can be broken by adding heavier hydrocarbons [59, 136-138]. The azeotrope was broken here by introducing a solvent stream at stage number 3 of the Extractive Column. The composition of the solvent stream varies between Cases I, II and III and is described in the next section.

The third column in Figure 14 denoted by *R* is the *Recovery Column* denoted by *R*, has a total of 50 stages. The bottoms products of distillation or the heavy stream from the *Extractive column* is used to feed this column. The feed stream consists of ethane ($C_2H_6$), propane ($C_3H_8$), n-butane (n-$C_4H_{10}$), iso-butane (i-$C_4H_{10}$), n-pentane (n-$C_5H_{12}$) and iso-pentane (i-$C_5H_{12}$). It separates ethane which is extracted in the distillate stream from the rest of the hydrocarbons. The solvent *Recovery column* operates at 24 bar. The reflux ratio in the *Solvent Recovery column* is 6 and the distillate to feed ratio is 0.13. Total type condenser, kettle reboiler and Peng-Robinson equation of state are used once again in this block.

Some of the most important parameters of columns *D*, *E* and *R* have been summarized in Table 2.

**Table 2 Some important column parameters**

| **Column specifics** | **D** | **E** | **R** |
|---|---|---|---|
| Total stages | 30 | 50 | 50 |
| Feed stage | 20 | 26 | 15 |
| Solvent stage | - | 3 | - |
| Pseudo streams | 28 | 0 | 0 |
| Reflux ratio | 2 | 3.3 | 6 |
| Boilup ratio | 5.79 | 0.68 | 0.88 |
| Distillate to Feed ratio | 0.85 | 0.12 | 0.13 |
| Pressure (bar) | 35 | 24 | 24 |

It should be mentioned, that the fractionating system is sensitive to the total number of stages, feed stage, solvent inlet stage, reflux ratio, operating pressures and solvent stream

composition. Some of these factors have been investigated. Furthermore, since columns *E* and *R* are coupled, the solvent stream composition affects the distillation process in both columns to a great extent. The coupling of the two columns makes the simulation very complex.

### *4.1.2 Case Studies*

To set up the solvent stream and study the effect of recycling the solvent stream on the system compared to no recycling, three cases have been set up. Case I refers to using a solvent stream that is an equal mixture of n-pentane and iso-pentane. This has been inspired by the work of Sterner [54]. Case II refers to a solvent stream which has a composition similar to the stream composition that is to be recycled from the solvent recovery column. The purpose of this case is to study how recycling can be implemented and how it can affect the overall system. It is also used to study how the coupling among the three columns can affect the system's performance. Case III utilizes a flow controller (FC) or stream splitter to control the solvent flow rate. Table 3 shows the solvent stream composition for the three cases. For Cases I and II the solvent stream needs to be preconditioned. For these simulations they were preconditioned to -10$^{o}$ C temperature and 30 bars pressure. For Case III the solvent stream has the physical properties and composition of the recycle stream from the flow controller or stream splitter and needs no further pre-conditioning. The ratio of the flow rate being recycled to that being stored away for other industrial applications is 1:2.6.

Table 3 shows the solvent stream composition for Cases I and II.

**Table 3 External solvent stream (no recycle) composition used in Case I and II**

| **Case 1: Arbitrary solvent composition to *extractive column*** | |
|---|---|
| Component | Mole fraction |
| n-$C_5H_{12}$ | 0.5 |
| i-$C_5H_{12}$ | 0.5 |
| **Case 2: Solvent stream composition similar to recycle stream** | |
| Component | Mole fraction |
| $CH_4$ | 0 |
| $CO_2$ | 0 |
| $C_2H_6$ | 0 |
| $C_3H_8$ | 0.11 |
| n-$C_4H_{10}$ | 0.11 |
| i-$C_4H_{10}$ | 0.06 |
| n-$C_5H_{12}$ | 0.388 |
| i-$C_5H_{12}$ | 0.332 |

The distillation results for column *D* are shown in Table 4. As expected, the distillation results of column *D* are identical for all three cases. The feed composition that has 85% methane has been purified to the desired level of below 50 ppm for safe industrial applications. The final distillate product in the *Demethanizer* column is methane that has purity greater than 99.99%. $CO_2$ is present in trace amounts to the order of 4.5 ppm. The purity of methane in the distillate is significantly below the desirable limit of 50 ppm of $CO_2$ contamination. All the LNG is distilled

into the distillate stream. The heavy stream or the bottoms product of column *D* contains only trace amounts of methane. The rest of the feed comprises of $CO_2$ and hydrocarbons.

Figure 16 shows the temperature profile of the *Demethanizer column* for stage 1 to 30 and the freezeout temperatures in the corresponding stages. It is noted, at all points in the *Demethanizer column* the freezeout temperature of $CO_2$ is below the operating temperature, as desired. Stages 28 and 29 are the "pinch points" and represent the locations in the system where the difference in the actual temperature and the freezeout temperature is the lowest. These are the stages that are most susceptible to freeze out. To a large extent the freezeout profile in Figure 16 can be explained by the concentration of $CO_2$ increases in the lower stages (stages 22 to 29).

The bottoms product of column *D* consists of $CO_2$ and $C_2H_6$ and forms an azeotrope and that is treated in column *E*. The composition of bottoms product of *D*, which acts as a feed to *E*, is listed in Table 5.

**Table 4 Distillation results of *Demethanizer* Column, *D* and *Extractive* Column, *E***

| ***Demethanizer column* light stream** | | | |
|---|---|---|---|
| Component | Mole fraction Case I | Mole fraction Case II | Mole fraction Case III |
| $CO_2$ | 4.527 ppm | 4.527 ppm | 4.527 ppm |
| $CH_4$ | 0.9999 | 0.9999 | 0.9999 |
| ***Extractive column* light stream** | | | |
| Component | Mole fraction Case I | Mole fraction Case II | Mole fraction Case III |
| $CO_2$ | 0.99714 | 0.98134 | 0.93719 |
| $C_2H_6$ | 6.522e-04 | 6.643e-4 | 0.0212 |

| *Extractive column* heavy stream | | | |
|---|---|---|---|
| $CO_2$ | 0.000371 | 0.002545 | 1.9e-05 |
| $C_2H_6$ | 0.181729 | 0.181727 | 0.1388 |

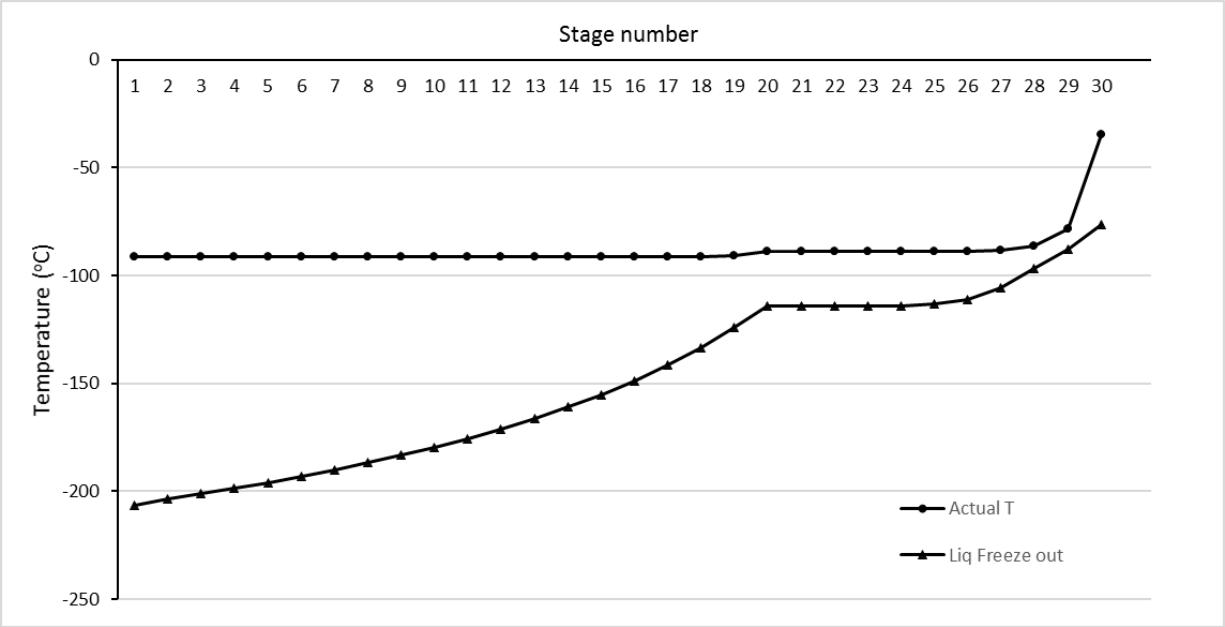


**Figure 16 Temperature profile of *Demethanizer* column from stage 1 to 30 and the freezeout temperature at corresponding stages**

**Table 5 Bottoms product of *Demethanizer Column* acts as feed to *Extractive Column***

| ***Demethanizer* heavy stream or Feed composition to E** | |
|---|---|
| Component | Mole fraction |
| $CH_4$ | 2.564e-05 |
| $CO_2$ | 0.1999 |
| $C_2H_6$ | 0.2667 |
| $C_3H_8$ | 0.1333 |
| n-$C_4H_{10}$ | 0.1333 |
| i-$C_4H_{10}$ | 0.0667 |
| n-$C_5H_{12}$ | 0.1333 |
| i-$C_5H_{12}$ | 0.0667 |
| Total flow rate | 1500 |

The temperature distributions across stages 1 to 50 in columns E and R are shown in Figure 17.

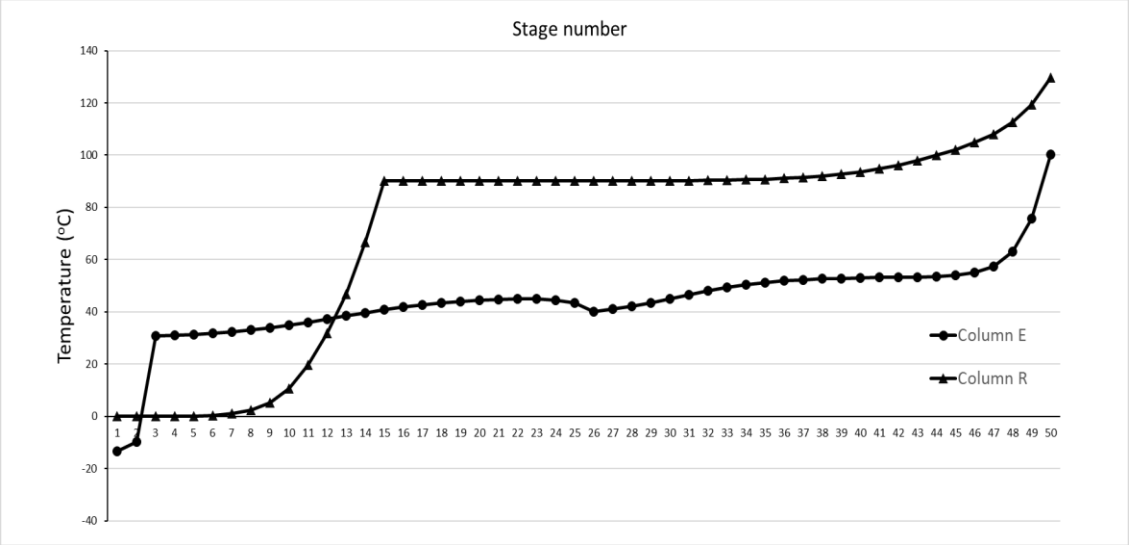


**Figure 17 Temperatures variation across extractive and recovery column through stages 1 to 50**

The results for the *Extractive* column can be seen in Table 4. Case I shows the best results by breaking the azeotrope to give 99.7% $CO_2$ in the distillate. The solvent used in case I is very close to an ideal solvent for this azeotrope. Case II and Case III give 98.13 % and 93.72 % of $CO_2$ respectively in the distillate. This is an instance that demonstrates how a very similar solvent composition can have a considerably different effect on the azeotrope as a result of coupling in Case III. The solvent composition in Case II has been matched to the heavy or bottoms product from column *R* up to four significant digits. The distillate obtained in the *Recovery column* is 99.99% ethane. Ethane is a very important industrial compound can be stored or used for various applications. The results for column the *Recovery Column* can be seen in Table 3, as solvent composition of Case II is a reflection of the distillation process in the *Recovery Column* and represents the heavy stream composition that is recycled. Depending on the number of compounds

that need to be separated additional distillation columns can be added and the relatively lighter hydrocarbon can be obtained in the distillate product.

### *4.1.3 Detailed results of a full three column distillation setup for purification of natural gas where full recycle is functional (Case III)*

Detailed results of a full three column fractionating system with a *Demethanizer Column, Extractive column* and *Solvent Recovery Column* has been shown for only one of the cases mentioned above. All three cases cannot be shown in details due space constrictions and *Case III* has been selected for this purpose. *Case III* has been chosen since it is the most interesting, involved and challenging case to set up and simulate, because of the implementation of solvent recycle from the *Recovery column* to the *Extractive column* and because of the coupling between the two columns.

Pipeline natural gas material that needs to be purified to acceptable industrial standards of methane purity is used as raw feed. The composition of the pipeline natural gas used in these simulations is based on the composition of natural gas found in the Barnett shale region in Texas reported by Bullen et al [1]. Figure 18 shows the composition of the feed used in the *Demethanizer column.* Temperature distribution in the *Demethanizer column* with the corresponding freezeout temperature of $CO_2$ has been shown in Figure 16 in the previous section with all three case studies.

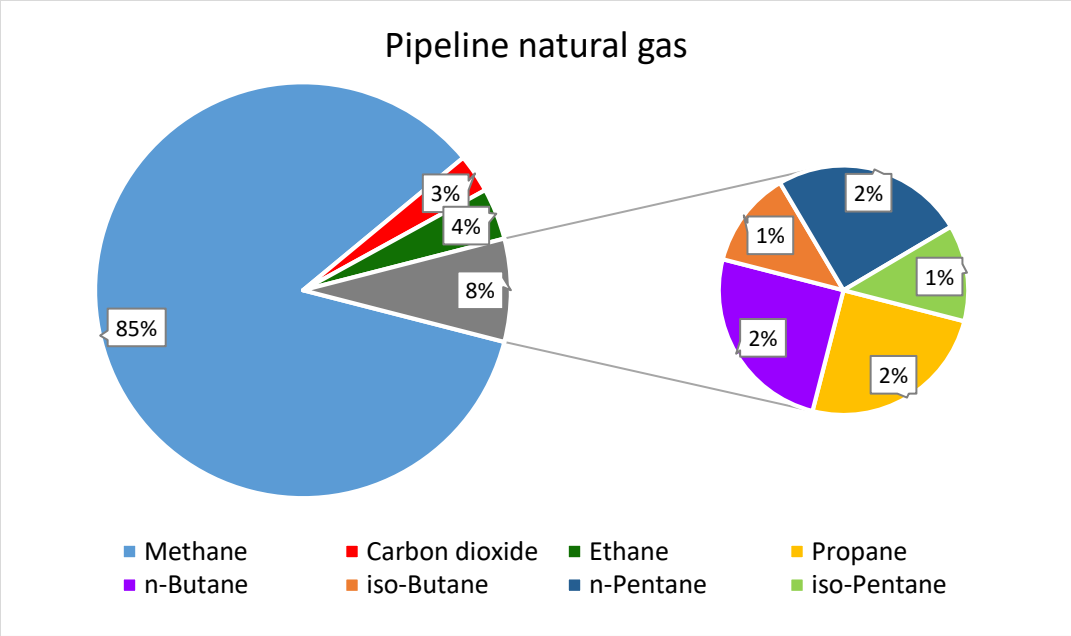


**Figure 18 Pipeline natural gas used in the current work or the feed composition to the *Demethanizer column***

Figure 19 - Figure 23 how the methane, carbon dioxide, ethane, heavier hydrocarbon (including propane, n-butane, iso-butane, n-pentane and iso-pentane) mole fraction and average molecular weight respectively. The plots show the variation of the respective properties with stage number in the *Demethanizer column*. This gives us an assessment of how the distillation process advances and the separating of lighter and heavier key components along the *Demethanizer column*. As expected methane mole fraction is almost at 1.0 at stage1 (top of the distillation column) since the distillate is almost entirely methane as mentioned in earlier results. Similarly ethane, carbon dioxide and heavier hydrocarbons show increasing mole fractions in the lower stages. The carbon dioxide profile is very important because it is a good indication of the *pinch points* or the points where the distillation column temperature comes close to the freeze out

temperature of $CO_2$ as can be seen in Figure 16. It also confirms the theory that freezeout temperature is heavily dependent on composition of the mixture or the concentration of $CO_2$. Heavier hydrocarbons have been bundled in the same figure to exhibit the solvent stream components in the *Demthanizer column.*

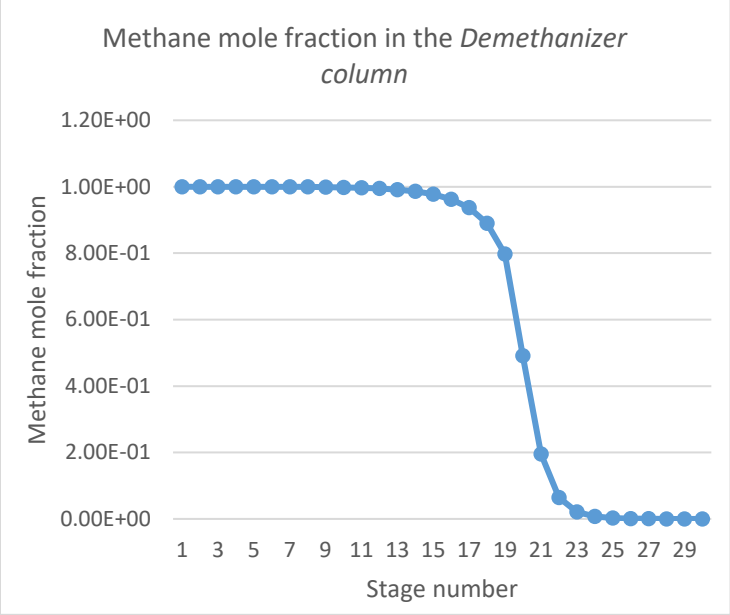


**Figure 19 Methane mole fraction variation with stage number in the *Demethanizer column***

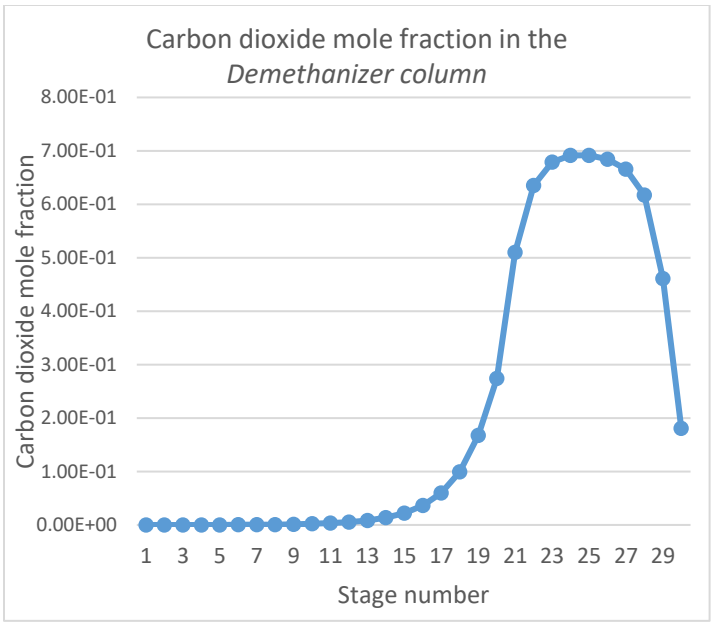


**Figure 20 Carbon dioxide mole fraction variation with stage number in the *Demethanizer column***

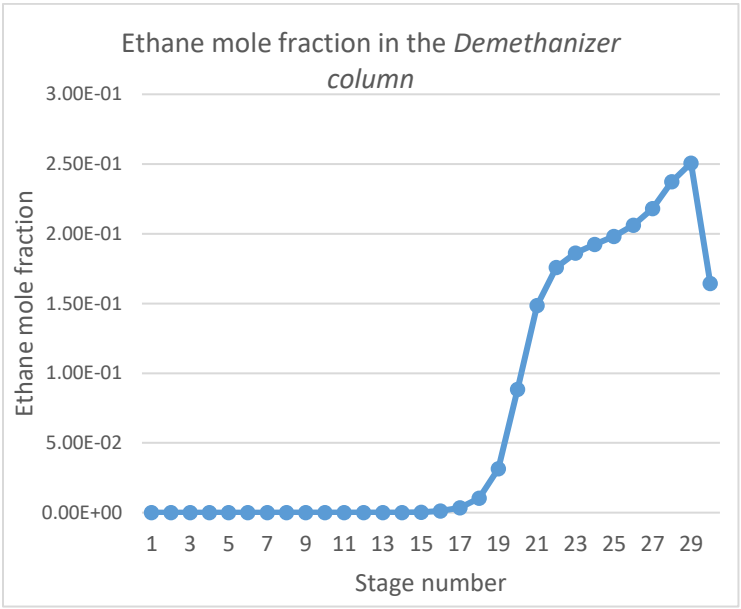


**Figure 21 Ethane mole fraction variation with stage number in the *Demethanizer column***

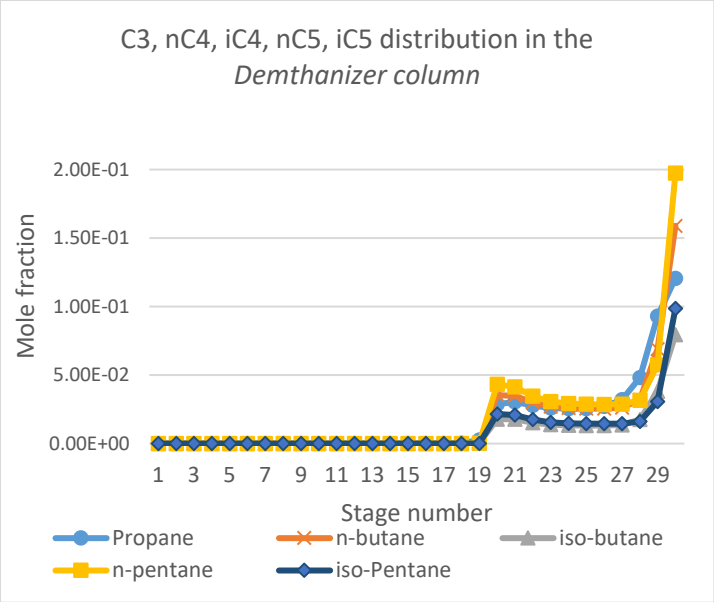


**Figure 22 Heavier hydrocarbon mole fraction variation with stage number in the *Demethanizer column***

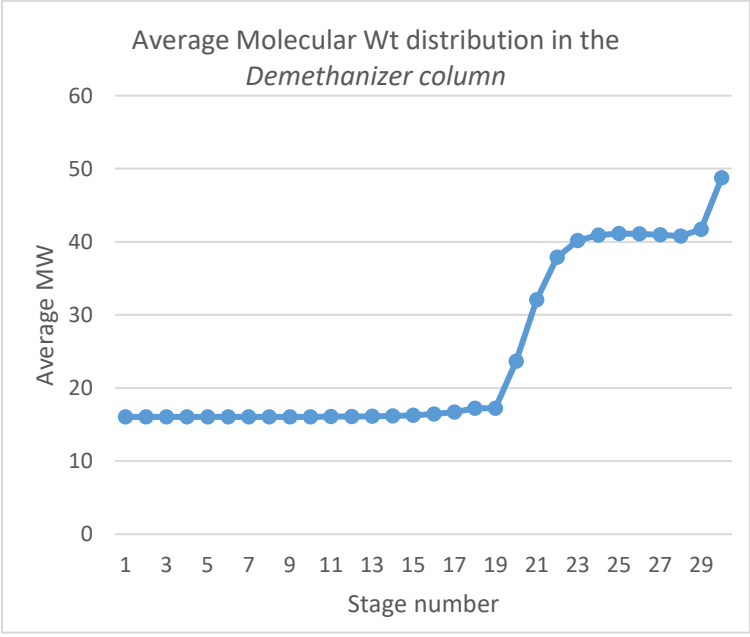


**Figure 23 Average molecular weight variation with stage number in the *Demethanizer column***

Figure 24 shows the feed to the Extractive column.

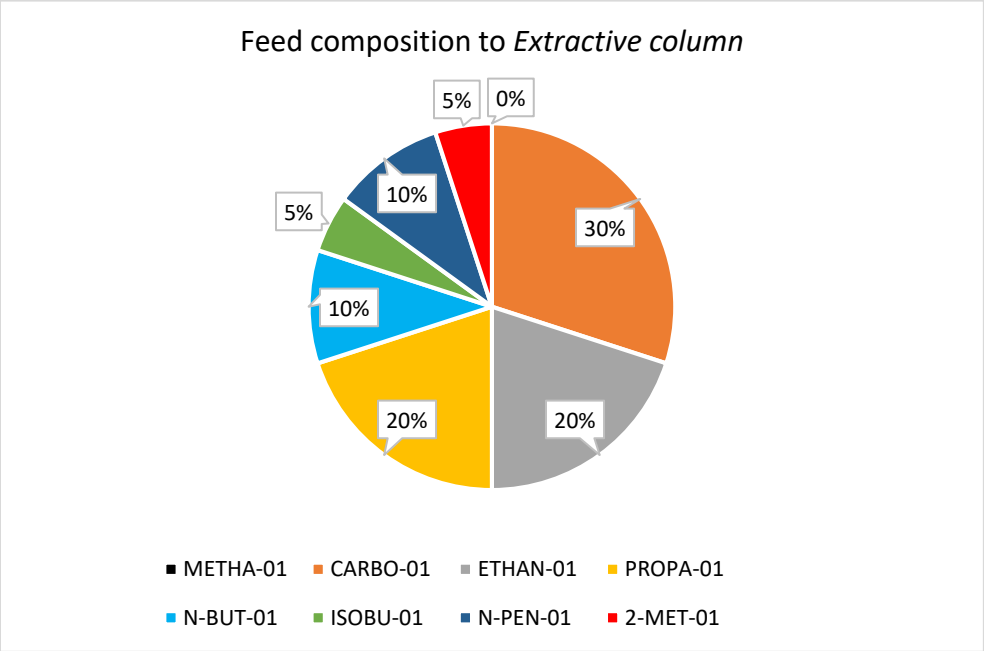


**Figure 24 Feed composition to the Extractive column, which is the bottoms product composition from the *Demethanizer column***

Similarly, figures Figure 25 - Figure 28 show the temperature, carbon dioxide, ethane and heavier hydrocarbon (including propane, n-butane, iso-butane, n-pentane and iso-pentane) mole fraction and how they vary with stage number in the *Extractive column*. As expected the mole fractions in the *Extractive column* reflect increasing carbon dioxide in the distillate stream or stage 1 and increasing ethane and heavier hydrocarbons at the bottom of the column. Methane mole fraction has not been shown because methane is assumed to be absent in this fractionating column. This is a valid assumption since methane mole fraction is to the order of E-16. There is a change in the slopes of the temperature and mole fraction profiles of the *Extractive column*. This can be explained by the feed stage being located at stage 15. Thus the upwards and downward flowrates of vapour and liquid respectively above and below the feed stage are different.

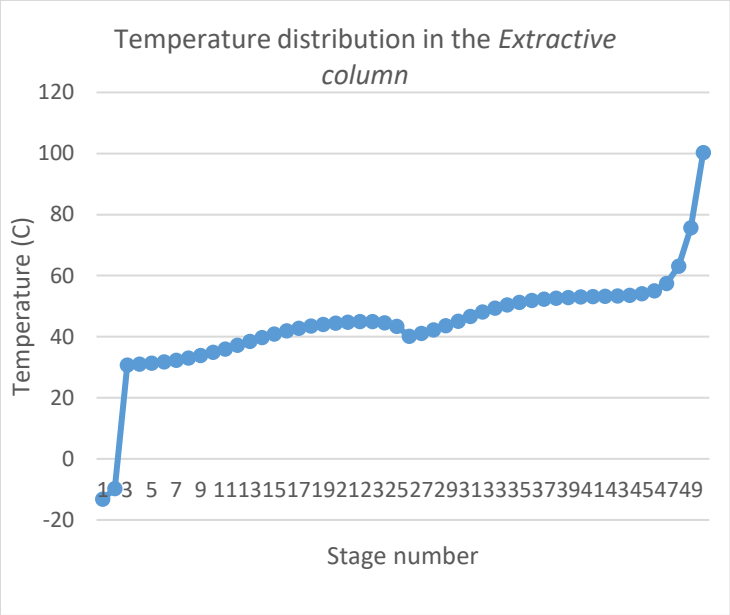


**Figure 25 Temperature variation with stage number in the *Extractive column***

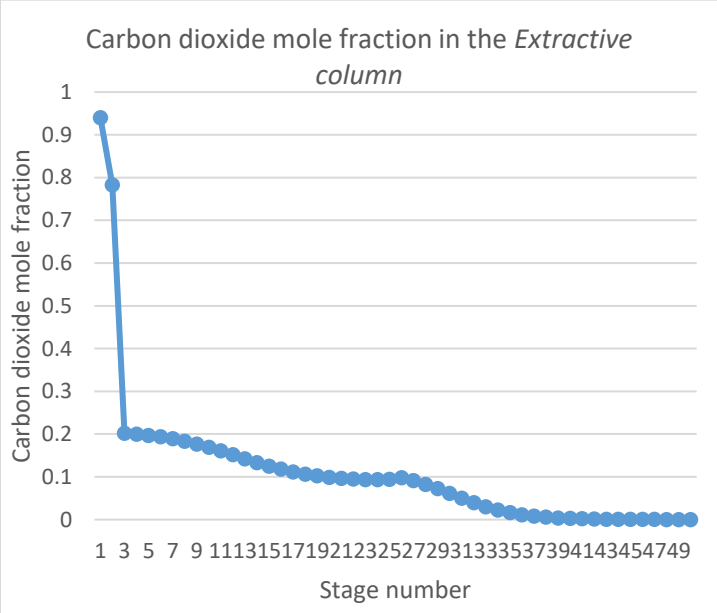


**Figure 26 Carbon dioxide mole fraction variation with stage number in the *Extractive column***

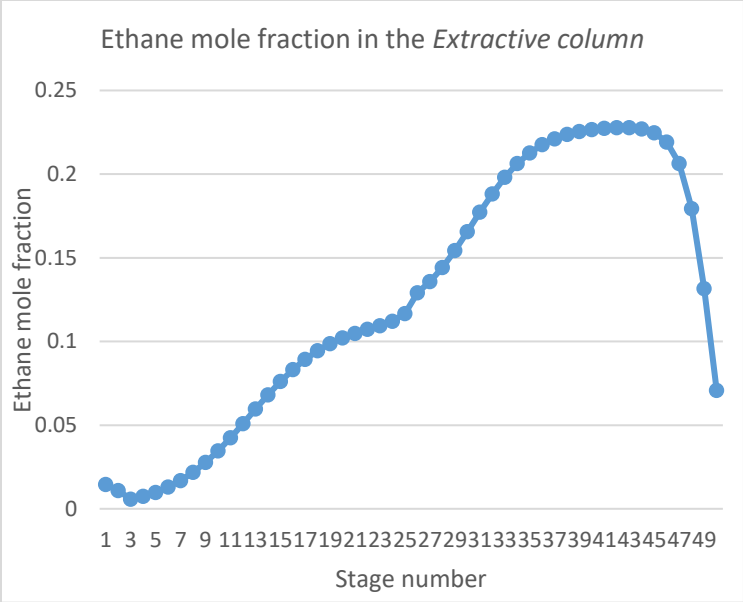


**Figure 27 Ethane mole fraction variation with stage number in the *Extractive column***

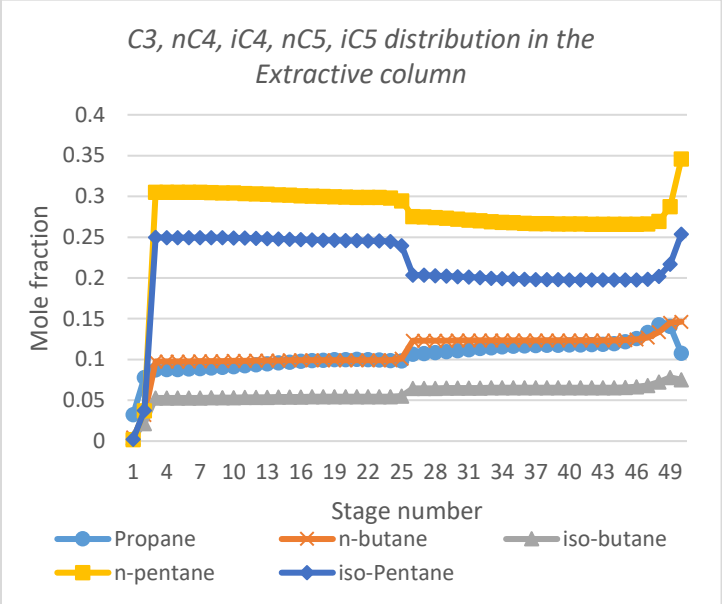


**Figure 28 Heavier hydrocarbon mole fraction variation with stage number in the *Extractive column***

Figure 29 - Figure 32 show how the temperature, carbon dioxide, ethane and heavier hydrocarbon (including propane, n-butane, iso-butane, n-pentane and iso-pentane) mole fraction and how they vary with stage number in the *Solvent Recovery column*. Ethane mole fraction nears unity at the top or in the distillate stream. The bottoms products comprising of mainly the heavier hydrocarbons are a good composition for breaking the azeotrope. Thus the bottoms product can be recycled.

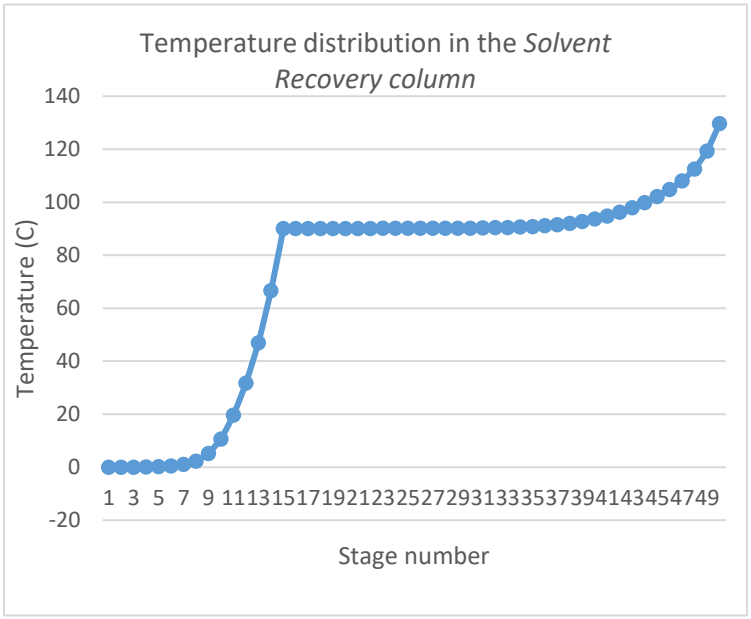


**Figure 29 Temperature variation with stage number in the Solvent *Recovery column***

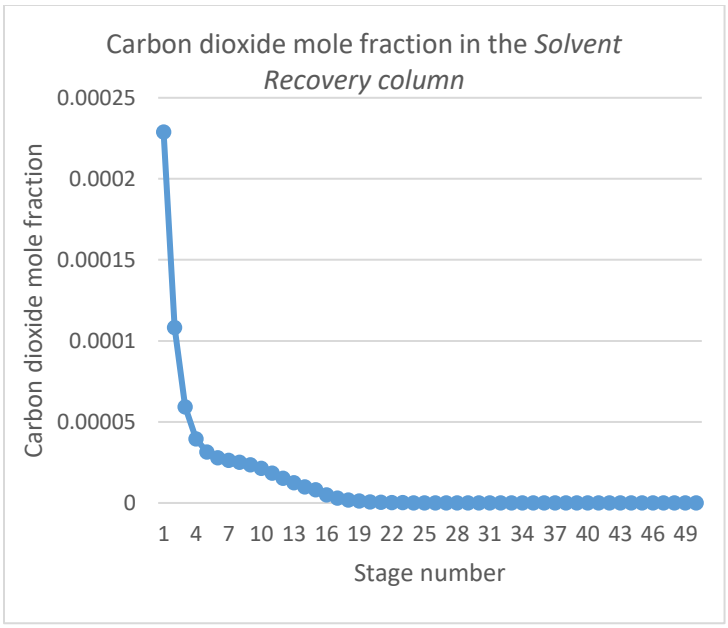


**Figure 30 Carbon dioxide mole fraction variation with stage number in the Solvent *Recovery column***

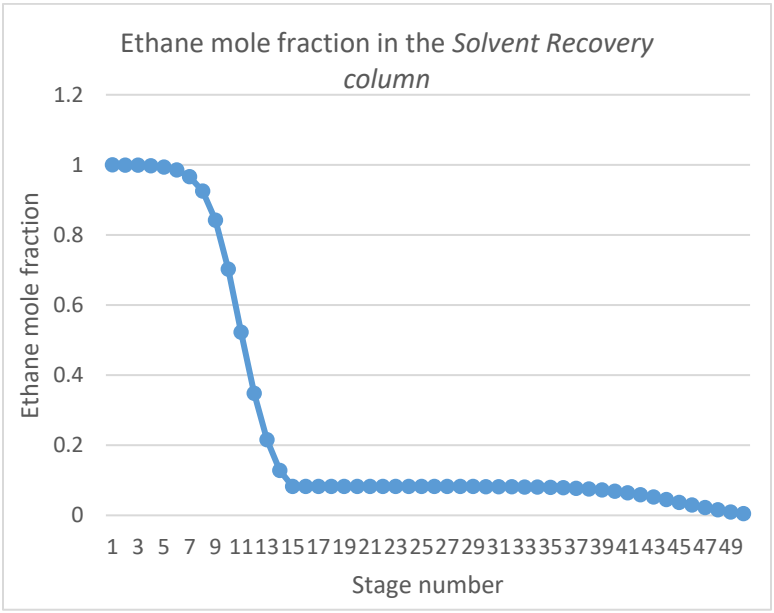


**Figure 31 Ethane mole fraction variation with stage number in the *Solvent Recovery column***

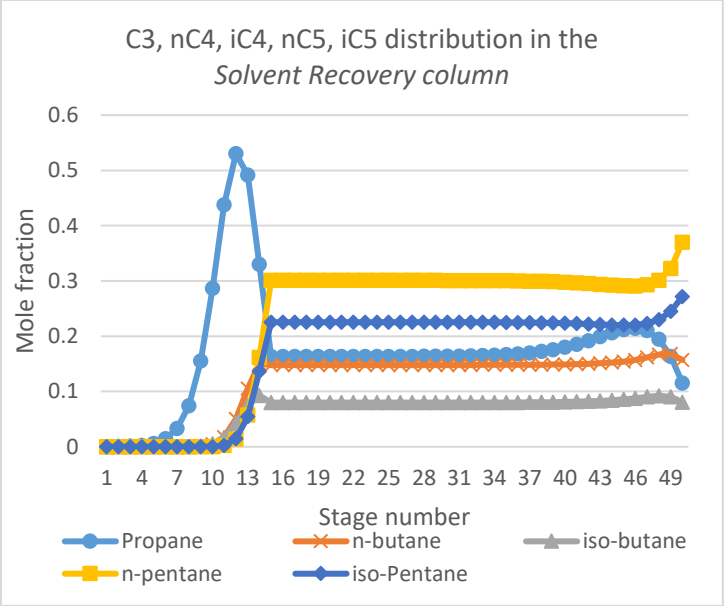


**Figure 32 Heavier hydrocarbon mole fraction variation with stage number in the Solvent *Recovery column***

The aforementioned results indicate that in theory a distillation-based $CO_2$ removal system for LNG is feasible. Evidently however, further study is needed in order to examine the energetic and economic aspects of such a system.

Simulations were also run to study the effect of using a different equation of state on the full three column distillation setup for purification of natural gas where full recycle is functional (Case III). The Redlich-Kwong-Soave (RKS) cubic equation of state for all thermodynamic properties. The Redlich-Kwong-Soave (RKS) method has been selected because this property method is comparable to the Peng-Robinson property method. Like the Peng Robinson this property method is also suited for nonpolar or mildly polar mixtures like hydrocarbons and light gases, such as carbon dioxide, hydrogen sulfide, and hydrogen. The applicability of this equation

of state less universal than the Peng-Robingson equation of state and Redlich-Kwong-Soave is particularly suitable in the high temperature and high pressure regions, such as in hydrocarbon processing applications or supercritical extractions. However it can be applied to the current simulations that are at high pressures and near critical point. The details of the comparison of equation of states can be found in Table 6. The Peng-Robinson and Redlich-Kwong-Soave both perform well for removal separating methane into the distillate stream from the other constituents of natural gas in the *Demethanizer Column.* However the RKS equation of state is not successful in breaking the azeotrope between $CO_2$ and $C_2H_6$. The 2:1 by volume azeotrope of $CO_2$ and $C_2H_6$ can be seen in the distillate stream of the *Extractive column*. This leads us to conclude that the equation of state being used in the simulations must be selected carefully and Redlich-Kwong-Soave equation of state does not perform well in low temperature conditions.

**Table 6 Comparison of the distillation separation process on the three column simulation using Peng-Robinson and Redlich-Kwong-Soave equations of states**

| ***Demethanizer column* light stream** | | |
|---|---|---|
| Component | Peng-Robinson EoS | Redlich-Kwong-Soave EoS |
| $CO_2$ | 4.527 ppm | 0.32 ppm |
| $CH_4$ | 0.9999 | 0.9999 |
| ***Extractive column* light stream** | | |
| Component | Peng-Robinson EoS | Redlich-Kwong-Soave EoS |
| $CO_2$ | 0.9371 | 0.619 |
| $C_2H_6$ | 0.0212 | 0.3212 |
| ***Extractive column* heavy stream** | | |
| $CO_2$ | 1.9e-05 | 0.2715 |
| $C_2H_6$ | 0.1388 | 0.7268 |

### *4.1.4 Parametric study of Extractive column*

This section illustrates the effect of some common distillation operating conditions on the fractionating or separation process. The *Extractive column* is chosen for this study since the *Demethanizer column* is tightly constrained by the $CO_2$ freezeout temperature and a wide range of parameters cannot be explored. Due to the nature of the azeotrope, the *Extractive column* is often the most difficult to converge and thus, is also the most interesting to study. Only the *Extractive column* is simulated for the purpose of this study, but the feed to the extractive column is unchanged from what was used earlier in the full three column distillation system, that is the heavy stream from the bottoms of the *Demethanizer column* is used to feed the *Extractive column.*

Effect of pressure

Keeping all other parameters constant, the pressure is varied in the *Extractive column.* The pressure is varied from 10 to 30 bar in increments of 5 bar. The reflux ratio is 3.5, solvent to feed ratio is 0.5, a 50-50 mixture of n-pentane and iso-pentane is used as solvent, the solvent feed stage is 3 and the total number of stages is 50 in the *Extractive column*.

The $CO_2$ concentration in the distillate stream increases as pressure increases, peaks at 20 bar at a value of 98.42% and then decreases with increasing pressure. In the pressure test matrix, the $CO_2$ varied between 98.31% and 98.42% in the distillate. Conversely the $CO_2$ in the heavy streams or bottoms product decreases with increasing pressure, reaches a low at 20 bar and increases again. However, the ethane trends are different with pressure variation. As pressure

increases ethane concentration in the distillate stream decreases and in the heavy stream increases. The rest of the hydrocarbons including propane, n-butane, i-butane, n-pentane and i-pentane are not affected by pressure variations and are almost entirely present only in the bottoms products as heavy components.

Since the main function of the *Extractive column* is to break the azeotrope between $CO_2$ and ethane, the operating conditions are based on their respective concentrations. An optimized pressure of 24 bar was thus selected to simulate the full three-column distillation system described earlier. Figure 33 -Figure 36 shows the mole fraction of carbon dioxide and ethane in the distillate stream and bottoms stream respectively.

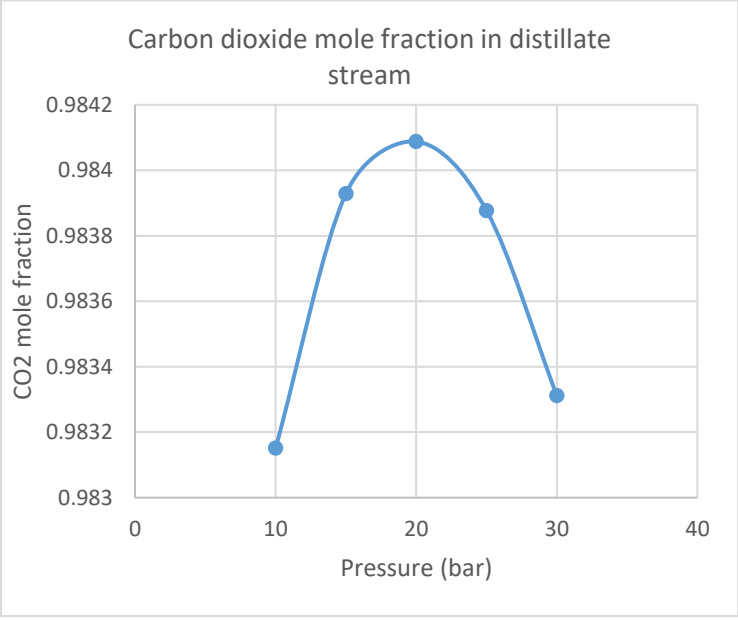


**Figure 33 Carbon dioxide mole fraction with pressure variation in the distillate stream of the *Extractive column***

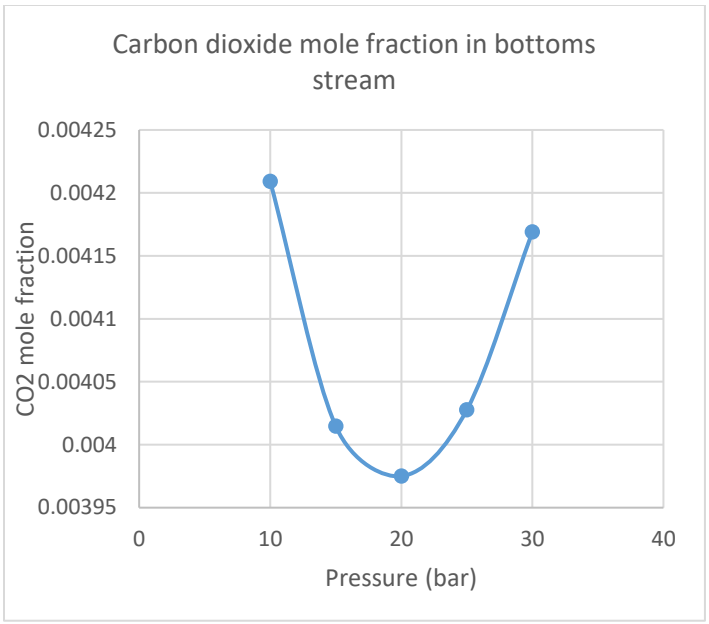


**Figure 34 Carbon dioxide mole fraction with pressure variation in the bottoms stream of the *Extractive column***

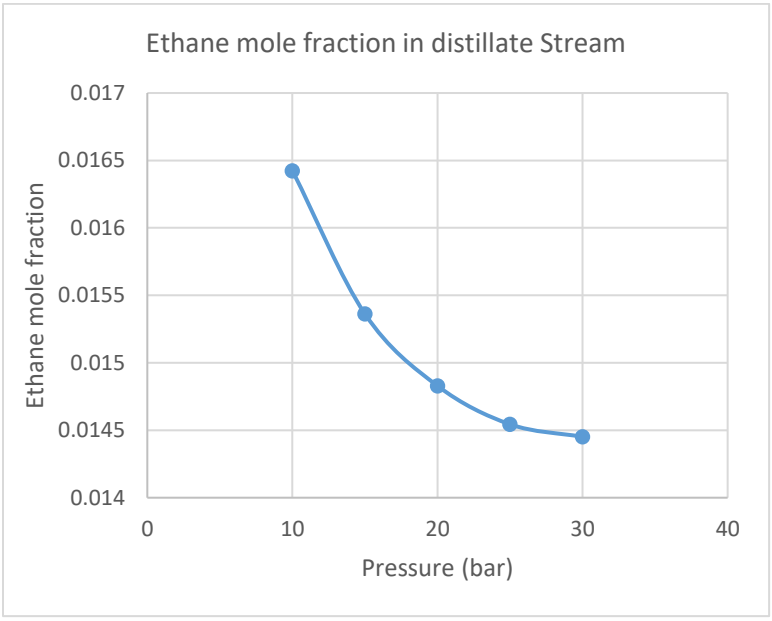


**Figure 35 Ethane mole fraction with pressure variation in the distillate stream of the *Extractive column***

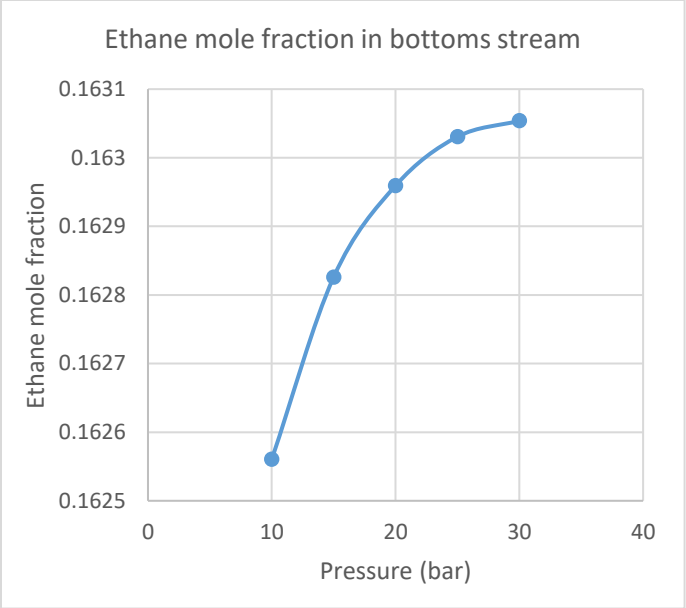


**Figure 36 Ethane mole fraction with pressure variation in the bottoms stream of the *Extractive column***

Effect of reflux ratio

To study the effect of reflux ratio on the extractive distillation process, all the parameters are kept constant and only the reflux ratio is varied. Reflux ratio is varied from 0.1 to 6.5 in increments of 0.5. The solvent to feed ratio is 0.5, a 50-50 mixture of n-pentane and iso-pentane is used as solvent, the solvent feed stage is 3, the total number of stages is 50 and the pressure in the *Extractive column* is 20 bar. As discussed earlier, the general rule is that as the reflux ratio increases the separation increases. However this is only true for simple distillation processes, azeotropic and extractive distillation have an interesting relationship with reflux ratio. There is a non-monotonic relationship between the mole fraction of key components being separated and reflux ratio. The Figure 37 and Figure 38 show that carbon dioxide mole fraction first increases

with reflux ratio and then instead of the expected trend of flattening out at near the peak value, the mole fraction of $CO_2$ then decreases with increasing reflux ratio. This peculiar behavior is typical of extractive distillation processes as excessive reflux ratio effectively dilutes the solvent thus worsening the separation. Conversely, ethane mole fraction in the distillate stream, first decreases, reaches a minimum value and then increases again as can be seen from Figure 39 and Figure 40. Non azeotropic components, in this case, the heavier hydrocarbons behave like simple distillation components and their respective mole fractions decrease in the distillate stream with increasing reflux ratio. An example can be seen in Figure 41, where n-pentane and iso- pentane concentrations decrease in distillate and the value flattens out after a certain reflux ratio.

It is clear that for extractive distillation processes, increasing the reflux ratio will not necessarily help the separation process, and sensitivity analysis must be done as a part of column design. Sometimes decreasing reflux can increase purity. In many, but not necessarily all cases, increasing reflux above a certain point decreases separation [146]. These trends of separation with variation of reflux ratio are in accordance to other extractive distillation studies found in literature [59, 137, 146].

It is interesting to note that the reflux ratio used for the full three-column distillation system described earlier is 3.3, even though it is determined that the reflux ratio corresponding to maximum separation in the *Extractive column* is close to 2. The value of reflux ratio corresponding to peak separation is dependent on many different parameters. The solvent stream composition used in those simulations are different than the simple 50-50 mixture of n-pentane and iso-pentane used for these parametric studies. This is the best case or ideal solvent. Also coupling of the *Solvent Recovery column* to the *Extractive column* changes the distillation dynamics and makes the system very complex. A detailed analysis was done for the entire system described in the previous section

to determine the best-operating conditions including reflux ratio of the *Extractive column* which was found to be 3.3

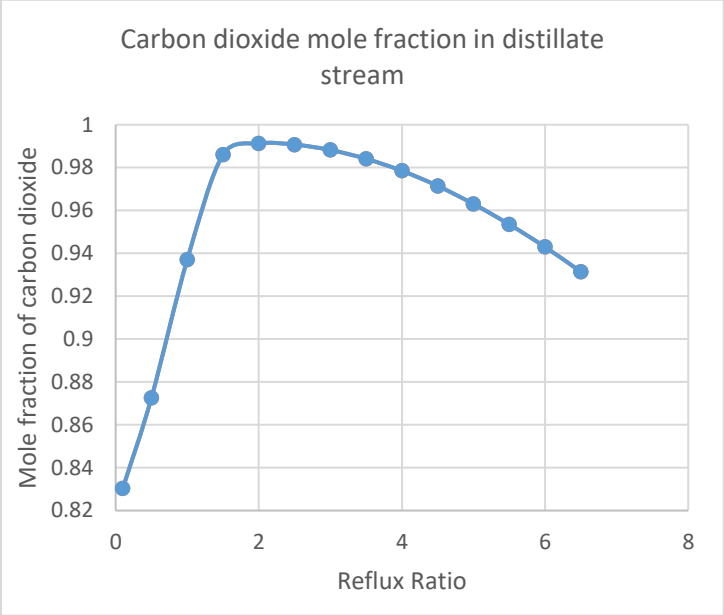


**Figure 37 Carbon dioxide mole fraction with reflux ratio variation in the distillate stream of the *Extractive column***

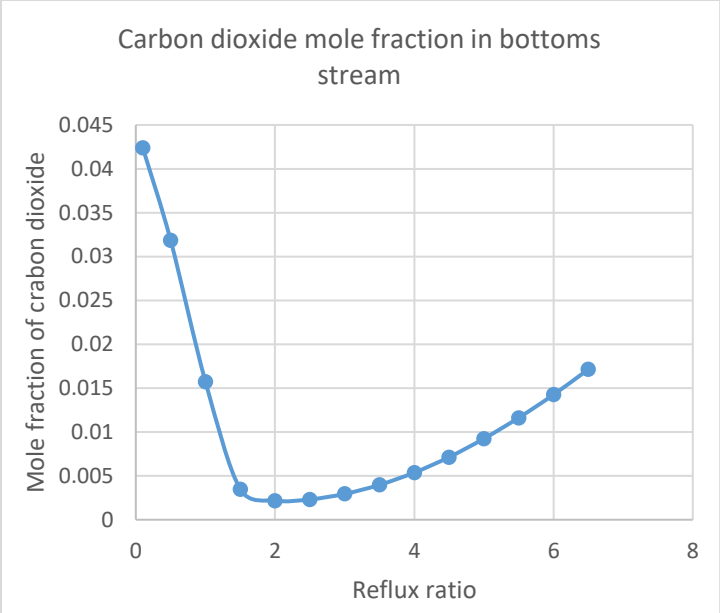


**Figure 38 Carbon dioxide mole fraction with reflux ratio variation in the bottoms stream of the Extractive column**

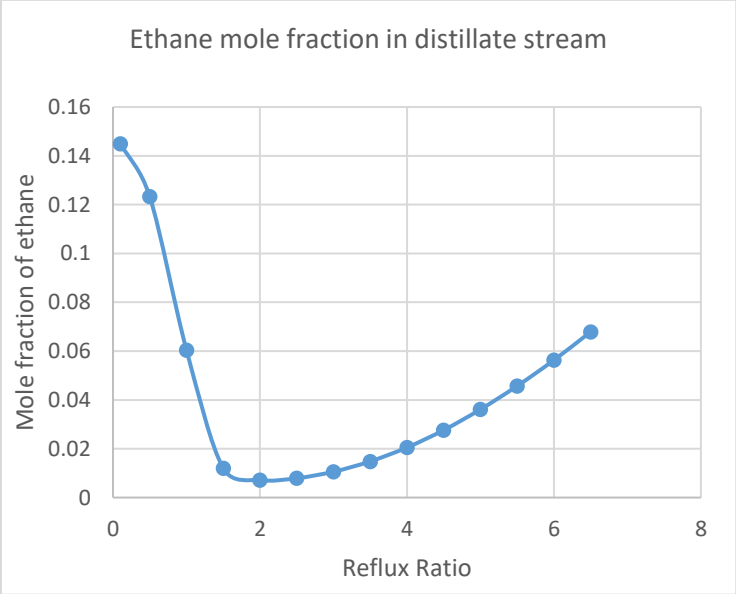


**Figure 39 Ethane mole fraction with reflux ratio variation in the distillate stream of the *Extractive column***

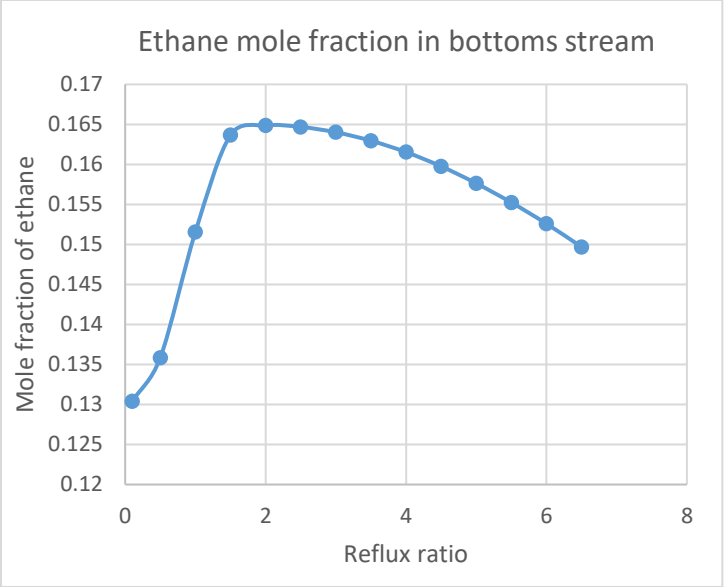


**Figure 40 Ethane mole fraction with reflux ratio variation in the bottoms stream of the *Extractive column***

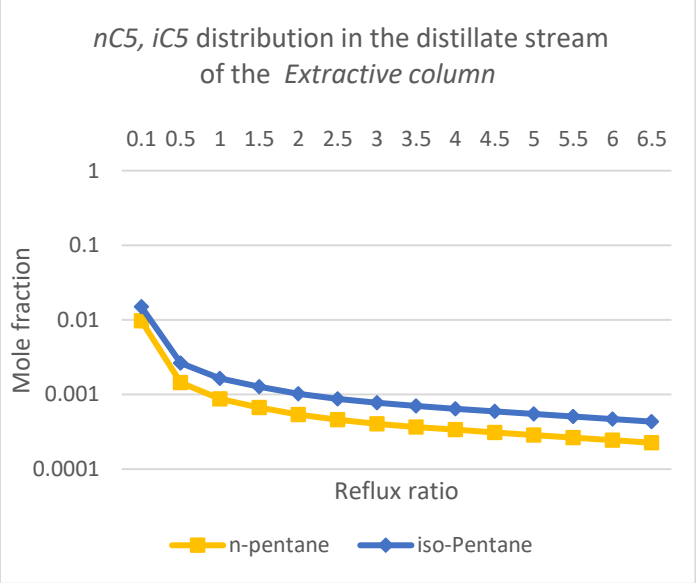


**Figure 41 n-pentane and iso-pentane mole fraction with reflux ratio variation in the distillate stream of the *Extractive column***

Effect of feed stage location

To study the effect of feed stage location all the parameters are kept constant and only the feed stage number is varied. Feed stage location number is varied from 2 to 38 in increments of 2 stages. The solvent to feed ratio is 0.5, a 50-50 mixture of n-pentane and iso-pentane is used as solvent, the solvent feed stage is 3, the total number of stages is 50, the pressure in the *Extractive column* is 20 bar and the reflux ratio, based on parametric studies is now kept constant at a value of 2.

Carbon dioxide mole fraction in the distillate stream increases as the feed inlet stage location increases or feed stage is lowered along the column. Ethane concentration follows the opposite trend: as feed stage location number increases, it decreases in the distillate stream. The $CO_2$ concentration reaches a maximum a little below the center tray and then remains constant with a flat profile. The compositions of carbon dioxide and ethane with variation in the feed stage location can be seen in Figure 42 - Figure 45.

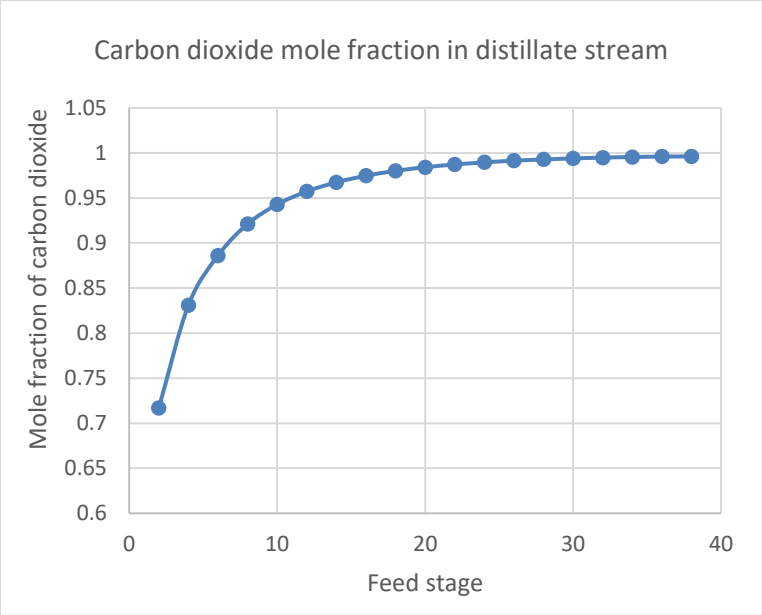


**Figure 42 Carbon dioxide mole fraction with feed stage variation in the distillate stream of the *Extractive column***

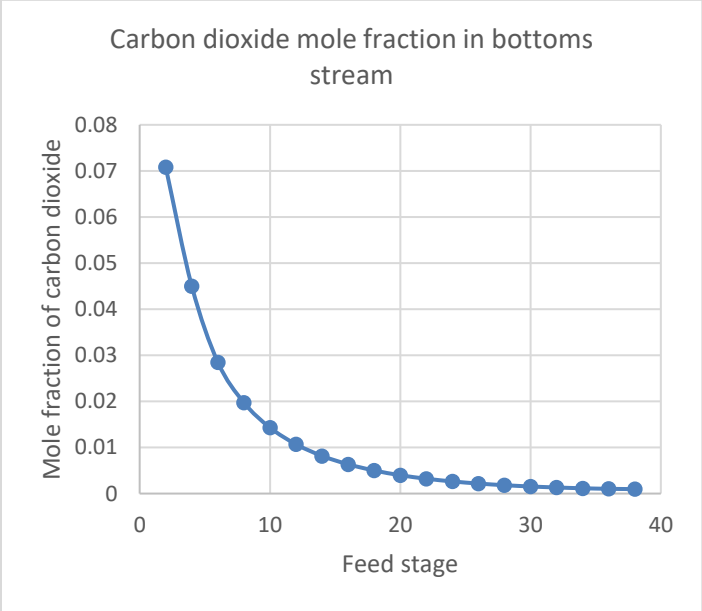


**Figure 43 Carbon dioxide mole fraction with feed stage variation in the bottoms stream of the *Extractive column***

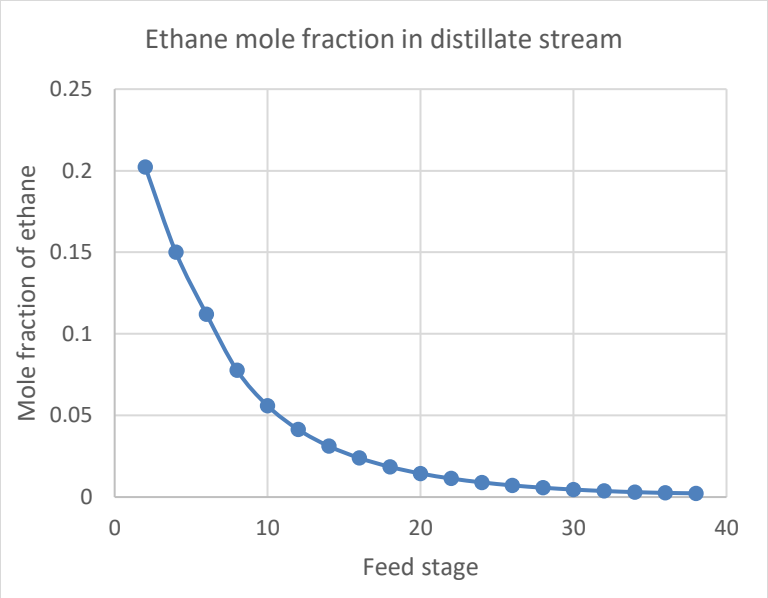


**Figure 44 Ethane mole fraction with feed stage variation in the distillate stream of the *Extractive column***

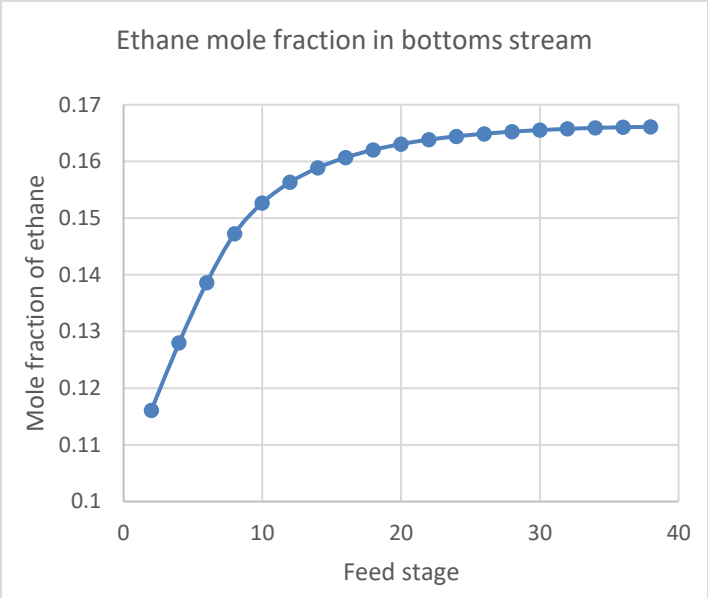


**Figure 45 Ethane mole fraction with feed stage variation in the bottoms stream of the *Extractive column***

Effect of reflux ratio on freeze-out

The effect of changing the reflux ratio on the $CO_2$ freezeout in a distillation column is studied. These tests are carried out in the *Demethanizer column* instead of the *Extractive column* since there is no freeze out in the *Extractive column.* The other parameters like the feed composition, feed conditions and pressure are unchanged. Reflux ratio is varied from 1 to 4 in increments of 1. It is found that for $CO_2$ –methane distillation systems as the reflux ratio increases the tendency of $CO_2$ to solidify also increases. This could be a result of better separation tendencies with increasing reflux ratio, thereby leading to higher $CO_2$ at earlier stages. If the $CO_2$ concentration increases at a rate that is faster than the corresponding stage temperature increase, then $CO_2$ will freeze out of the mixture. Figure 46 - Figure 50 show the freezeout temperature and the actual temperature or distillation stage temperature at each stage of the distillation column. As the reflux increases the pinch stages decrease or move up the column. Once again this can be explained by the tendency to have better separation. For reflux ratio = 1 the pinch stage is at 23 where the actual temperature comes closest to the freezeout temperature. Whereas for reflux ratio = 3 and 4, freeze out occurs at stages 18 and 19, where actual temperature in the distillation column is lower than the freeze out temperature of $CO_2$.

A property set called TFREEZE was developed and was found to be conservative, which means it predicts freezeout of $CO_2$ at a temperature a little higher than the actual freezeout temperature determined by experiments. Thus there is a possibility that there is no freeze out in any of the cases shown below. However, the trends observed are accurate and very helpful in studying distillation dynamics and developing a good understanding distillation processes for methane-carbon dioxide systems.

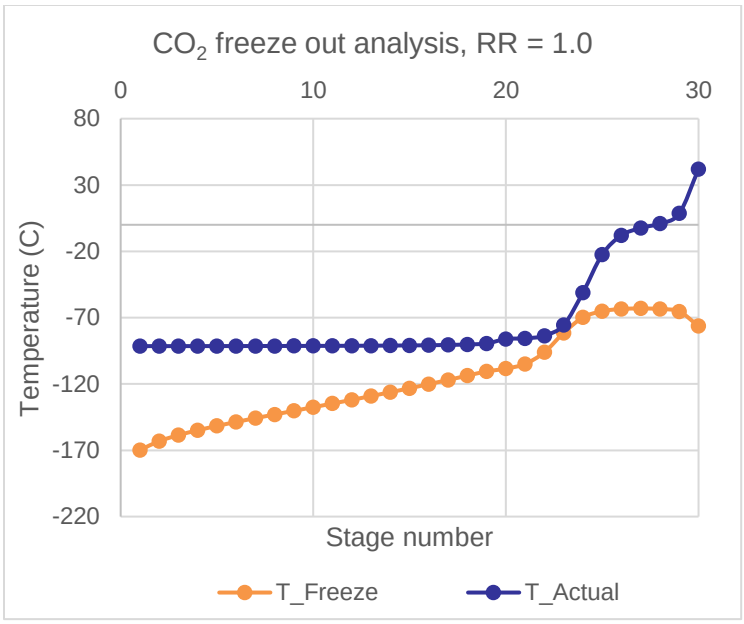


**Figure 46 Freezeout temperature and actual column temperature along all the stages in the *Demethanizer column* for reflux ratio = 1.0**

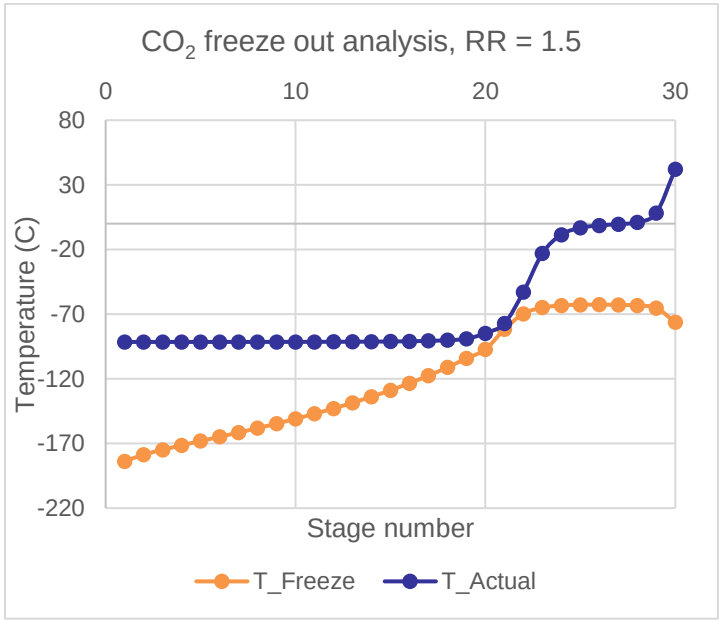


**Figure 47 Freezeout temperature and actual column temperature along all the stages in the *Demethanizer column* for reflux ratio = 1.5**

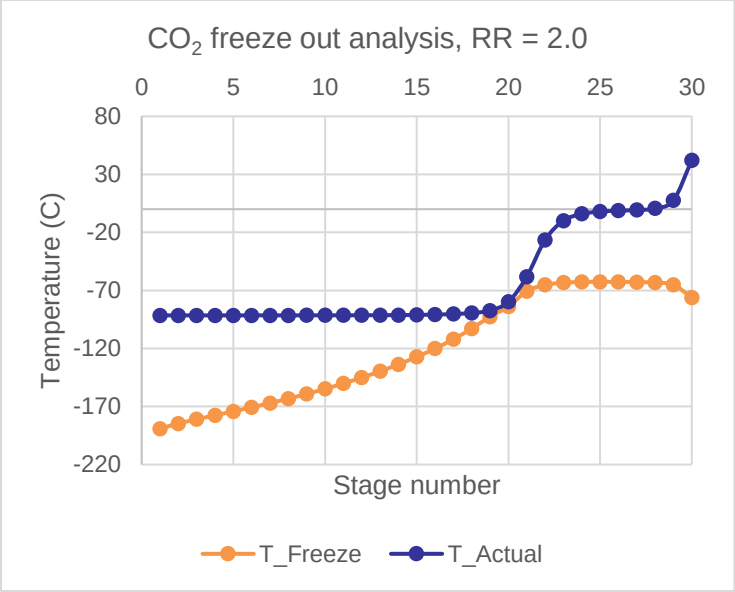


**Figure 48 Freezeout temperature and actual column temperature along all the stages in the *Demethanizer column* for reflux ratio = 2.0**

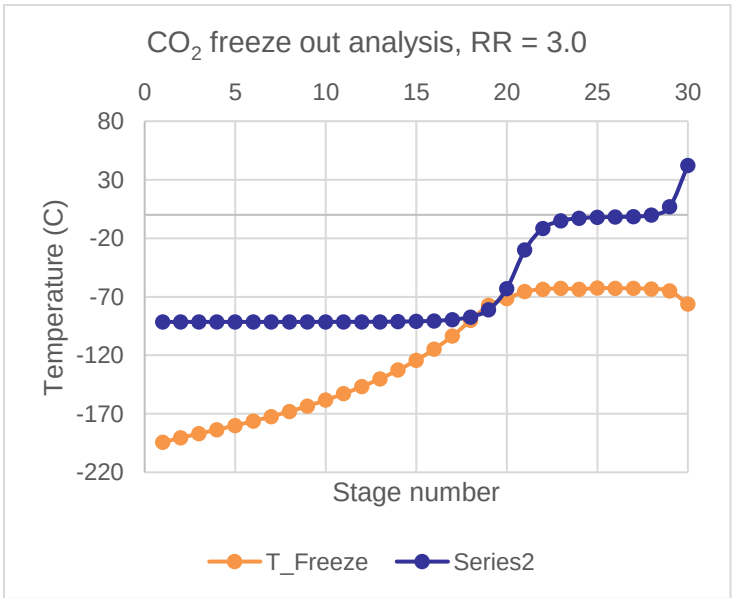


**Figure 49 Freezeout temperature and actual column temperature along all the stages in the *Demethanizer column* for reflux ratio = 3.0**

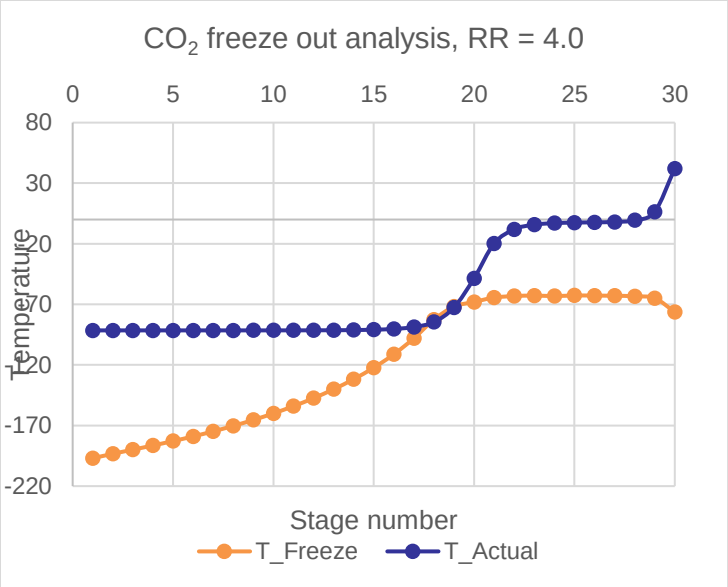


**Figure 50 Freezeout temperature and actual column temperature along all the stages in the *Demethanizer column* for reflux ratio = 4.0**

## 4.2 Hydrodynamics of a double helicoidally-coiled heat exchanger

### *4.2.1 Single-phase Flow Hydrodynamic Experiments*

In the single-phase hydrodynamic experiments the intention is to measure and correlate the friction factor in the helically coiled flow passage. These experiments are performed with gas and liquid separately. Single-phase flow experiments, besides being valuable and critically important in their own right, are essential for the development of empirical correlations for two-phase flow. LabVIEW, a systems engineering software, is used for data acquisition and visualization. Inlet and outlet pressures and temperatures for both fuel and coolant and the weight of the fuel cylinder are recorded at intervals of 1 second. The Mach number for both water and nitrogen single-phase experiments are to the order of 0.01 and thus compressibility effects can be neglected.

Conservation equations used for hydrodynamic analysis of single-phase flow through a double helically coiled tube

A constant flow rate is imposed through the coil, and once steady-state is achieved the total pressure drop in the coil is measured. The friction factor is calculated from the two-phase momentum equation [114] in the following form:

$$\left(-\frac{\partial P}{\partial z}\right)_{total}=\left(-\frac{\partial P}{\partial z}\right)_{ta}+\left(-\frac{\partial P}{\partial z}\right)_{sa}+\left(-\frac{\partial P}{\partial z}\right)_{g}+\left(-\frac{\partial P}{\partial z}\right)_{fr} \tag{26}$$

Where,

$\left(-\frac{\partial P}{\partial z}\right)_{total}$ = channel total pressure gradient

$\left(-\frac{\partial P}{\partial z}\right)_{ta}$ = temporal mixture acceleration

$\left(-\frac{\partial P}{\partial z}\right)_{sa}$ = spatial mixture acceleration

$\left(-\frac{\partial P}{\partial z}\right)_{g}$ = hydrostatic pressure acceleration

$\left(-\frac{\partial P}{\partial z}\right)_{fr}$ = frictional pressure gradient

The pressure gradient terms in Equation (26) can be written as

$$\left(-\frac{\partial P}{\partial z}\right)_{total} = \cancel{\left(\frac{\partial G}{\partial t}\right)_{ta}} + \frac{1}{A}\frac{\partial}{\partial z}\left(\frac{G^2}{\rho}\right)_{sa} + \cancel{\left(\rho g \sin\theta\right)_{g}} + \left(\frac{fG^2}{2D\rho}\right)_{fr} \tag{27}$$

Integrating both sides, we get:

$$\left(P_{in} - P_{exit}\right)_{total} = \int_0^L \left( \cancel{\left(\frac{\partial G}{\partial t}\right)_{ta}} + \frac{1}{A}\frac{\partial}{\partial z}\left(\frac{G^2}{\rho}\right)_{sa} + \cancel{\left(\rho g \sin\theta\right)_{g}} + \left(\frac{fG^2}{2D\rho}\right)_{fr} \right) dz + \sum_{i=1}^{N} \Delta P_i \tag{28}$$

Where, $\sum_{i=1}^{N} \Delta P_i$ = is the total pressure drop due to flow disturbance i, and N is the total number of flow disturbances (valves, orifices, flow area changes, etc.). The only disturbances that cause pressure drop in this case are the inlet and outlet of the coiled tubes.

The frictional pressure drop, and the friction factor, are then calculated via the following rendition of the 1D momentum conservation equation.

$$\left(P_{in}-P_{exit}\right)_{total}=G^2\left(\frac{1}{\rho_{exit}}-\frac{1}{\rho_{in}}\right)_{sa}+\left(\frac{fLG^2}{2D\rho}\right)_{fr}+K_{in}\frac{1}{2}\rho_{in}U_{in}^2+K_{exit}\frac{1}{2}\rho_{exit}U_{exit}^2 \tag{29}$$

where the left side represents the total (measured) pressure drop, $K_{in}$ and $K_{exit}$ are the inlet and exit loss coefficients, respectively, and $f$ is the average Darcy friction factor. This equation can evidently account for the compressibility of the fluid.

The cross-section of the double helicoidally-coiled tubes is a near-circular elliptical, as described earlier in Section 3.2.1), thus the eccentricity of the ellipse needs to be taken into account while calculating the Reynold number. Thus we define

$$\mathrm{Re}_D=\frac{\rho jD}{\mu}=\frac{GD}{\mu} \tag{30}$$

where $\mathrm{Re}_D$ is the Reynold number of a circular cross sectional pipe having the same diameter as the effective diameter of the elliptical cross-section pipe, and D is the effective diameter of the coiled tubes. For an ellipse the following equations can be used [147]

$$a=\frac{D_a}{2};b=\frac{D_b}{2} \tag{31}$$

$$\alpha^*=\frac{b}{a};\xi=1-\left(\alpha^*\right)^2 \tag{32}$$

$$E_{\xi} = \frac{\pi}{2}\left[1 - \left(\frac{1}{2}\right)^2 \xi^2 - \left(\frac{1*3}{2*4}\right)^2 \frac{\xi^4}{3} - \left(\frac{1*3*5}{2*4*6}\right)^2 \frac{\xi^6}{5}\right] \quad (33)$$

$$D_i = \pi \frac{b}{E_{\xi}} \quad (34)$$

$$Area = \pi ab \quad (35)$$

where, $D_a$ and $D_b$ are the major and minor axes of the ellipsoid, a is half of the major axis, b is half of the minor axis, α* is the aspect ratio, $E_\xi$ is the complete elliptical integral of the second kind.

The range of Reynold number for which the single-phase flow experiments have been carried out are shown in Table 7. Tests are performed for $Re_D$ = 2613 to 47811. Single-phase water tests were performed between Reynold numbers of 2613 to 19288 and single-phase nitrogen gas tests were performed between Reynolds numbers of 11889 to 47811.

**Table 7 Range of Reynolds number for single-phase flow hydrodynamic analysis of a double helicoidally coiled pipe**

| **Range of Reynolds numbers for single-phase flow experiments** | |
|---|---|
| Component | $Re_D$ |
| Water | 2613 - 19288 |
| Nitrogen | 11889 - 47811 |

Error analysis and uncertainties

Physical quantities measured in experiments, e.g., velocity, temperature, pressure, concentration, heat fluxes, etc., are subject to error. Two broad categories of error are taken into account in the current work [148]: precision errors and bias errors. Precision errors or random errors have various sources like the “least count” of the scale, fluctuating experimental conditions, repeatability associated errors, etc. Bias errors or systematic errors arise from sources like calibration error in a measuring instrument, sensitivity or span errors, and hysteresis associated errors. Some errors that are generally referred to as hidden errors [148] may also be present in the experiments. For example a hidden error in the current experimental set up may be the possibility that the thermocouple attached to the surface on the primary and secondary side walls do not read the surface temperature unless there is a good thermal contact between the sensor and surface; if not, the thermocouple will give a value somewhere between the true surface temperature and the ambient temperature. These types of errors will be hard to isolate since all the thermocouples have been welded into the test section during manufacturing and is not accessible easily. The concept of accuracy that is often quoted by the manufacturer includes errors from all sources. In the current analysis as soon as an error from a particular source is seen to be significantly smaller than other errors present, it is given no further consideration. Whenever feasible, experiments were repeated under identical conditions to check for repeatability and data scatter.

For hydrodynamic analysis of single-phase flow in determining the friction factor f, we can estimate the error, by analyzing the dependence of $f$ on different measured parameters.

Error is propagated through the following equation

$$U_Y = \sqrt{\left(\frac{\partial Y}{\partial X_1}U_{X_1}\right)^2 + \left(\frac{\partial Y}{\partial X_2}U_{X_2}\right)^2 + \ldots\ldots\ldots + \left(\frac{\partial Y}{\partial X_n}U_{X_n}\right)^2} \quad (36)$$

$$Y = f(X_1, X_2, \ldots X_n) \quad (37)$$

where, $Y$ is a function of variables $X_1, X_2, \ldots X_n$

$U_Y$, $U_{X_1}$, $U_{X_2}$ ….. $U_{X_n}$ are the uncertainties of variables $Y, X_1, X_2, \ldots X_n$ respectively

$\frac{\partial Y}{\partial X_1}, \frac{\partial Y}{\partial X_2} \ldots\ldots\ldots \frac{\partial Y}{\partial X_n}$ are the influence coefficients or partial derivatives of the variables $X_1, X_2, \ldots X_n$ respectively

Friction factor, *f* is defined as

$$f = \frac{2(P_i - P_o)D\rho}{LG^2} \quad (38)$$

Writing *f* in terms of experimentally measured parameters

$$f = \frac{2(P_i - P_o)D\rho}{L\left(\frac{\dot{m}}{\frac{\pi}{4}D^2}\right)^2} \quad (39)$$

$$\text{Since, } G = \frac{\dot{m}}{A} = \frac{\dot{m}}{\frac{\pi}{4}D^2} \quad (40)$$

$$f = \frac{(P_i - P_o)D^5 \rho \pi^2}{8L\dot{m}^2} \tag{41}$$

The error propagation equation for $f$ can be written as

$$U_f = \sqrt{\left(\frac{\partial f}{\partial P_i}U_{P_i}\right)^2 + \left(\frac{\partial f}{\partial P_o}U_{P_o}\right)^2 + \left(\frac{\partial f}{\partial D}U_D\right)^2 + \left(\frac{\partial f}{\partial \rho}U_\rho\right)^2 + \left(\frac{\partial f}{\partial L}U_L\right)^2 + \left(\frac{\partial f}{\partial \dot{m}}U_{\dot{m}}\right)^2} \tag{42}$$

(43)

The influence coefficients are be shown to be

$$\frac{\partial f}{\partial P_i} = \frac{D^5 \rho \pi^2}{8L\dot{m}^2} \tag{44}$$

$$\frac{\partial f}{\partial P_o} = -\frac{P_o D^5 \rho \pi^2}{8L\dot{m}^2} \tag{45}$$

$$\frac{\partial f}{\partial D} = \frac{(P_i - P_o)5D^4 \rho \pi^2}{8L\dot{m}^2} \tag{46}$$

$$\frac{\partial f}{\partial \rho} = \frac{(P_i - P_o)D^5 \pi^2}{8L\dot{m}^2} \tag{47}$$

$$\frac{\partial f}{\partial L} = -\frac{(P_i - P_o)D^5 \rho \pi^2}{8L^2\dot{m}^2} \tag{48}$$

$$\frac{\partial f}{\partial \dot{m}} = -2\frac{(P_i - P_o)D^5 \rho \pi^2}{8L\dot{m}^3} \tag{49}$$

The uncertainties can be found from the manuals and using least count of the measuring devices.

$$U_{P_i} = U_{P_o} = \pm 0.25\% 16mA \tag{50}$$

$$U_T = 0.5\% \ \ above \ \ 0^o C \ \ or \ 1.7K \tag{51}$$

$$U_L = \frac{2 \times least count}{\sqrt{6}} \tag{52}$$

$$U_D = \frac{2 \times least count}{\sqrt{6}} \tag{53}$$

$U_{\dot{m}}$ is calculated differently based on the phase being considered. For water or liquid phase a flowmeter is used, so uncertainty is based on the flowmeter. For gas phases both nitrogen and air, accurate measurements are obtained using a weighing balance and then calculating the mass flow rate using slope against time. Regression analysis of the slope is performed using a linear polynomial fitting model in to calculate the uncertainty in mass flow rate of the gas phases. It is observed that the gas phase mass flow rate has less uncertainties than the liquid phase. A larger percentage of the error for both phases comes from the mass flow rate. The error in density is so small that it can be neglected.

Experimental results of the single-phase flow hydrodynamic tests

Figure 51 shows the variation of the friction factor of the double helically coiled heat exchanger with Reynolds number. The experiments were run over a large enough range of Reynolds numbers to encompass laminar, transition and turbulent flows regimes. The triangular markers (in blue) are the friction factor for single-phase tests with water and are mostly in the laminar regime, but show transition to the turbulent regime. The circular markers (in orange) exhibit the single-phase friction factors using nitrogen gas. The nitrogen gas tests show transition leading up to well-developed turbulent flow at high Reynolds numbers. The single-phase tests using nitrogen show some scatter in the friction factor that are not encompassed by the error bars. This can be partially attributed to the error introduced in the results from repeatability. The tests show good repeatability for the same flow conditions, however.

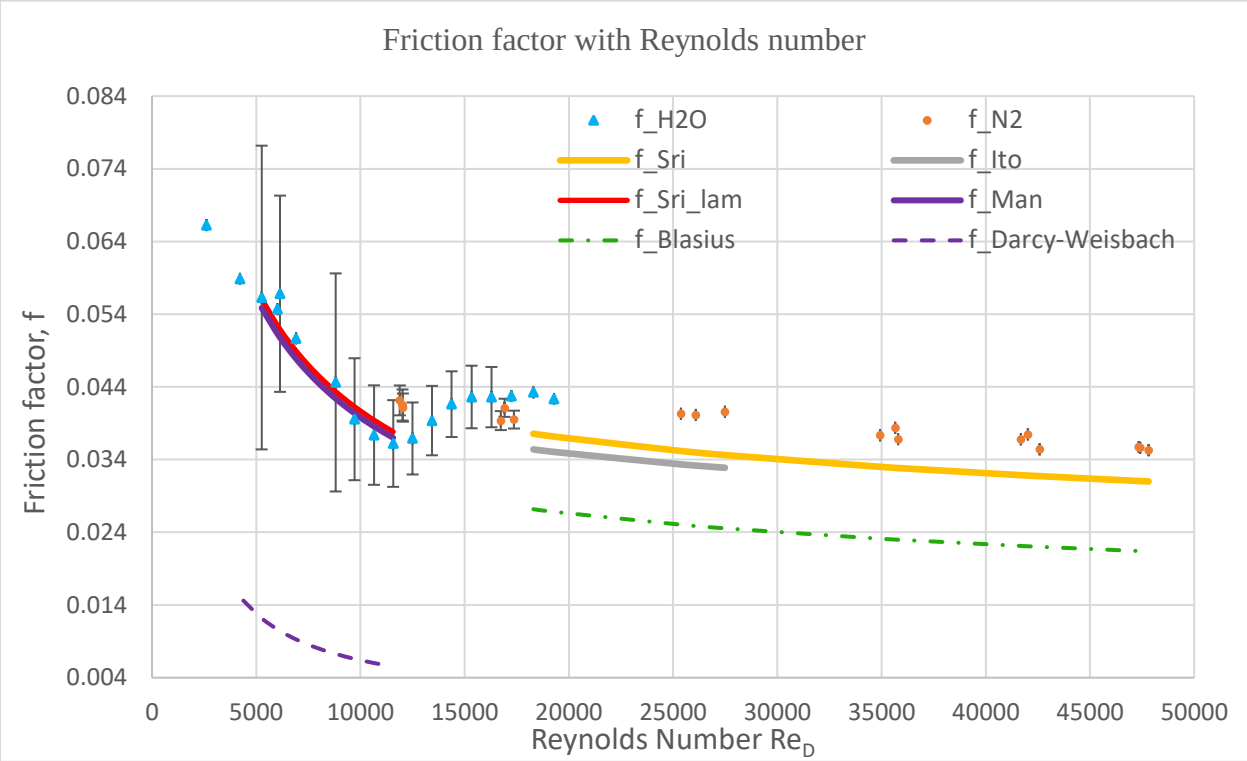


**Figure 51 Friction factor of the double helically coiled tube as a function of Reynolds number for single-phase flow tests using water and nitrogen as the test fluids**

It is observed that the transition from laminar flow to turbulent flows is delayed in comparison to a straight pipe ~2100 under similar conditions. The critical Reynolds number for curved tubes is delayed because the secondary flow stabilizes the laminar flow. It is also observed that for the laminar flow, the friction factors line up well with existing friction factor correlations found in literature for helical flows. The friction factors determined from experiments are compared in the figure with several correlations. The correlation of Srinivasan et al. [79] for laminar flow is

$$\frac{f_c}{f_s} = \begin{pmatrix} 1 & for & Dn < 30 \\ 0.419 Dn^{0.275} & for & 30 < Dn < 300 \\ 0.1125 Dn^{0.5} & for & Dn > 300 \end{pmatrix} \tag{54}$$

Where the range of applicability is $7 < \frac{R_{cl}}{R_i} < 140$

The friction factor for laminar flows can also be found from the correlation of Manalpaz and Churchhill [81]

$$\frac{f_c}{f_s} = \left[ \left( 1.0 - \frac{0.18}{\left\{ 1 + \left( 35 / Dn \right)^2 \right\}^{0.5}} \right)^m + \left( 1 + \frac{R_i / R_{cl}}{3} \right)^2 \left( \frac{Dn}{88.3} \right) \right]^{0.5} \tag{55}$$

where,

$m = 2 \quad for \quad Dn < 20$
$m = 1 \quad for \quad 20 < Dn < 40$
$m = 0 \quad for \quad Dn > 40$

The parameters $f_s$ and $f_c$ are friction factors for a straight line, and friction factor representing the helicoidally coiled tube, respectively.

It is interesting to note that for laminar flows in helical pipes the friction factor in the current work and those in literature trends are all comparable and show the same trends.

The critical Reynolds number for laminar-turbulent flow regime change proposed by Schmidt [75] for simple helicoidal tubes is

$$\mathrm{Re}_{critical} = 2300\left(1+8.6\left(R_i / R_{cl}\right)^{0.45}\right) \tag{56}$$

A correlation for the same critical Reynolds number proposed by Srinivasan et al. [76] is

$$\mathrm{Re}_{critical} = 2100\left(1+12\left(R_i / R_{cl}\right)^{0.5}\right) \tag{57}$$

The above correlations predict a critical Reynold number of 9378 and 10144 respectively for our test section. The critical Renolds numbers observed in the single-phase experiments are only slightly higher, and are about ~12000.

Our data indicate that the minimum Reynolds number for fully turbulent flow regime is about ~18000. The transition from laminar to turbulent flow and the onset of turbulence is captured by the water experiments, but the majority of the flow in turbulent regime is captured by the gas nitrogen tests. Beyond the transition regime the water and nitrogen results align with each other quite well, thereby confirming the reliability of the experimental procedure. The friction factor for turbulent flows of helically coiled pipes have been compared to some widely-used correlation in literature, including the correlation of Ito [74]

$$f_c\left(\frac{R_{cl}}{R_i}\right)^{0.5} = 0.029 + 0.304\left[\mathrm{Re}_D\left(\frac{R_{cl}}{R_i}\right)^{-2}\right]^{(-0.25)} \tag{58}$$

$$\text{where, } 0.034 < \mathrm{Re}_D\left(\frac{R_{cl}}{R_i}\right)^{-2} < 300, \tag{59}$$

and the correlation of Srinivasan et al. [79]

$$f_c\left(\frac{R_{cl}}{R_i}\right)^{0.5} = 0.336 * \left[\mathrm{Re}_D\left(\frac{R_{cl}}{R_i}\right)^{-2}\right]^{(-0.2)} \tag{60}$$

$$\text{where, } \mathrm{Re}_D\left(\frac{R_{cl}}{R_i}\right)^{-2} < 700 \quad \text{and} \quad 7 < \frac{R_{cl}}{R_i} < 104. \tag{61}$$

The friction factors determined from experiments in the turbulent regime are higher than those of Srinivasan and Ito. It must also be noted that for turbulent flows the correlations of Srinivasan and Ito are not completely aligned. Although the experimental friction factors and the friction factors predicted by the aforementioned two correlations are not equal, their trends are quite similar. Since the friction factor in the turbulent flow regime for helicoidal pipes determined by experiments are higher that those found in literature rather significantly, the following new correlation for the friction factor is proposed

$$f_{turb} = 0.306\,\mathrm{Re}_D^{-0.2} \tag{62}$$

The average deviation of this correlation (or equivalently the experimentally measured f=values of friction factor) from Srinivasan friction factor is about 12.7%. The higher friction

factor is due to a higher pressure loss for the same Reynold number and thus can be at least partially attributed to the asymmetric or elliptical cross section of the double helicoidal pipes. The way the pipes were manufactured during the process of extrusion and then coiled, resulted in a slightly flattened portion of the ellipse being on the outside of the coil, i.e the major axis of the ellipse is parallel to the axis of the helix. The secondary vortices caused by unbalanced centrifugal forces have more contact surface area with the internal walls of the pipe as compared to an equivalent helix with a circular cross-section. Thus additional kinetic energy is lost as shear stress or pressure drop between the walls and the fluid. This results in a higher friction factor for the same Reynolds number.

### *4.2.2 Two-phase Flow Hydrodynamic Experiments*

In the two-phase hydrodynamic experiments the intention is to measure and correlate the pressure drop due to friction in the double helically coiled flow passages for two-phase flow without phase change. These experiments are performed with immiscible mixtures of gas and liquid phases. The gas phase used for these tests is air, and the liquid phase used is water.

Single-phase flow results derived in section 0 are used here, for the development of empirical correlations for two-phase flow. LabVIEW is used for data acquisition and visualization. Inlet and outlet pressures and temperatures for air-water mixtures in the helicoidally coiled tubes and the weight of the liquid supply cylinder are recorded at intervals of 1 second.

Equations used for hydrodynamic analysis of two-phase flow through a double helically coiled tube

The hydrodynamic aspects of two-phase flow in helicoidally-coiled tubes were discussed in some detail earlier in Section 2.2. As mentioned, two-phase multipliers are commonly used by researchers to analyze two-phase flows. The concept of two-phase multipliers was developed from the derivation of the expression of two phase frictional pressure drop in homogenous flows of non-miscible liquids. In homogenous flows the two phase multipliers have a well-defined form that has been derived based on a homogenous mixture viscosity (see Section 2.2). In homogenous flow this parameter is a function of fluid properties but for more realistic flow this multiplier must analyzed and determined through experimental or numerical methods. In general, for separated flow, the two-phase pressure drop can be expressed in four different but equivalent forms as discussed in section 2.2.1. The following two of those form are used in the current analysis [114].

$$\left(-\frac{\partial P}{\partial z}\right)_{fr} = \Phi_L^2 \left(-\frac{\partial P}{\partial z}\right)_{fr,L} \tag{63}$$

$$\left(-\frac{\partial P}{\partial z}\right)_{fr} = \Phi_G^2 \left(-\frac{\partial P}{\partial z}\right)_{fr,G} \tag{64}$$

where the left-hand side terms in the equations $(-\partial P/\partial z)_{fr}$ is the two-phase pressure drop due to frictional losses. The pressure loss terms on the right-hand side $(-\partial P/\partial z)_{fr,L}$ and $(-\partial P/\partial z)_{fr,G}$ represent frictional pressure losses in single-phase flows. The subscript L is the frictional pressure gradient when only pure liquid at a mass flux of G(1-x) flows in the channel, and subscript G represents the case when pure gas at mass flux, Gx flows in the channel. The parameters $\Phi^2_L$ and

$\Phi^2_G$ are two-phase multipliers for liquid and gas and are found from the aforementioned Equations (63) and (64) as the ratio of the frictional pressure drop in the two-phase flow divided by the frictional pressure drop in the single-phase flow of their respective liquid or gas components

$$\Phi_L^2 = \frac{\left(-\frac{\partial P}{\partial z}\right)_{fr}}{\left(-\frac{\partial P}{\partial z}\right)_{fr,L}} \tag{65}$$

$$\Phi_G^2 = \frac{\left(-\frac{\partial P}{\partial z}\right)_{fr}}{\left(-\frac{\partial P}{\partial z}\right)_{fr,G}} \tag{66}$$

Some fundamental flow parameters of two-phase flows that are used to derive the expression for the two-phase pressure multipliers are defined below. These include quality, x, liquid and gas mass fluxes $G_L$ and $G_G$, total mass flux, G, liquid and gas Reynolds number, and $Re_L$ and $Re_G$

$$x = \frac{\dot{m}_G}{\left(\dot{m}_G + \dot{m}_L\right)} \tag{67}$$

$$G_L = \frac{\dot{m}_L}{A} \tag{68}$$

$$G_G = \frac{\dot{m}_G}{A} \tag{69}$$

$$\dot{m} = \dot{m}_G + \dot{m}_L \tag{70}$$

$$G = G_G + G_L = \frac{\rho_G \dot{V}_G}{A} + \frac{\rho_L \dot{V}_L}{A} \tag{71}$$

$$\mathrm{Re}_L = \frac{\dot{m}_L}{A}\frac{D_i}{\mu_L} \tag{72}$$

$$\mathrm{Re}_G = \frac{\dot{m}_G}{A}\frac{D_i}{\mu_G} \tag{73}$$

The frictional pressure losses in the single-phase liquid flow in Equation (63) can be derived using the Equations (67) – (73)

$$\left(-\frac{\partial P}{\partial z}\right)_{fr,L} = \frac{f_L G_L^2}{2D_i \rho_L} \tag{74}$$

$$\left(-\frac{\partial P}{\partial z}\right)_{fr,L} = \frac{f_L}{2D_i \rho_L}\left(\frac{\dot{m}_L}{A}\right)^2 \tag{75}$$

$$\left(-\frac{\partial P}{\partial z}\right)_{fr,L} = \frac{f_L}{2D_i \rho_L}\left(\mathrm{Re}_L \frac{\mu_L}{D_i}\right)^2 \tag{76}$$

$$\left(-\frac{\partial P}{\partial z}\right)_{fr,L} = \frac{f_L \,\mathrm{Re}_L^2 \,\mu_L^2}{2D_i^3 \rho_L} \tag{77}$$

Similarly, the frictional pressure losses in the single-phase gas flow in Equation (64) can be derived as follows

$$\left(-\frac{\partial P}{\partial z}\right)_{fr,G} = \frac{f_G G_G^2}{2D_i \rho_G} \tag{78}$$

$$\left(-\frac{\partial P}{\partial z}\right)_{fr,G} = \frac{f_G}{2D_i \rho_G}\left(\frac{\dot{m}_G}{A}\right)^2 \tag{79}$$

$$\left(-\frac{\partial P}{\partial z}\right)_{fr,G} = \frac{f_G}{2D_i \rho_G}\left(\mathrm{Re}_G \frac{\mu_G}{D_i}\right)^2 \tag{80}$$

$$\left(-\frac{\partial P}{\partial z}\right)_{fr,G} = \frac{f_G \,\mathrm{Re}_G^2 \,\mu_G^2}{2D_i^3 \rho_G} \tag{81}$$

The single-phase flow friction factor proposed in section 0 can be used to find the friction factor of water and air $f_L$ and $f_G$, when the corresponding liquid and gas flow regimes are turbulent

$$f_{turb} = 0.306\,\mathrm{Re}_D^{-0.2}$$

The frictional pressure losses in the single-phase liquid and gas flow derived in Equation (77) and (81) can be used to find the two-phase pressure multipliers in Equations (65) and (66).

The Martinelli parameter, defined earlier in Section 2.2, and is defined below for convenience, is used as an empirical parameter for the correlations

$$X^2 = \frac{\Phi_G^2}{\Phi_L^2} = \frac{\left(-\frac{\partial P}{\partial z}\right)_{fr,L}}{\left(-\frac{\partial P}{\partial z}\right)_{fr,G}} \tag{82}$$

For empirical modeling, when liquid and gas are both turbulent when they flow alone in the flow passage, the Martinelli parameter can be shown to be

$$X_{tt} = \left(\frac{\rho_G}{\rho_L}\right)^{0.5} \left(\frac{\mu_L}{\mu_G}\right)^{0.1} \left(\frac{1-x}{x}\right)^{0.9} \tag{83}$$

$$X_{tt}^2 = \left(\frac{\mu_L}{\mu_G}\right)^{0.25} \left(\frac{1-x}{x}\right)^{1.75} \frac{\rho_G}{\rho_L} \tag{84}$$

Flow parameters of two-phase flow experiments

The two-phase flow experiments are run in sets of constant liquid mass flow rate. For each set of constant liquid mass flow rate, the gas mass flow rate is increased. For the next set of experiments the liquid mass flow rate is increased and the tests are repeated for all the gas flow rates at the new liquid mass flow rate. Table 8 shows the range of Reynolds numbers for the air-water experiments and the range of liquid and gas Reynolds numbers that were tested. The column on the right with the liquid Reynolds number is the average Reynolds number for all experiments run at the same mass flow rate. There is a slight fluctuation in $Re_L$ at constant mass flow rate because the temperature of the water varies during an experiment. However the variation is slight and average values of Reynolds number is a good approximation for the set of experiments.

**Table 8 Range of water and air Reynolds number for two-phase flow hydrodynamic analysis of a double helicoidally coiled pipe**

| **Range of Reynolds numbers for two-phase flow air-water experiments** | |
|---|---|
| Average $Re_L$ | $Re_G$ |
| 1035 | 2530 - 17302 |
| 1271 | 2690 - 17429 |
| 1360 | 2668 - 17526 |
| 1890 | 2256 - 17732 |
| 2260 | 2719 - 15132 |
| 2677 | 2840 - 16073 |
| 3448 | 2821 - 11962 |
| 4054 | 2809 - 10114 |
| 4191 | 3010 - 9197 |

| | |
|---|---|
| 5345 | 3147 - 7531 |
| 6652 | 3400 – 5362 |

As can be observed from Table 8 as the average liquid Reynolds number increases, or with increasing water mass flow rates, the range of air Reynolds number decreases. This is because as water mass flow rate increases the back pressure on the air side required to match the pump pressure head increases. This in turn requires a higher pressure on the air cylinder side and to achieve higher air mass flow rate, the liquid mass flow rate required to be pumped cannot be satisfied. For each liquid mass flow rate there is a maximum air mass flow rate that can be achieved without damaging the liquid supply apparatus.

Experimental results of the two-phase flow tests

Figure 51 shows the pressure drop ($\Delta P$ in Pa) recorded in the air-water two-phase flow tests in the double helicoidally coiled tubes. The tests are categorized into sets with each set representing a constant liquid Reynolds number. It is observed that as the Reynolds number of air increases the pressure drop across the helical test section also increases. As the water Reynolds number increases for a comparable air Reynolds number, the pressure drop also increases.

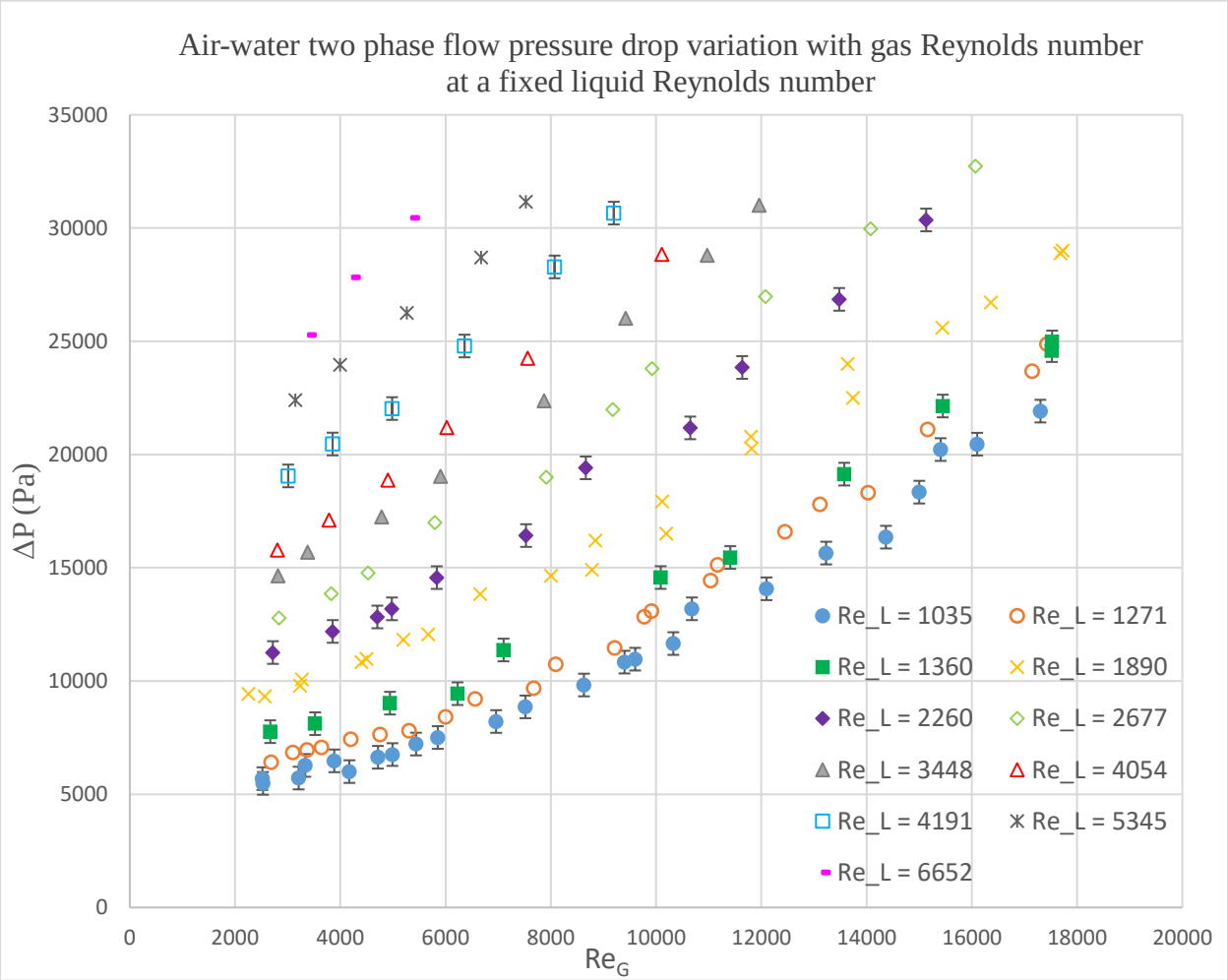


**Figure 52 Pressure drop recorded in air-water two-phase flow experiments with variation in gas Reynolds number. Each data series consists of data obtained with a fixed liquid Reynolds number while increasing the gas Reynols number.**

Figure 53 through Figure 63 show the dependence of the two-phase multiplier $\Phi_L^2$ on the Martinelli parameter for each set of liquid Reynolds number. The results have been compared to the predictions of the correlations of Xin et al. [124] and Colorado et al. [130]. The two-phase

multipliers determined from our experiments lie in between the correlations of Xin and Colorado. For a set of experiments with constant Reynold number of water, the liquid two-phase pressure multiplier decreases as the Martinelli parameter increases.

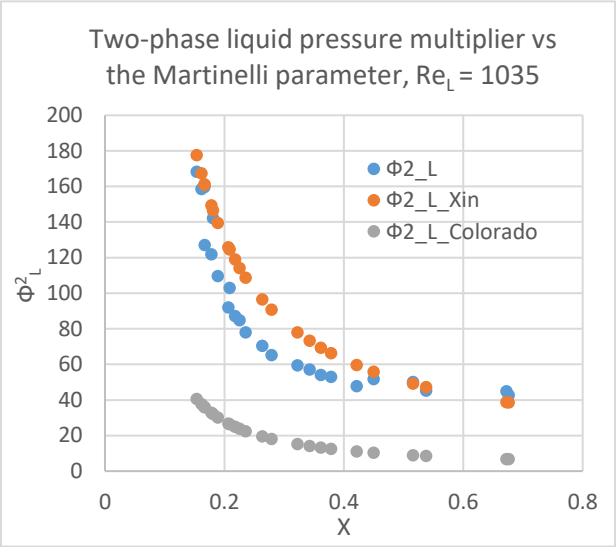


**Figure 53 Two-phase pressure multiplier found from experiments and comparison with two published correlations vs the Martinelli parameter for an average liquid Reynolds number of 1035**

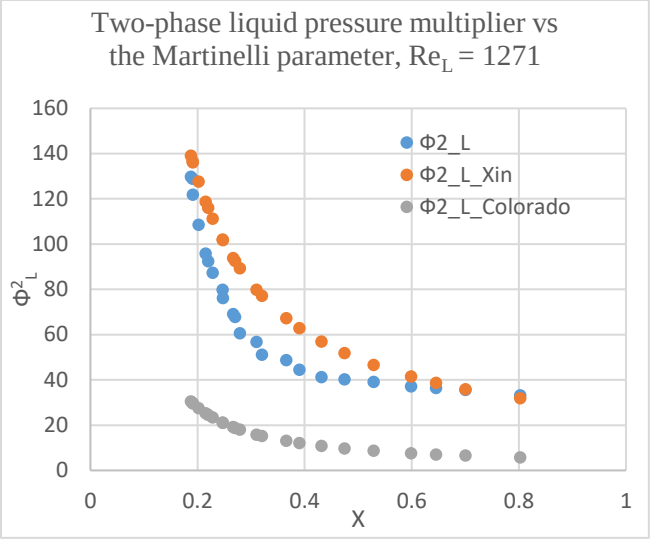


**Figure 54 Two-phase pressure multiplier found from experiments and comparison with two published correlations vs the Martinelli parameter for an average liquid Reynolds number of 1271**

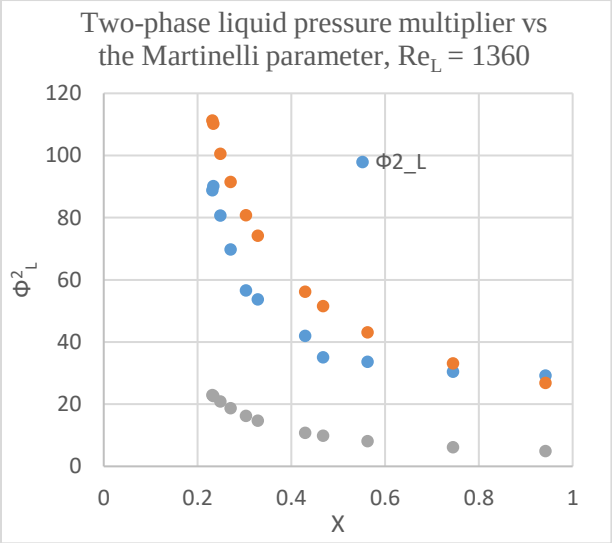


**Figure 55 Two-phase pressure multiplier found from experiments and comparison with two published correlations vs the Martinelli parameter for an average liquid Reynolds number of 1360**

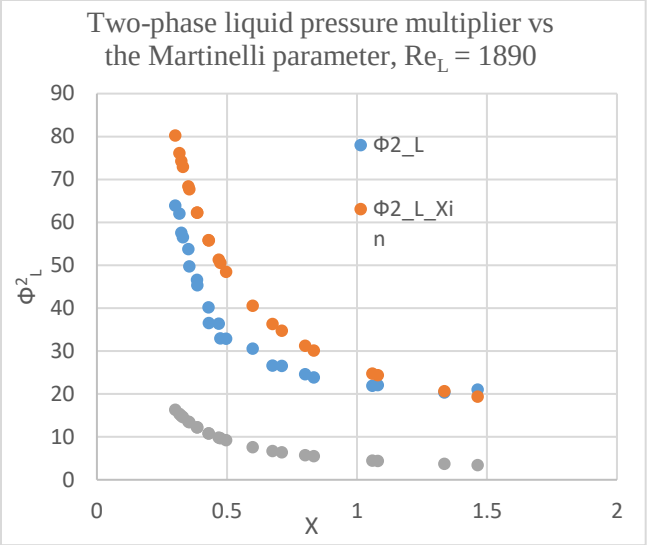


**Figure 56 Two-phase pressure multiplier found from experiments and comparison with two published correlations vs the Martinelli parameter for an average liquid Reynolds number of 1890**

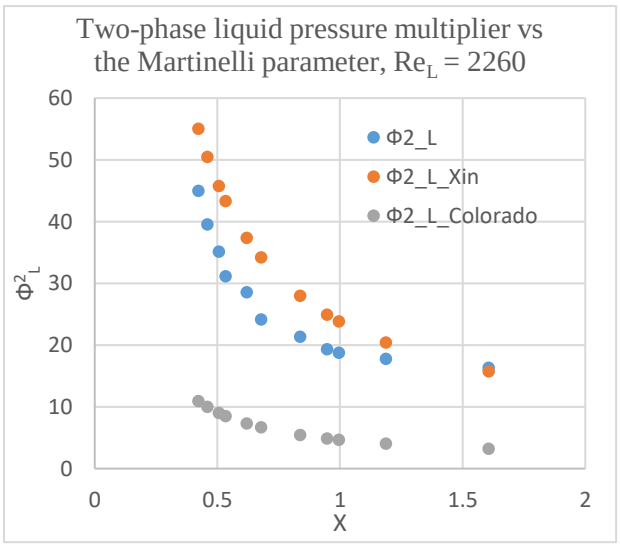


**Figure 57 Two-phase pressure multiplier found from experiments and comparison with two published correlations vs the Martinelli parameter for an average liquid Reynolds number of 2260**

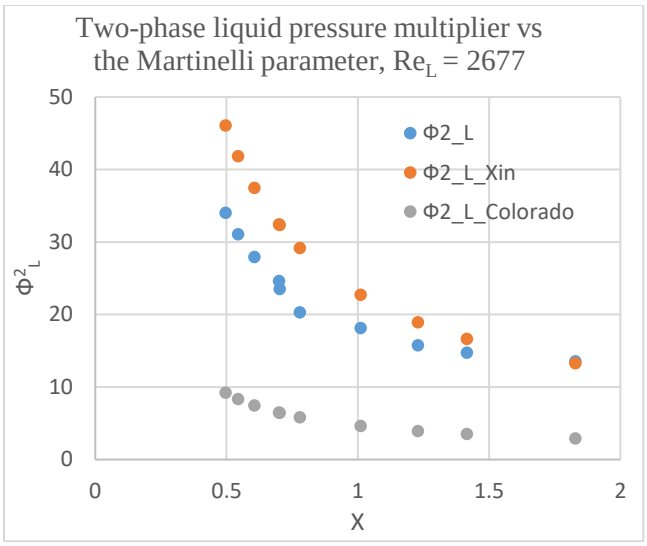


**Figure 58 Two-phase pressure multiplier found from experiments and comparison with two published correlations vs the Martinelli parameter for an average liquid Reynolds number of 2677**

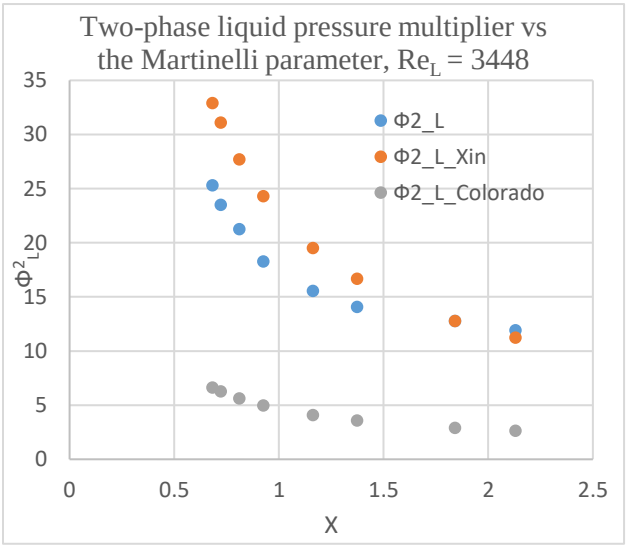


**Figure 59 Two-phase pressure multiplier found from experiments and comparison with two published correlations vs the Martinelli parameter for an average liquid Reynolds number of 3448**

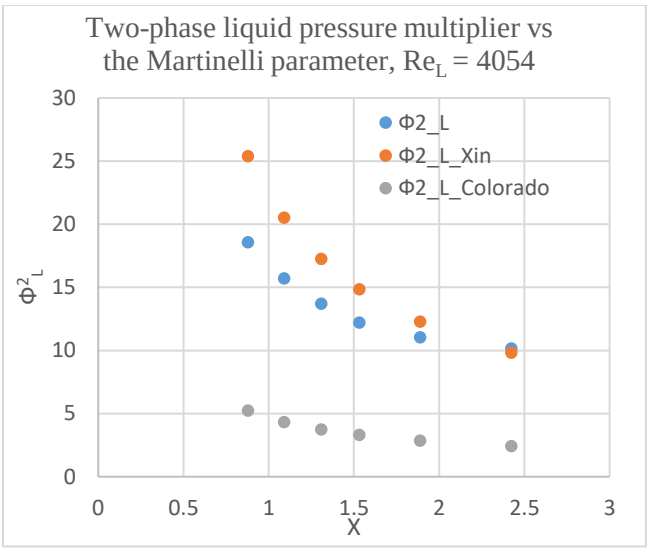


**Figure 60 Two-phase pressure multiplier found from experiments and comparison with two published correlations vs the Martinelli parameter for an average liquid Reynolds number of 4054**

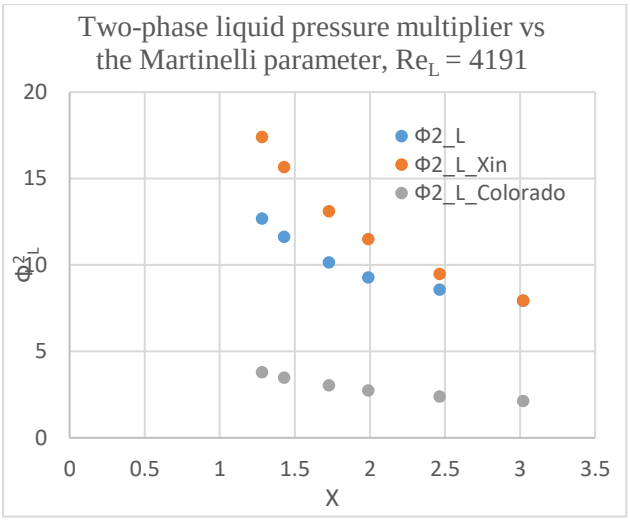


**Figure 61 Two-phase pressure multiplier found from experiments and comparison with two published correlations vs the Martinelli parameter for an average liquid Reynolds number of 4191**

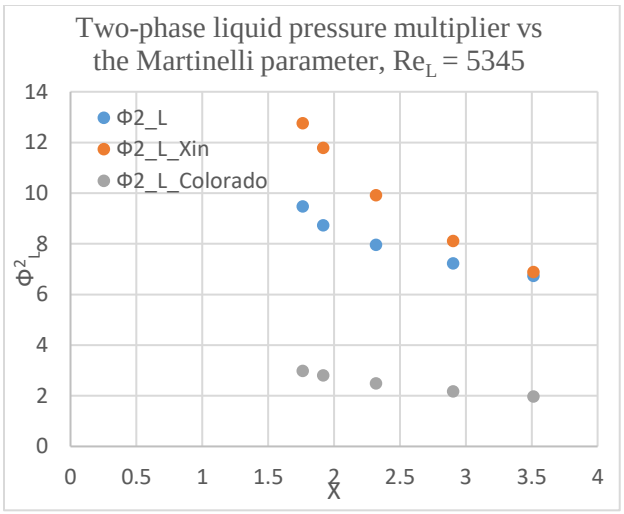


**Figure 62 Two-phase pressure multiplier found from experiments and comparison with two published correlations vs the Martinelli parameter for an average liquid Reynolds number of 5345**

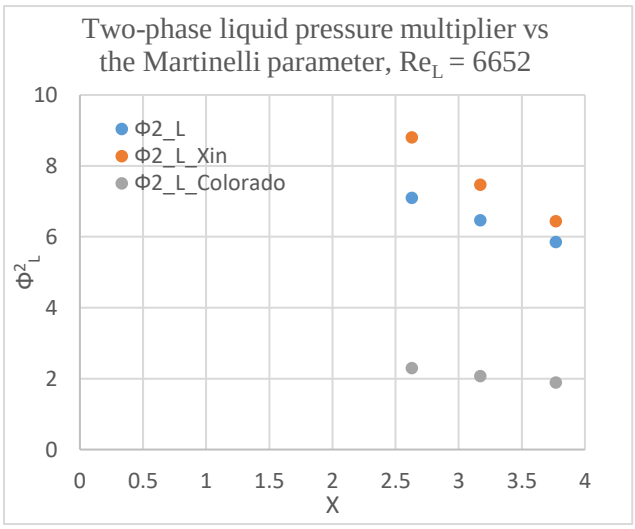


**Figure 63 Two-phase pressure multiplier found from experiments and comparison with two published correlations vs the Martinelli parameter for an average liquid Reynolds number of 6652**

Figure 64 - Figure 74 show the dependence of the two-phase multiplier $\Phi_G^2$ on the Martinelli parameter for each set of liquid Reynolds number. The liquid Reynolds numbers are also shown for reference. The two-phase pressure drop multiplier $\Phi_G^2$ increases with an increase in the Martinelli parameter.

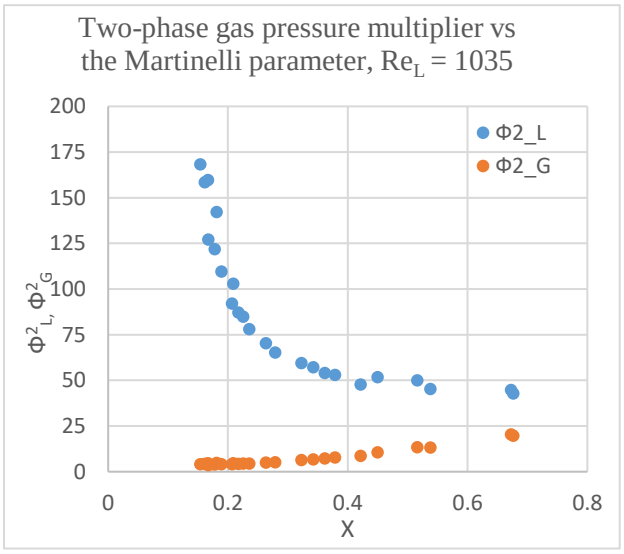


**Figure 64 Two-phase pressure multipliers found from experiments vs the Martinelli parameter for an average liquid Reynolds number of 1035**

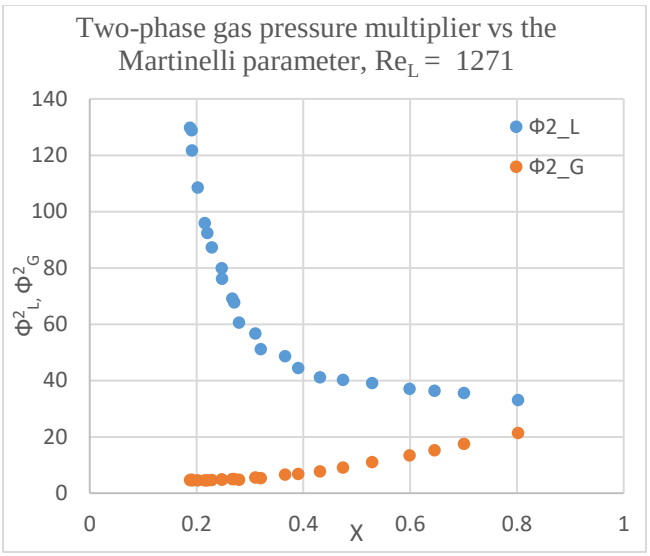


**Figure 65 Two-phase pressure multipliers found from experiments vs the Martinelli parameter for an average liquid Reynolds number of 1271**

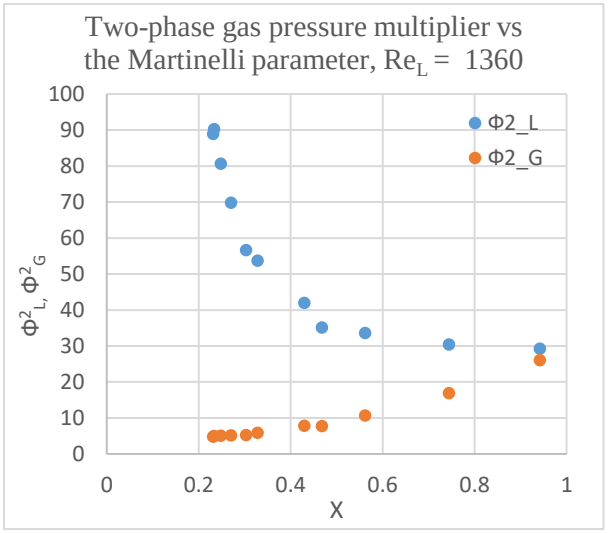


**Figure 66 Two-phase pressure multipliers found from experiments vs the Martinelli parameter for an average liquid Reynolds number of 1360**

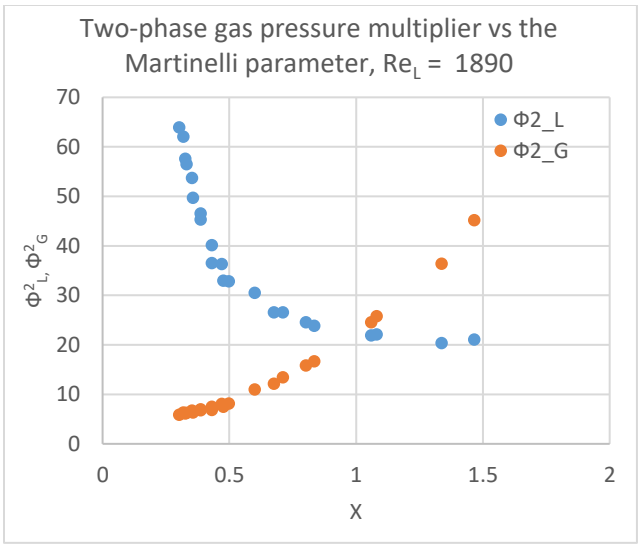


**Figure 67 Two-phase pressure multipliers found from experiments vs the Martinelli parameter for an average liquid Reynolds number of 1890**

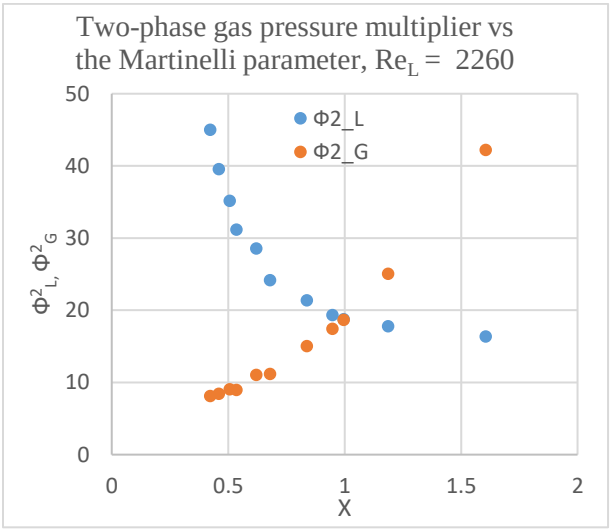


**Figure 68 Two-phase pressure multipliers found from experiments vs the Martinelli parameter for an average liquid Reynolds number of 2260**

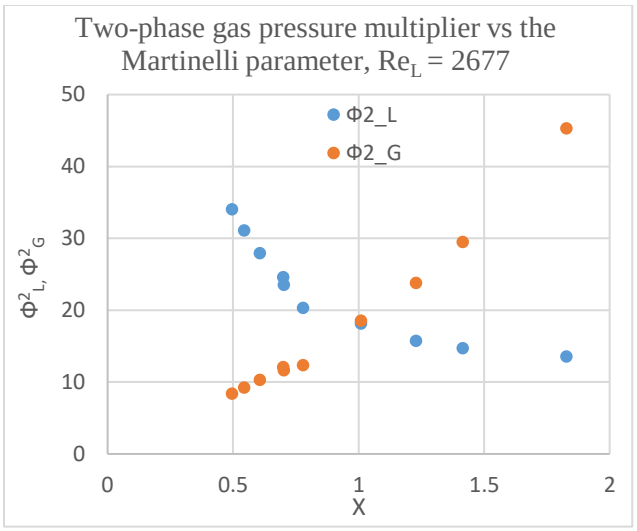


**Figure 69 Two-phase pressure multipliers found from experiments vs the Martinelli parameter for an average liquid Reynolds number of 2677**

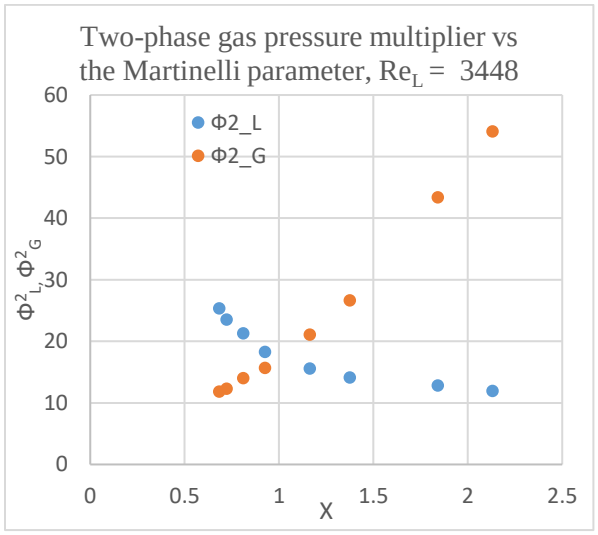


**Figure 70 Two-phase pressure multipliers found from experiments vs the Martinelli parameter for an average liquid Reynolds number of 3448**

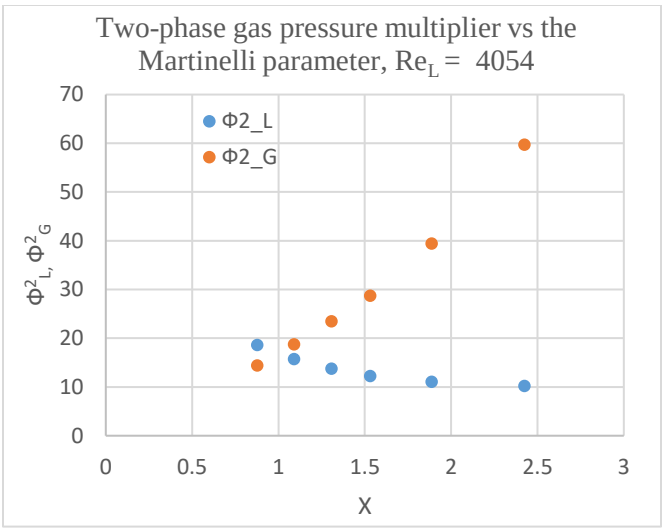


**Figure 71 Two-phase pressure multipliers found from experiments vs the Martinelli parameter for an average liquid Reynolds number of 4054**

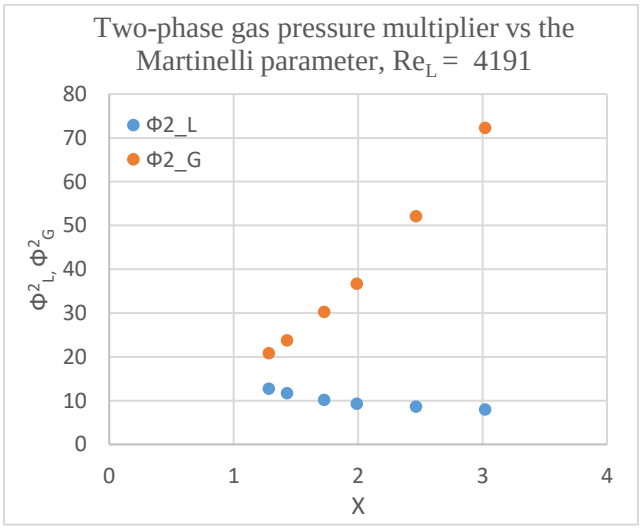


**Figure 72 Two-phase pressure multipliers found from experiments vs the Martinelli parameter for an average liquid Reynolds number of 4191**

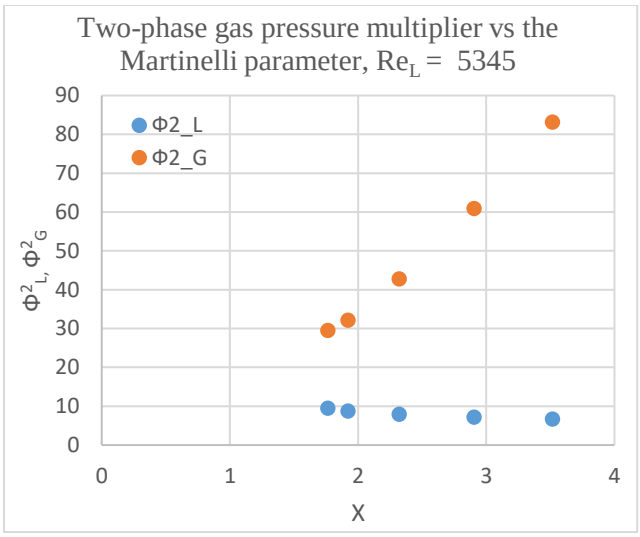


**Figure 73 Two-phase pressure multipliers found from experiments vs the Martinelli parameter for an average liquid Reynolds number of 5345**

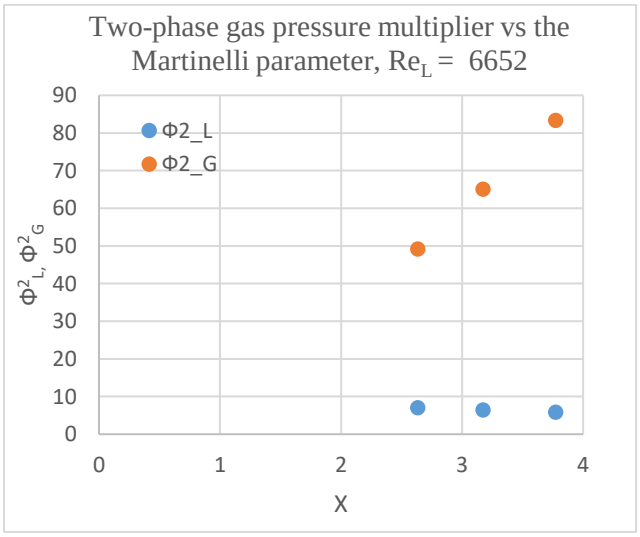


**Figure 74 Two-phase pressure multipliers found from experiments vs the Martinelli parameter for an average liquid Reynolds number of 6652**

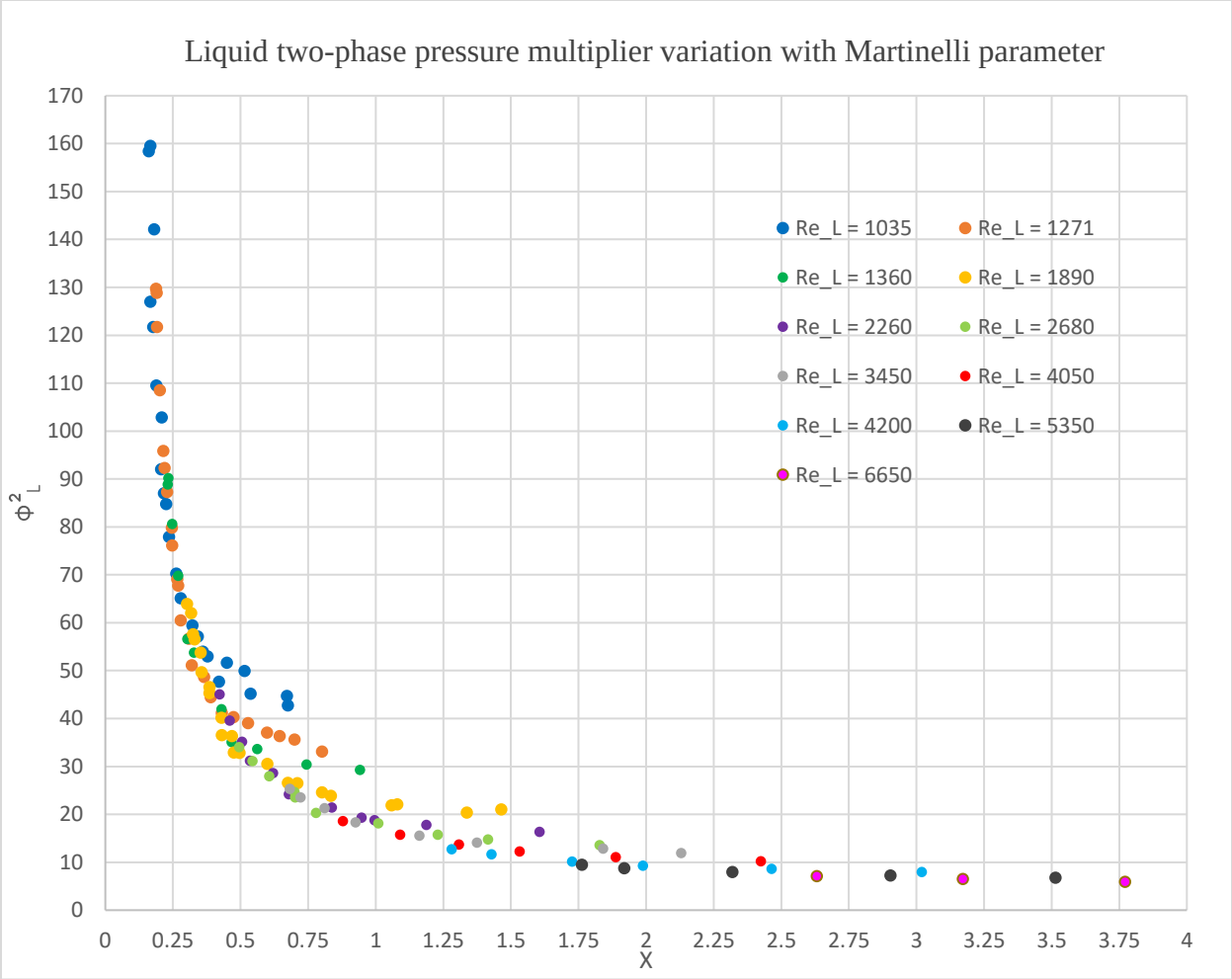


**Figure 75 Two-phase pressure muliplier $\Phi_L^2$ variation with the Martinelli parameter for all air and water Reynolds numbers**

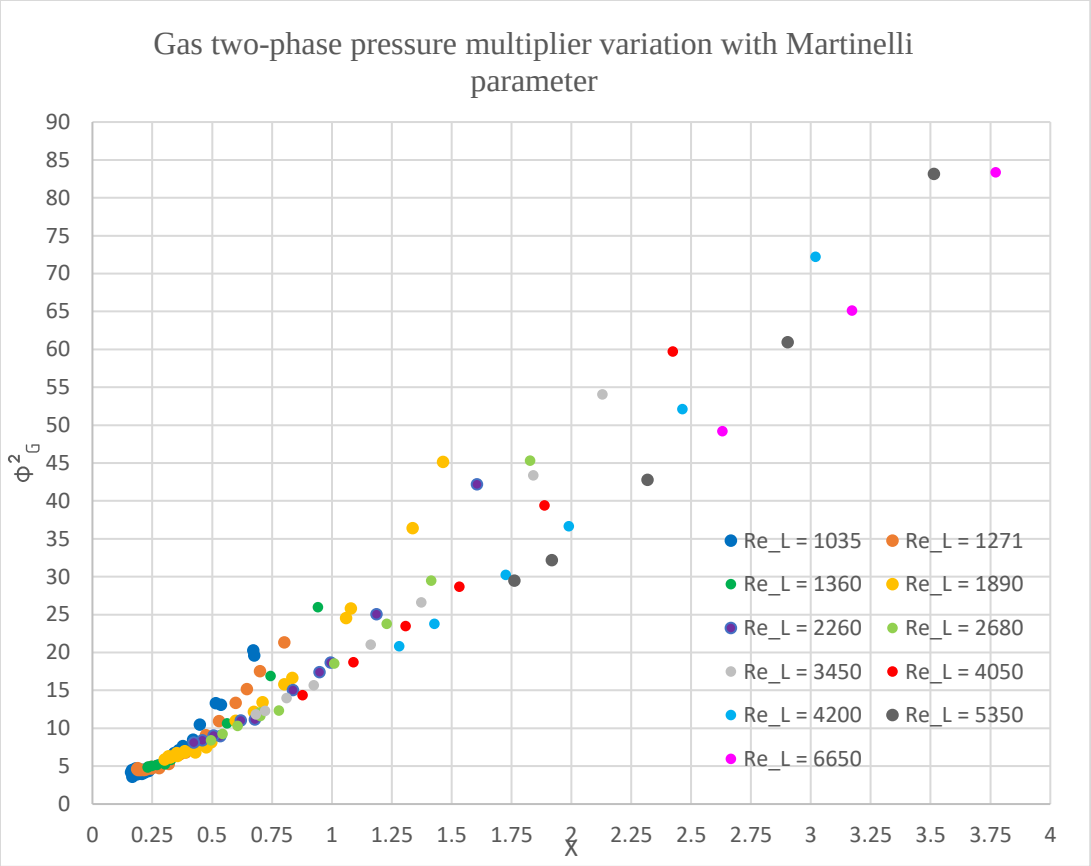


**Figure 76 Two-phase pressure multiplier $\Phi^2_G$ variation with the Martinelli parameter for all air and water Reynolds numbers**

Figure 75 and Figure 76 show the two-phase pressure multipliers $\Phi^2_L$ and $\Phi^2_G$, respectively, and their variation with the Martinelli parameter for all air and water Reynolds numbers. As can be seen in Figure 75 , $\Phi^2_L$ monotonically decreases as the liquid Reynolds number increases. For some of the lower liquid Reynolds numbers a slight deviation from the base curve is noticed. This deviation or scatter occurs at low liquid and gas Reynolds numbers that correspond to the laminar flow of either phase when it flows alone in the tube. This behavior can thus be attributed to the flow not being fully turbulent (turbulent-turbulent).

Further analysis of the experimental data shows that the scatter or deviation occurs at Reynold number of air less than ~ 4200 and Reynold number of water less than ~2800. This can be interpreted as the critical Reynolds number for two-phase flows of an air-water system in a double helically coiled pipe.

$$\mathrm{Re}_{G,critical} \approx 4200 \tag{85}$$

$$\mathrm{Re}_{L,critical} \approx 2800 \tag{86}$$

**The base curve of the liquid two-phase pressure multiplier for a turbulent-turbulent air-water system in helicoidal pipes is shown in**

**Figure 77. The forthcoming new correlation is proposed and is shown as the red dotted line in**

Figure 77:

$$\Phi_L^2 = 18.75 X^{-1.032} \tag{87}$$

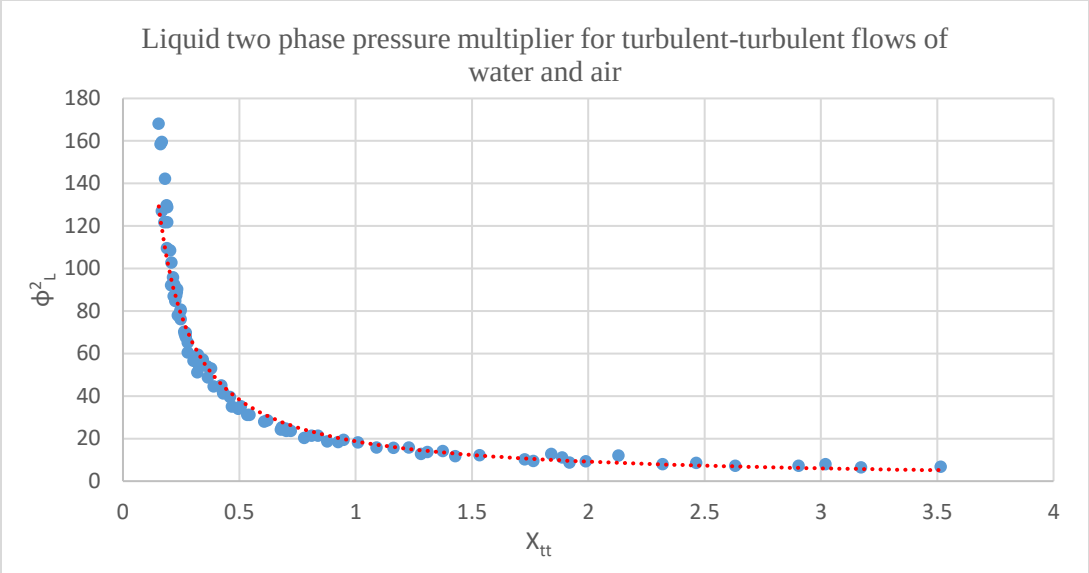


**Figure 77 Liquid two-phase pressure multiplier for turbulent-turbulent flows of water and air for all ranges of flow rates and Reynolds numbers of air and water**

# CHAPTER 5. CONCLUSION AND RECOMMENDATIONS

## 5.1 LNG Purification

The feasibility of designing a multi- stage distillation based $CO_2$ removal system for LNG is examined, where freeezeout of $CO_2$ and azeotropes are avoided. A comprehensive and complete separation by distillation three tower approach is developed and theoretically demonstrated. A self-sustaining, multi-tower pseudo-closed loop distillation system with solvent recovery which can be recycled back into the system has been addressed in the current research.

A methodology for the design of a multi-tower distillation system for the removal of carbon dioxide from natural gas was proposed and demonstrated by simulation. The removal of $CO_2$ from natural gas is imperative because of various reasons, and a comprehensive study to achieve an industrially acceptable grade of liquefied natural gas that contains less than 50 ppm of $CO_2$ is conducted. Natural gas used as feed in these simulations is pipeline natural gas. The natural gas that is being used as feed contains 85% methane and 3% carbon dioxide. A distillation system has been designed that can purify natural gas initially having 3% carbon dioxide (pipeline natural gas) to as low as 4.53 ppm of CO2, and therefore render natural gas suitable for industrial applications which require the carbon dioxide levels to be below 50 ppm. Natural gas with a purity of 99.99% methane purity is obtained in the distillate. The multi-tower distillation design is for medium-sized plants (37.85 $m^3/s$, equivalent to 10,000 gallon/day of LNG) that may not be viable using normal large scale $CO_2$ removal techniques that are commonly used in the industry. The type of distillation adopted in all stages of the multi-tower distillation system is equilibrium distillation. In this

technique it is assumed that all the components in the mixture existing in the liquid phase also exist in the vapor phase and equilibrium is achieved. The maximum relative difference in the concentration of the substances in the phases, thereby maximum separation occurs when the mixture constituents are in a state of physical equilibrium. Therefore, attainment of equilibrium conditions is desirable in the distillation process and most design techniques use equilibrium as one of the boundary conditions for quantitative calculations. Equilibrium is closely approximated by adjustment of temperature and pressure in the different stages of the distillation towers. There are two major technical challenges in the distillation-based removal of $CO_2$ from natural gas. Both of these issues have been addressed and a suitable solution has been proposed. The first problem is that the CO2 freezes out in the Demethanizer distillation column. This problem is due to the nature of the phase diagram of $CO_2$-$CH_4$ makes it impossible to get pure methane at a constant pressure without $CO_2$ freezeout so $C_{3+}$ hydrocarbons are added to the distillation column by incorporating a multicomponent feed thereby circumventing the freezeout problem. By-products of distillation find many uses in the distillation plant/industry for different applications. Separating these components requires additional distillation towers and units. The second major problem associated with distillation-based removal of CO2 from NG is that $CO_2$ and ethane, the second largest constituents of NG after methane, form an azeotrope in the bottom streams of *Demethanizer* distillation system. The second distillation or the Extractive Column is added to perform extractive distillation and break the azeotrope between $CO_2$ and $C_2H_6$ so the components can be further separated by using a solvent stream. A solvent stream consisting of heavier hydrocarbons is used in this *Extractive Column*, the azeotrope is broken and a high percentage of $CO_2$ is extracted in the distillate. The distillate of the *Extractive Column* contains 93.72% carbon dioxide and 2.12 % ethane. While extraction of side products has advantages by adding an additional distillation for

every additional side product to be obtained, in this particular work due to the nature of the azeotrope a different route is taken which satisfies the solvent production needs in the current fractionating system. A third column, referred to as the *Solvent Recovery Column*, denoted by *R*, that produces ethane as a distillate or light key component which is treated as an additional side product and heavier hydrocarbons like propane, butane and pentane are obtained as the bottoms product or heavy key component of distillation, that can be recycled back to the *Extractive column* to be used as the solvent stream to break the azeotrope. In addition, parametric studies on the effect of some common distillation operating conditions on the fractionating or separation process are performed in the *Extractive column.* The effect of pressure, reflux ratio, and feed stage location is studied and reported. The effect of reflux ratio on the freeze out phenomenon in the *Demethanizer Column* is also simulated. The highest composition of carbon dioxide in the distillate in the *Extractive Column* occurs at 20 bar, while the lowest composition of ethane occurs at 30 bar. An optimized pressure of 24 bar was thus selected to simulate the full three column distillation system. Separation due to reflux ratio variation for an ideal solvent in the *Extractive Column* peaks at a value of 2. Carbon dioxide mole fraction first increases with reflux ratio and then instead of the expected trend of flattening out at near the peak value, the mole fraction of CO2 then decreases with increasing reflux ratio. This peculiar behavior is typical of Extractive distillation processes as excessive reflux ratio effectively dilutes the solvent thus worsening the separation. The efficiency of the separation increases as the feed inlet stage location increases or feed stage is lowered along the column and reaches a maximum performance a little below the centre tray and then remains constant with a flat profile. The tendency of carbon dioxide to freezeout in the *Demethanizer Column* increases as reflux ratio increases. Pinch stages are observed well below the centre of the column.

### *5.1.1 Future Work and Recommendations*

The parametric study on the Extractive column can be extended to encompass the effect of solvent amount, the effect of inlet solvent stage, and boil-up ratio. Simulations can be carried out to determine how the solvent amount and solvent feed stage affects the distillation results. It is commonly seen that solvent acts like the reflux ratio effect demonstrated in the current research. There is an optimum amount at which the distillation efficiency reaches its peak value. In the case of the extractive column the solvent feed stage plays a very important role. If the solvent is not injected high enough breaking the azeotrope can be difficult. It will be interesting to study how low the solvent can be injected while still breaking the azeotrope. The effect of pressure and reflux ratio on the other two columns, the *Demethanizer column* and the *Solvent Recovery column* can also be examined.

The aforementioned results confirm that in theory a distillation based CO2 removal system for LNG is feasible. Evidently, however, further study is needed in order to examine the energetic and economic aspects of such a system, in particular for commercial plant scales. Comparisons between the classic scheme like amines used for separation and the low-temperature schemes like distillation should be examined to deduce which is more profitable on an energy basis. The energy efficiency of a low-temperature distillation process can also be compared to a classic process with regards to natural gas composition or the percentage of $CO_2$, $H_2S$ and $C_{2+}$ contents present in the natural gas, to determine if there is a bias based on the composition or gas source/reserve.

## 5.2 Double Helicoidally Coiled Tube and Heat Exchanger

The hydrodynamic characteristics of a double helicoidally coiled tube heat exchanger that is used in LNG transportation is investigated. An instrumented test loop is used for this purpose, which represents a prototypical fuel delivery system in large vehicles. The test loop comprises of a double-helically coiled tube heat exchanger that carries LNG placed in a shell-confined secondary side through which the engine coolant flows. The helicoidally coiled tube is made of 301 Stainless Steel and have horizontal axes. The cross-section of the tubes become slightly distorted and form an ellipsoid during coiling and extrusion, with the equivalent circular diameter of the ellipsoidal cross-section being 0.874 cm.

The double helicoidally heat exchanger was completely characterized for hydrodynamics properties The single-phase flow tests measure and correlate the friction factor in the helically coiled flow passage and experiments are performed to determine the friction factor. These experiments were performed with gas and liquid separately. The fluids used for tests are nitrogen and water. The range of Reynold number for which the single-phase flow experiments are performed is $Re_D$ = 2613 to 47811. Single-phase water tests were performed between Reynold numbers of 2613 to 19288 and single phase nitrogen gas tests were performed between Reynolds numbers of 11889 to 47811.

Single-phase flow experiments, besides being valuable and critically important in their own right, are essential for the development of empirical correlations for two-phase flow. Laminar, transition and turbulent profiles are captured and the complete range of the flow has been characterized. The friction factor has been compared to existing correlations. In the laminar flow regime it aligned with the published data. In the turbulent regime the values of friction factor determined by experiments and analysis in the current work is higher than published correlations. It must be noted that the published correlations show some disparity among each other as well. A new empirical correlation for the friction factor in the turbulent flow regimes of a double helicoidal pipe has been proposed as follows:

$$f_{turb} = 0.306\,\mathrm{Re}_D^{-0.2} \tag{88}$$

The higher friction factor is due to a higher pressure loss for the same Reynold number is attributed to the asymmetric or elliptical cross-section of the double helicoidal pipes. The major axis of the ellipse (pipe cross-section) is parallel to the axis of the helix (coil). The secondary vortices caused by unbalanced centrifugal forces have more contact surface area with the internal walls of the pipe as compared to an equivalent helix with a circular cross-section. Thus additional kinetic energy is lost as shear stress or pressure drop between the walls and the fluid. This results in a higher friction factor for the same Reynolds number.

Once single-phase flow behaviour of the test section was fully characterized, two-phase flows experiments were performed to measure and correlate the pressure drop due to friction in

the double helically coiled flow passage. These experiments were performed with immiscible gas and liquid phases simultaneously. The gas phase used for these tests is air, and the liquid phase used is water. The range of Reynolds number for the two-phase gas-liquid tests are the Reynolds number of water ranging from 1035 – 6652, and the Reynolds number of air ranging from 2530 – 17526. The concept of two-phase multipliers has been introduced and analyzed for the air-water two phase flow tests. The results are compared to existing publications. Modifications and a new correlation of the liquid two-phase multiplier has been proposed as follows

$$\Phi_L^2 = 18.75 X^{-1.032} \tag{89}$$

The two new correlations for friction factor of turbulent single phase flows and two phase pressure multipliers for turbulent-turbulent immiscible fluid that have been proposed in the current work are novel in many aspects. These correlations can be applied to double helicoidal heat exchangers in the LNG transport and delivery industry with near circular cross sections. During mass production of heat exchangers in industries, it is pertinent to prioritize the cost of production over the accuracy with which a circular cross-section of the helical pipe must be manufactured. The correlations proposed for the double helical coil have many practical and industrial applications. Furthermore, the data available in literature is not as extensive as it looks. Particularly two phase flow data for horizontal coils are very limited and they actually do not agree with our data. With respect to heat transfer the situation is worse and there is no data for non-boiling two phase flow at all. The proposed correlation strives to predict and accurately quantify the two-phase flows of non-miscible fluids in a double helically coiled pipe.

### *5.2.1 Future Work and Recommendations*

The hydrodynamic analysis of any flow is coupled to the heat transfer analysis. With a good understanding of the hydrodynamic characteristics of the double helically coiled heat exchangers used in LNG transport and delivery, the next steps in the current research can be extended to encompass heat transfer characterization of the same heat exchanger. The flow field that has been characterized in this work is tied to the pressure drop which in turn is coupled to the heat transfer. Thus this work provides a good basis for understanding and extending the current analysis to correlate the heat transfer coefficient variation of the double helically coiled heat exchanger with the flow variations.

Furthermore, an investigation of the geometric parameters of the double helically coiled heat exchanger used in LNG transport and delivery can be conducted. It would be interesting to study the effect of some parameters like total length of the heat exchanger, pitch, coil radius on the friction factor. The effect of the elliptical cross section of the helical pipe can be quantified by running experiments on test sections having different major axis to minor axes (a to b) ratios. The effect of having multiple parallel coils or helices can also be analyzed.

# APPENDIX A: SINGLE-PHASE FLOW HEAT TRASNSFER EXPERIMENTS

In heat transfer experiments the main objective is to measure the coil average heat transfer coefficient, even though the pressure drop and as a result the average friction factor are also measured. In these experiments first a steady flow of gas or liquid is established through the coil. The secondary side heater is then turned on and a constant flow rate of the secondary flow is also imposed. The system is then allowed to reach steady state. The measured parameters include the coiled tube flow rate and inlet and outlet temperatures and pressures, as well as the secondary side flow rate and inlet and outlet temperatures. The energy equation for the fluid in the coiled tube can be represented as [114]

$$\rho \frac{Dh}{Dt} + \rho \frac{D}{Dt}\left(\frac{1}{2} j^2\right) + gj\rho \sin\theta = \frac{q'' p_{heat}}{A} + \dot{q}_v + \frac{\partial P}{\partial t} \tag{90}$$

Expanding the material derivative and assuming that the system is steady, the helix axis is not tilted an angle and the rate of volumetric energy generation is 0 (91) – (94),

$$\frac{D}{Dt} = \frac{\partial}{\partial t} + j\frac{\partial}{\partial z} \tag{91}$$

$$\frac{\partial}{\partial t} = 0 \tag{92}$$

$$\theta = 0 \tag{93}$$

$$\dot{q}_v = 0 \tag{94}$$

We get

$$\cancel{\rho \frac{\partial h}{\partial t}} + \rho j \frac{\partial h}{\partial z} + \cancel{\rho \frac{\partial}{\partial t}\left(\frac{1}{2} j^2\right)} + \rho j \frac{\partial}{\partial z}\left(\frac{1}{2} j^2\right) + gj\rho \cancel{\sin\theta}$$

$$= \frac{q'' p_{heat}}{A} + \cancel{\dot{q}_v} + \cancel{\frac{\partial P}{\partial t}} \tag{95}$$

$$\rho j \frac{\partial h}{\partial z} + \frac{1}{2} \rho j \frac{\partial}{\partial z}\left(j^2\right) = \frac{q'' p_{heat}}{A} \tag{96}$$

Since, $G = \rho j$ (97)

$$G \frac{\partial h}{\partial z} + \frac{1}{2} G \frac{\partial}{\partial z}\left(\frac{G^2}{\rho^2}\right) = \frac{q'' p_{heat}}{A} \tag{98}$$

$$G \frac{\partial h}{\partial z} + \frac{1}{2} G^3 \frac{\partial}{\partial z}\left(\frac{1}{\rho^2}\right) = \frac{q'' p_{heat}}{A} \tag{99}$$

Since, $dh = C_p dT$ and $P = \rho R_{N_2} T$ (100)

$$GC_p \frac{\partial T}{\partial z} + \frac{1}{2} G^3 \frac{\partial}{\partial z}\left(\frac{R_{N_2}^2 T^2}{P^2}\right) = \frac{q'' p_{heat}}{A} \tag{101}$$

$$GC_p \frac{\partial T}{\partial z} + \frac{1}{2} G^3 R_{N_2}^2 \left\{ \frac{-2T^2}{P^3} \frac{dP}{dz} + \frac{2T}{P^2} \frac{dT}{dz} \right\} = \frac{q'' p_{heat}}{A} \tag{102}$$

$$GC_p \frac{\partial T}{\partial z} - \frac{G^3 R_{N_2}^2}{P^3} \frac{dP}{dz} T^2 + \frac{G^3 R_{N_2}^2}{P^2} T \frac{dT}{dz} = \frac{q'' p_{heat}}{A} \tag{103}$$

Since, $p_{heat} = \pi D_i$ (104)

And heat flux, $q'' = \dfrac{T_o - T}{\dfrac{1}{h_i} + \dfrac{r_i}{k_\omega} \ln \dfrac{r_o}{r_i} + \dfrac{r_i}{h_o r_o}}$ (105)

$$GC_p \frac{\partial T}{\partial z} - \frac{G^3 R_{N_2}^2}{P^3} \frac{dP}{dz} T^2 + \frac{G^3 R_{N_2}^2}{P^2} T \frac{dT}{dz}$$

$$= \frac{\pi D_i}{A} \frac{T_o - T}{\dfrac{1}{h_i} + \dfrac{r_i}{k_\omega} \ln \dfrac{r_o}{r_i} + \dfrac{r_i}{h_o r_o}} \tag{106}$$

$$\int_{T_{in}}^{T_{out}} \left( GC_p \frac{\partial T}{\partial z} - \frac{G^3 R_{N_2}^2}{P^3} \frac{dP}{dz} T^2 + \frac{G^3 R_{N_2}^2}{P^2} T \frac{dT}{dz} \right) \partial T$$

$$= \frac{\pi D_i}{A} \int_{z=0}^{z=L} \left( \frac{T_o - T}{\dfrac{1}{h_i} + \dfrac{r_i}{k_\omega} \ln \dfrac{r_o}{r_i} + \dfrac{r_i}{h_o r_o}} \right) \partial z \tag{107}$$

To calculate the heat transfer coefficient inside the coiled tube, $h_i$, evidently the heat transfer coefficient on the outside, $h_o$, is needed. Local measurement of $h_o$ is impractical, however. CFD simulation have shown that $h_o$ varies significantly along the coiled tube. Thus, in data analysis $h_o$ is found from detailed CFD simulation.

CFD simulation of the secondary side or shell side of the helically coiled heat exchanger is performed on Ansys Fluent and the CFD model is shown below in Figure 78. The primary and secondary flows are not coupled and the heat transfer analysis on the secondary side or shell side can be performed independently with the known boundary conditions on the secondary side to determine $h_o$.

Experiments were run for increasing Reynolds number of the primary flow or nitrogen. For each mass flow rate of nitrogen, three different secondary flow rates were tested. The range of Reynolds number of nitrogen tested is 11889 – 47811. From the hydrodynamic analysis of the single phase flow it can be concluded that the heat transfer tests were run in the turbulent flow regime for the helicoidal heat exchanger. For each fuel flow rate three different coolant flow rates at the same secondary inlet temperature were tested. The secondary side inlet temperature is fixed at 82 $^{o}$C (180 $^{o}$F).

Simulations are performed with two different turbulence models: k-ε and k-ω turbulence models and the results were comparable. Table 9 shows the tests matrix that were run and Table 10 shows the results of the CFD simulations.

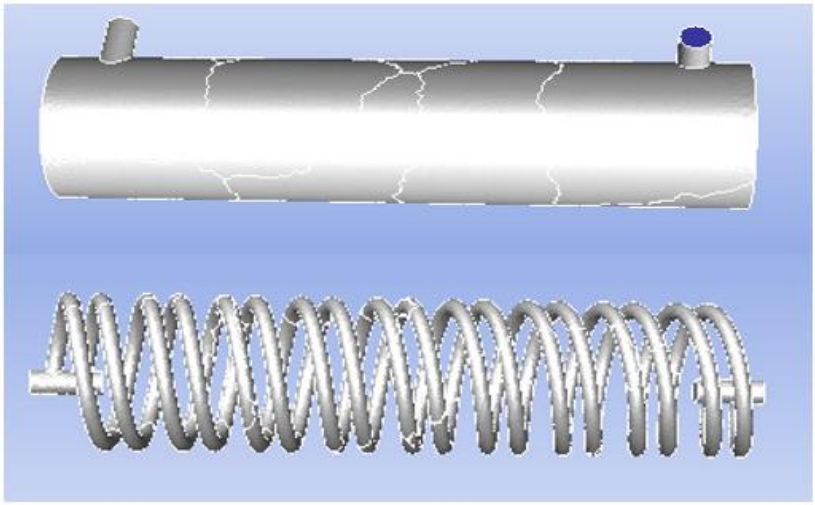

**Figure 78 Ansys Fluent model used for CFD simulation of the secondary side to calculate the outside heat transfer coefficient**

**Table 9 Test matrix for the single phase heat transfer experiments with the range of Reynolds numbers of nitrogen and the corresponding coolant (secondary fluid) flow rate**

| **Range of Reynolds numbers of nitrogen and corresponding coolant flow rates** | |
|---|---|
| Re in the primary side | Flow rates in the secondary side (gpm) |
| 11889 – 12037 | 3, 4 and 5 |
| 16476 – 17366 | 3, 4 and 5 |
| 25373 – 27485 | 3, 3, 4 and 5 |
| 3234 – 23690 | 3, 4 and 5 |
| 34932 – 35797 | 3, 4 and 5 |
| 41682 – 42582 | 3, 4 and 5 |
| 47337 - 47811 | 3, 4 and 5 |

**Table 10 CFD simulation results for the heat transfer coefficient on the secondary or coolant side of the helically coiled heat exchanger**

| $h_o$ values determined from CFD simulations of the secondary side | |
|---|---|
| k-ε turbulence model | |
| Coolant Flow rate (gpm) | $h_o$ (W/m$^2$-K) |
| 3 | 26.24 |
| 4 | 31.80 |
| 5 | 37.71 |
| k-ω turbulence model | |
| 3 | 30.43 |
| 4 | 36.28 |
| 5 | 40.03 |

Equation (107) that is derived for single phase heat transfer in helical coils has limits of integration on the RHS as z = 0 to L, where L is the total length of the primary side of the coiled heat exchanger. However, this is true if L is less than thermal equilibrium length. In the current case thermal equilibrium is achieved at some unknown length inside the heat exchanger. In order to proceed with the numerical integration and analysis, the length at which thermal equilibrium is achieved must be determined. A new design for the heat exchanger has been proposed and discussed.

**Future Work and Recommendations**

The heat transfer experiment results with single phase nitrogen gas showed that the length of the heat exchanger is an overkill. The primary side or fuel reaches thermal equilibrium with the secondary or coolant side before reaching the heat exchanger exit. A new shorter design is proposed. Reducing the length will save on space and material costs.

New experiments have been designed to determine the ideal length for both single phase and two phase flows. In the current test section the thermocouples are placed only at the inlet and exit of the primary and secondary side of the heat exchanger because it was assumed that thermal equilibrium is not achieved in the heat exchanger. Figure 79 shows the new test section with 14 thermocouples on the primary side. There are 12 thermocouples on the secondary side of the heat exchanger.

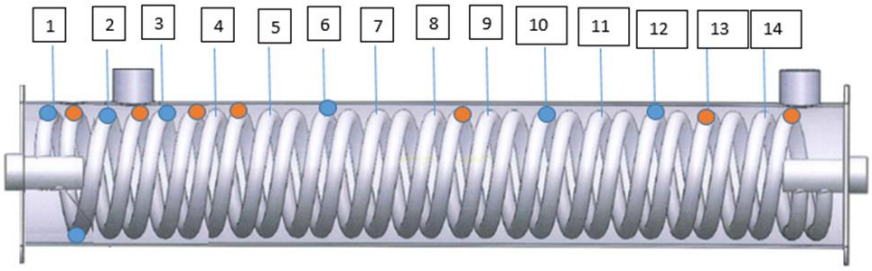


**Figure 79 Thermocouple placement on the primary and secondary side of the new proposed helecoidal heat exchanger test section. Blue dots represent thermocouples on Pipe 1 and orange dots represent Pipe 2 of the double helically coiled heat exchanger.**

The 12 total thermocouples placed on secondary side are one each at inlet, outlet, 1/6th, 1/3rd, ½ and 2/3rd of total length on both pipes. The thermocouples on the secondary side can be seen in Figure 80

**Figure 80 Placement of thermocouples on both the primary and secondary side**

This design will help determine the thermal equilibrium length L so the equation (107) can be numerically integrated correctly, from z = 0 to $L_{Eq}$. The outside heat transfer coefficient has already been calculated from CFD simulations and tabulated in Table 10. Thus the inside heat transfer coefficients can also be calculated. These will be compared to the heat transfer empirical correlations for fully developed flow turbulent flow through circular helically coiled tubes. Some of them are listed below

Schmidt [75]

$$\frac{Nu_{D,c}}{Nu_{D,s}} = 1.0 + 3.6\left[1 - \left(\frac{R_i}{R_{cl}}\right)\right]\left(\frac{R_i}{R_{cl}}\right)^{0.8} \tag{108}$$

Where, $2\times10^4 < \mathrm{Re}_D < 1.5\times10^5$

$5 < R_{cl}/R_i < 84$

$\mathrm{Pr} \geq 0.7$

Pratt [149]

$$\frac{Nu_{D,c}}{Nu_{D,s}} = 1.0 + 3.4\left(\frac{R_i}{R_{cl}}\right) \tag{109}$$

Where, $2\times10^4 < \mathrm{Re}_D < 1.5\times10^5$

Orlov and Tselishchev [150]

$$\frac{Nu_{D,c}}{Nu_{D,s}} = \left[1 + 3.54\left(\frac{R_i}{R_{cl}}\right)\right]\left(\frac{\mathrm{Pr}_m}{\mathrm{Pr}_s}\right)^{0.25} \tag{110}$$

Where, $R_{cl}/R_i > 6$

# APPENDIX B: FLOW BOILING EXPERIMENTAL

These experiments are carried out using liquid nitrogen (LN2) as the fluid flowing inside the coiled tube. These experiments intrinsically involve both hydrodynamics and heat transfer. In all tests LN2 at inlet to the test section is either in a slightly subcooled liquid state, a saturated liquid, or a saturated liquid-vapor mixture with very low vapor quality. LN2 undergoes boiling inside the coiled tube and emerges from the test section as a superheated vapor. As a result, all boiling heat transfer regimes, as well as all the corresponding two-phase flow regimes, occur in a typical test.

The analysis of these data requires the numerical integration of the two-phase momentum and energy conservation equations. These equations can be cast as [114]

$$G^2 \frac{\partial}{\partial z}\left[\frac{(1-x)^2}{\rho_L(1-\alpha)}+\frac{x^2}{\rho_G \alpha}\right] = -\frac{\partial P}{\partial z} - \bar{\rho} g \sin\theta - \left(-\frac{\partial P}{\partial z}\right)_{fr} \tag{111}$$

$$G\frac{\partial h}{\partial z} + G^3 \frac{\partial}{\partial z}\left(\frac{1}{2}\left[\frac{(1-x)^3}{\rho_L^2(1-\alpha)^2}+\frac{x^3}{\rho_G^2\alpha^2}\right]\right) + g\sin\theta G = \frac{4}{D} q''_w \tag{112}$$

Where, $x$ and α are the local quality and void fraction, respectively, and $h = h_f + x h_{fg}$

Some results of experiments have been shown in the Appendix. However complete analysis has not been possible due to time constraints. To apply these equations to the experimental data, evidently models/correlations are needed for two-phase flow friction factor, the void fraction, and

heat transfer coefficient. The experimental data will thus be analyzed by solving these equations and applying the best available flow boiling maps and two-phase pressure drop multiplier correlations, as well as utilizing the most appropriate void-quality correlations [114]. For the numerical integration of these equations the available commercial software, in particular SINDA [151] and Thermal Desktop [152] will be used, and wherever possible and appropriate modifications will be made to their constitutive and closure relations (i.e., empirical correlations) to bring about agreement between the experimental data and model predictions.

**Boiling data: Heat exchanger with insulation**

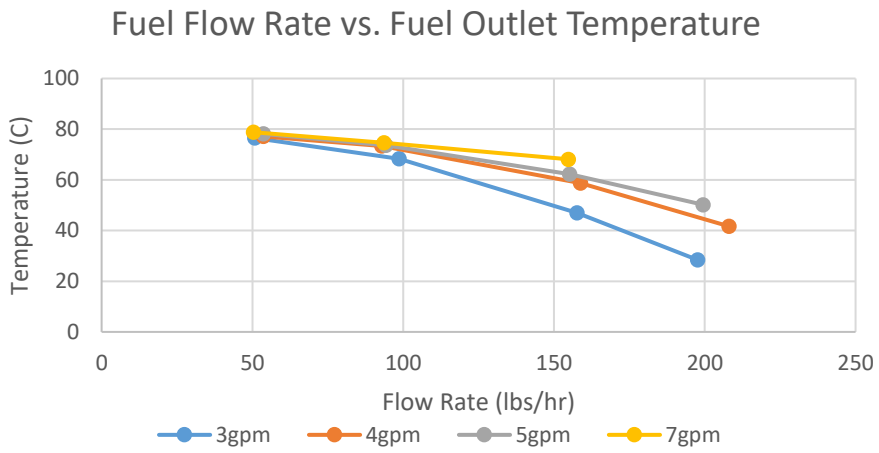


**Figure 81 Boiling experiments of liquid nitrogen with insulation showing the fuel outlet temperature variation with fuel mass flow rate for different coolant flow rates**

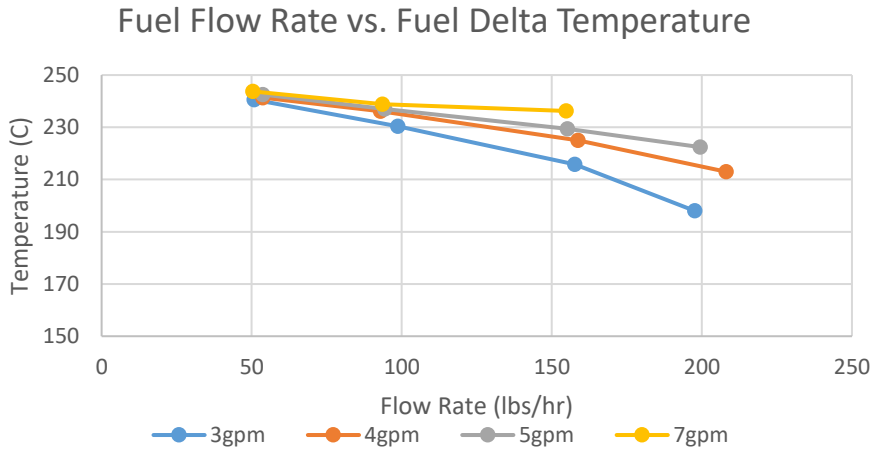


**Figure 82 Boiling experiments of liquid nitrogen with insulation showing the fuel delta temperature variation with fuel mass flow rate for different coolant flow rates**

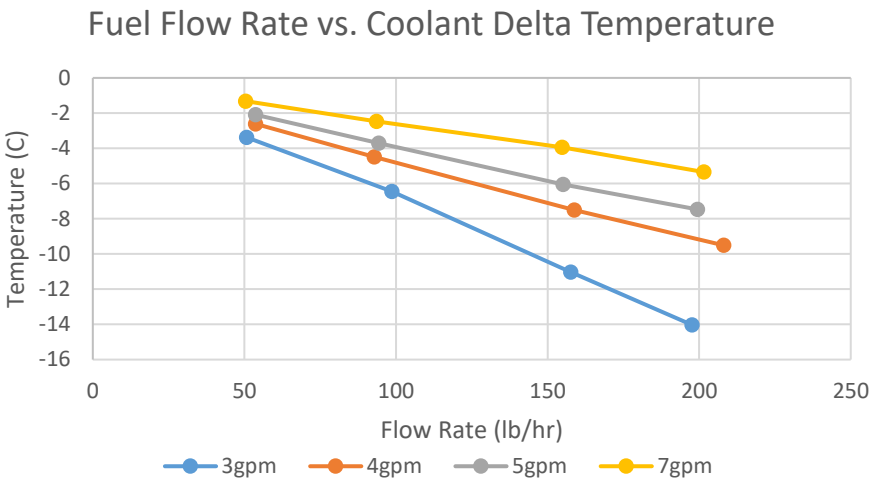


**Figure 83 Boiling experiments of liquid nitrogen with insulation showing the coolant delta temperature variation with fuel mass flow rate for different coolant flow rates**

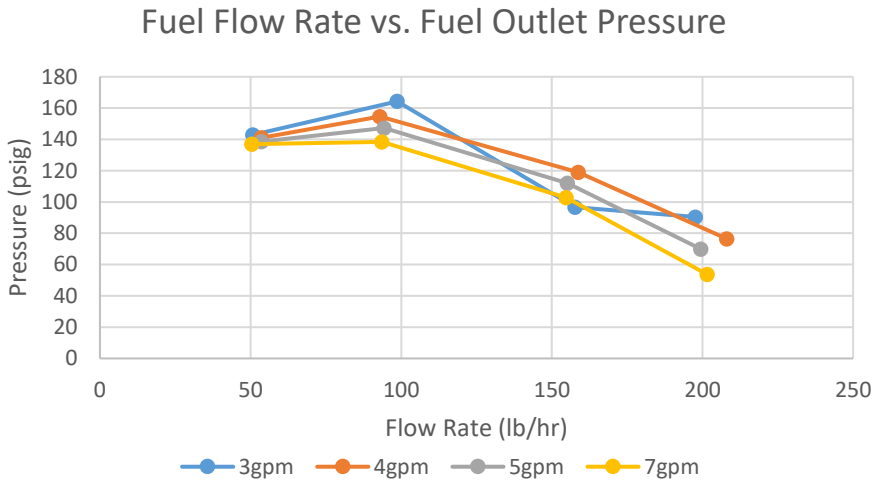


**Figure 84 Boiling experiments of liquid nitrogen with insulation showing the fuel outlet pressure variation with fuel mass flow rate for different coolant flow rates**

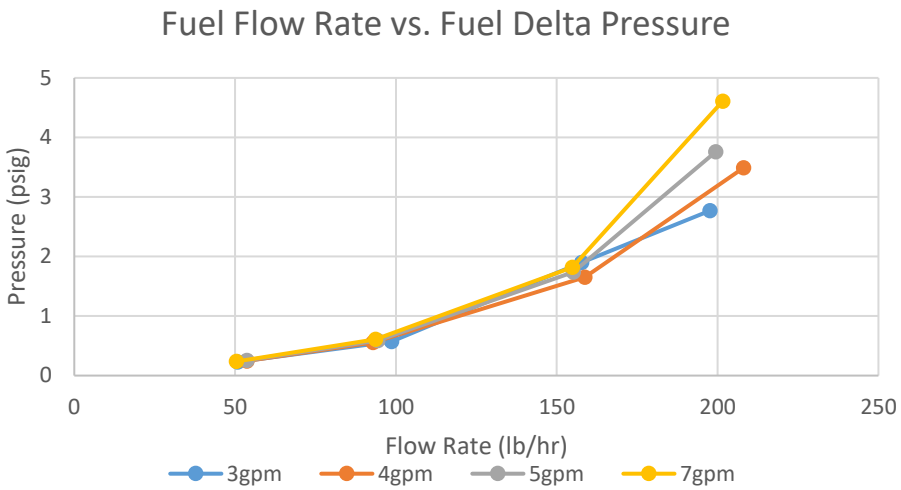


**Figure 85 Boiling experiments of liquid nitrogen with insulation showing the fuel delta pressure variation with fuel mass flow rate for different coolant flow rates**

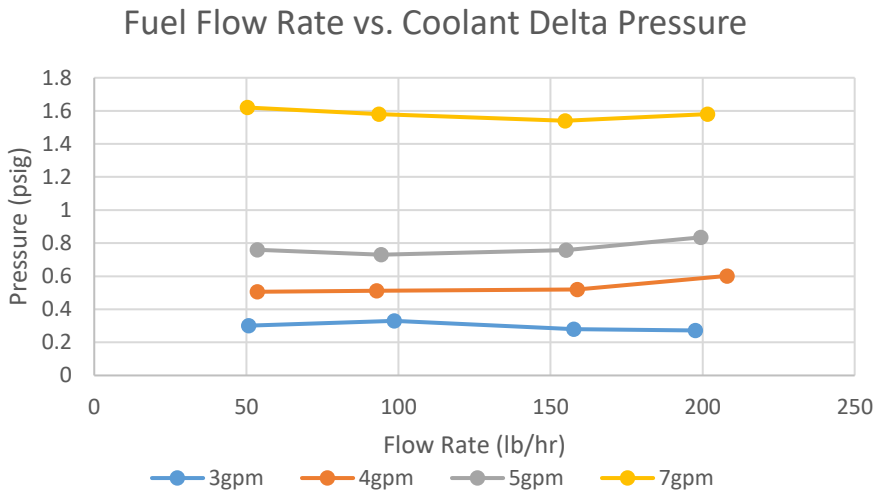


**Figure 86 Boiling experiments of liquid nitrogen with insulation showing the coolant delta pressure variation with fuel mass flow rate for different coolant flow rates**

**Boiling data: Heat exchanger with insulation**

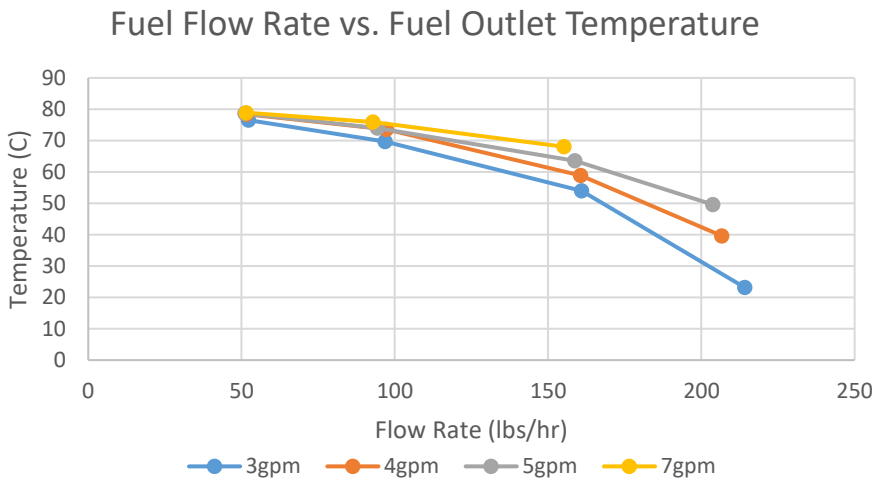


**Figure 87 Boiling experiments of liquid nitrogen with insulation showing the fuel outlet temperature variation with fuel mass flow rate for different coolant flow rates**

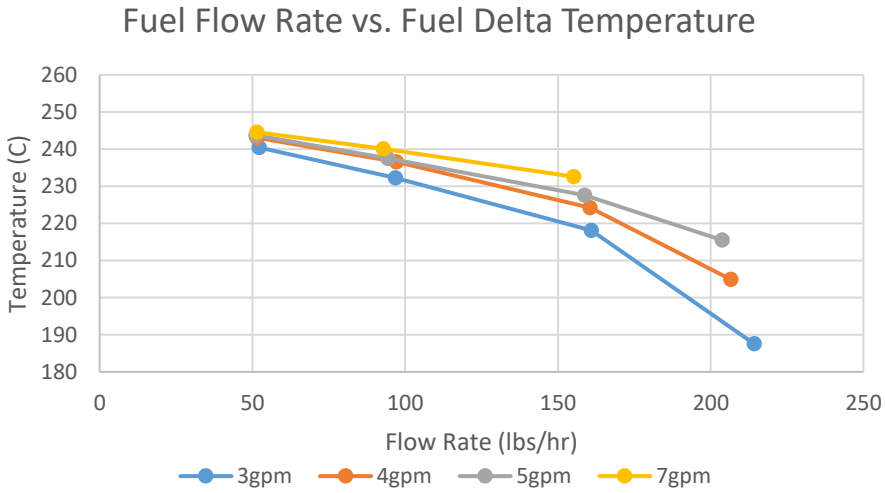


**Figure 88 Boiling experiments of liquid nitrogen without insulation showing the fuel delta temperature variation with fuel mass flow rate for different coolant flow rates**

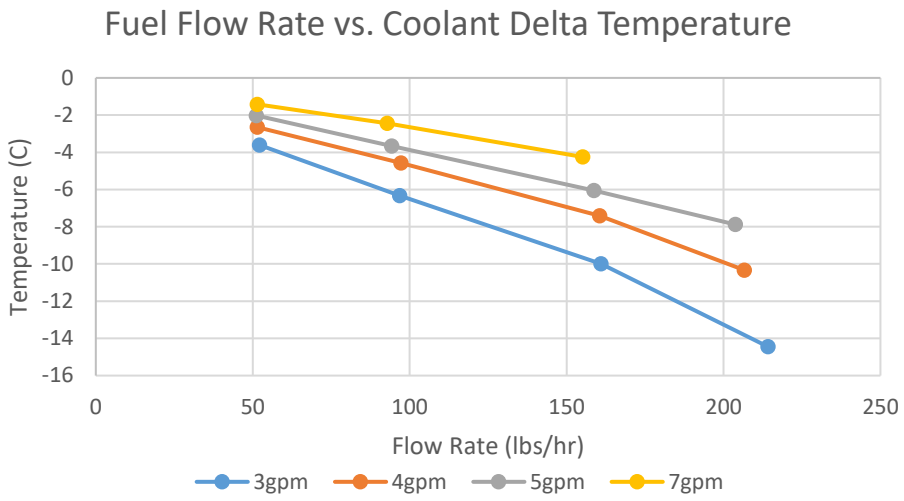


**Figure 89 Boiling experiments of liquid nitrogen without insulation showing the coolant delta temperature variation with fuel mass flow rate for different coolant flow rates**

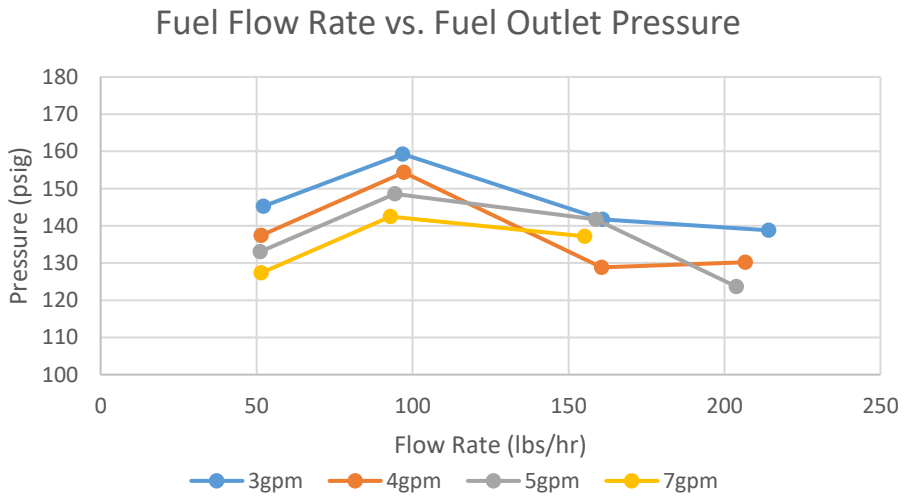


**Figure 90 Boiling experiments of liquid nitrogen without insulation showing the fuel outlet pressure variation with fuel mass flow rate for different coolant flow rates**

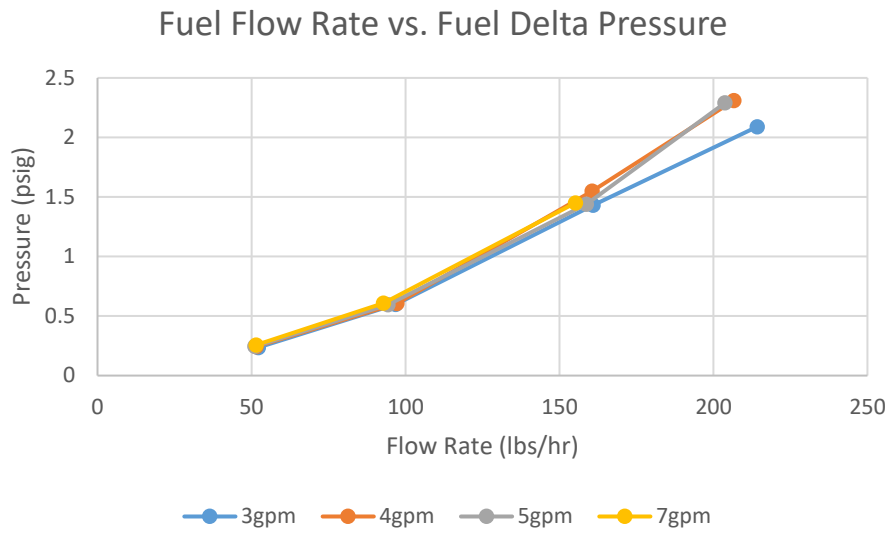


**Figure 91 Boiling experiments of liquid nitrogen without insulation showing the fuel delta pressure variation with fuel mass flow rate for different coolant flow rates**

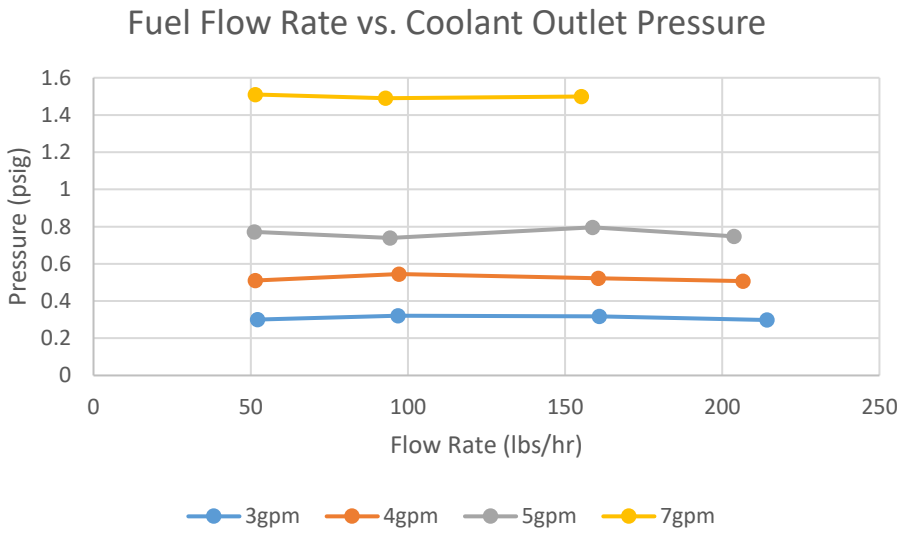


**Figure 92 Boiling experiments of liquid nitrogen without insulation showing the coolant outlet pressure variation with fuel mass flow rate for different coolant flow rates**

# APPENDIX C: DEMTHANIZER COLUMN COMPOSITION

| Stage | METHA-01 | CARBO-01 | ETHAN-01 | PROPA-01 |
|---|---|---|---|---|
| 1 | 0.999987583 | 1.24168943E-05 | 4.5654915E-11 | 1.54898527E-20 |
| 2 | 0.99997009 | 2.99094355E-05 | 2.05335762E-10 | 2.00584543E-19 |
| 3 | 0.999941999 | 5.80004674E-05 | 6.84120989E-10 | 1.79853494E-18 |
| 4 | 0.999896885 | 0.000103112619 | 2.1197099E-09 | 1.55943653E-17 |
| 5 | 0.999824431 | 0.000175562406 | 6.42420398E-09 | 1.34706767E-16 |
| 6 | 0.999708057 | 0.000291924033 | 1.93310155E-08 | 1.16321109E-15 |
| 7 | 0.999521109 | 0.000478832525 | 5.80321521E-08 | 1.00453904E-14 |
| 8 | 0.999220716 | 0.00077910999 | 1.74081131E-07 | 8.67702172E-14 |
| 9 | 0.998737825 | 0.00126165255 | 5.22080395E-07 | 7.49775822E-13 |
| 10 | 0.997961 | 0.00203743451 | 1.56571216E-06 | 6.48254363E-12 |
| 11 | 0.996709792 | 0.00328551189 | 4.69584486E-06 | 5.61001231E-11 |
| 12 | 0.994690091 | 0.00529582219 | 1.40859232E-05 | 4.86237901E-10 |
| 13 | 0.991417972 | 0.00853976068 | 4.22635791E-05 | 4.22484029E-09 |

| | | | | |
|---|---|---|---|---|
| 14 | 0.986083038 | 0.0137900631 | 0.000126861843 | 3.68589643E-08 |
| 15 | 0.977288708 | 0.022329879 | 0.00038108592 | 3.23796975E-07 |
| 16 | 0.962524477 | 0.0363265086 | 0.00114606845 | 2.87799288E-06 |
| 17 | 0.936937162 | 0.0595802508 | 0.0034548598 | 2.61399375E-05 |
| 18 | 0.890265774 | 0.0989964167 | 0.0104482653 | 0.000247172167 |
| 19 | 0.797057902 | 0.16732765 | 0.0315716806 | 0.00252476222 |
| 20 | 0.490758932 | 0.274002182 | 0.0884545155 | 0.028797313 |
| 21 | 0.195673647 | 0.51037512 | 0.148603432 | 0.0304705982 |
| 22 | 0.0639383123 | 0.635127908 | 0.17575906 | 0.0278108443 |
| 23 | 0.0213895909 | 0.679189574 | 0.186283798 | 0.0259924228 |
| 24 | 0.00730479344 | 0.691641304 | 0.192340991 | 0.0254019298 |
| 25 | 0.00252567523 | 0.691706656 | 0.198203274 | 0.0256053066 |
| 26 | 0.000882522303 | 0.684279944 | 0.206062841 | 0.0270757669 |
| 27 | 0.000312277333 | 0.665996864 | 0.218134764 | 0.032115693 |
| 28 | 0.00011169043 | 0.617070439 | 0.237241592 | 0.0482523109 |
| 29 | 3.71691702E-05 | 0.461138336 | 0.250690833 | 0.0930392625 |
| 30 | 8.44003369E-06 | 0.180514743 | 0.164469718 | 0.120595761 |

**Demthanizer column composition (contd)**

| Stage | N-BUT-01 | ISOBU-01 | N-PEN-01 | 2-MET-01 |
|---|---|---|---|---|
| 1 | 3.64318795E-30 | 2.38076744E-27 | 5.41462841E-39 | 6.508660E-39 |
| 2 | 1.4798571E-28 | 6.67206888E-26 | 6.22399392E-37 | 7.231110E-37 |
| 3 | 4.05691905E-27 | 1.26884247E-24 | 4.79057974E-35 | 5.380220E-35 |
| 4 | 1.09921082E-25 | 2.37304401E-23 | 3.67186141E-33 | 3.985731E-33 |
| 5 | 2.97728332E-24 | 4.43462135E-22 | 2.81464716E-31 | 2.952901E-31 |
| 6 | 8.06530626E-23 | 8.28797464E-21 | 2.15806389E-29 | 2.18818E-29 |
| 7 | 2.18540198E-21 | 1.5493103E-19 | 1.65527475E-27 | 1.622083E-27 |
| 8 | 5.92404346E-20 | 2.89725828E-18 | 1.270402E-25 | 1.20311547E-25 |
| 9 | 1.60689692E-18 | 5.42115104E-17 | 9.75974193E-24 | 8.931713E-24 |
| 10 | 4.36328542E-17 | 1.01532957E-15 | 7.50968492E-22 | 6.640430E-22 |
| 11 | 1.18677709E-15 | 1.90450118E-14 | 5.79303106E-20 | 4.948505E-20 |
| 12 | 3.23683989E-14 | 3.58125557E-13 | 4.48734211E-18 | 3.701812E-18 |
| 13 | 8.86774013E-13 | 6.7614439E-12 | 3.4994024E-16 | 2.786461E-16 |
| 14 | 2.44733365E-11 | 1.28505977E-10 | 2.75930696E-14 | 2.118971E-14 |
| 15 | 6.83838905E-10 | 2.46984306E-09 | 2.21664302E-12 | 1.639336E-12 |

| | | | | |
|---|---|---|---|---|
| 16 | 1.95160651E-08 | 4.83861219E-08 | 1.83832627E-10 | 1.306073E-10 |
| 17 | 5.78990291E-07 | 9.81833754E-07 | 1.61596655E-08 | 1.097962E-08 |
| 18 | 1.84753178E-05 | 2.12895247E-05 | 1.58571807E-06 | 1.021090E-06 |
| 19 | 0.000680933998 | 0.0005269662 | 0.0001941035 | 0.0001160018 |
| 20 | 0.035348373 | 0.0178170926 | 0.0431925145 | 0.0216290771 |
| 21 | 0.0348412828 | 0.0176872868 | 0.0414945661 | 0.020854066 |
| 22 | 0.0299149318 | 0.015286454 | 0.0346672211 | 0.0174952689 |
| 23 | 0.0269818507 | 0.013839732 | 0.030760031 | 0.0155630006 |
| 24 | 0.0258724605 | 0.013289687 | 0.0293065439 | 0.014842291 |
| 25 | 0.0254765749 | 0.0130962206 | 0.028798157 | 0.0145881353 |
| 26 | 0.0254288037 | 0.0131064569 | 0.0286502928 | 0.0145133726 |
| 27 | 0.0262230423 | 0.0136932042 | 0.0288766192 | 0.0146475356 |
| 28 | 0.0321567071 | 0.0175010238 | 0.0314831064 | 0.0161831302 |
| 29 | 0.0688749619 | 0.038101024 | 0.0574709491 | 0.0306474648 |
| 30 | 0.158956662 | 0.079478331 | 0.197317564 | 0.0986587818 |

**Extractive Column composition**

| Stage | METHA-01 | CARBO-01 | ETHAN-01 | PROPA-01 |
|---|---|---|---|---|
| 1 | 4.39625032E-05 | 0.940082825 | 0.0145387575 | 0.0326898288 |
| 2 | 7.42570406E-06 | 0.782718915 | 0.0109040816 | 0.0779215634 |
| 3 | 1.7986894E-06 | 0.201707151 | 0.00564074465 | 0.0874089076 |
| 4 | 1.89099075E-06 | 0.199616663 | 0.00745032944 | 0.0876582594 |
| 5 | 1.91509479E-06 | 0.196878308 | 0.00982958614 | 0.0879865049 |
| 6 | 1.91555668E-06 | 0.193343666 | 0.012915657 | 0.0884126073 |
| 7 | 1.90630815E-06 | 0.188867356 | 0.0168486054 | 0.0889556992 |
| 8 | 1.89143143E-06 | 0.183333612 | 0.0217495882 | 0.0896318571 |
| 9 | 1.87192467E-06 | 0.17669287 | 0.0276887093 | 0.0904494762 |
| 10 | 1.84798198E-06 | 0.169001028 | 0.0346471821 | 0.0914040526 |
| 11 | 1.81983758E-06 | 0.160446898 | 0.0424855761 | 0.0924741529 |
| 12 | 1.78811412E-06 | 0.151350651 | 0.0509349087 | 0.0936208542 |
| 13 | 1.75392547E-06 | 0.142123754 | 0.0596237325 | 0.094792137 |
| 14 | 1.71878547E-06 | 0.133198198 | 0.0681396666 | 0.0959315289 |

| | | | | |
|---|---|---|---|---|
| 15 | 1.68436539E-06 | 0.124949377 | 0.0761055081 | 0.0969879572 |
| 16 | 1.65219316E-06 | 0.117640219 | 0.0832418504 | 0.0979230042 |
| 17 | 1.62341046E-06 | 0.111401784 | 0.0893967195 | 0.098713096 |
| 18 | 1.59866582E-06 | 0.106247731 | 0.0945407638 | 0.0993463823 |
| 19 | 1.57815064E-06 | 0.102108637 | 0.0987408318 | 0.0998155148 |
| 20 | 1.56173353E-06 | 0.0988712618 | 0.102128884 | 0.100107576 |
| 21 | 1.54914152E-06 | 0.0964139209 | 0.104880104 | 0.100191888 |
| 22 | 1.54017359E-06 | 0.0946375709 | 0.107211275 | 0.10000822 |
| 23 | 1.53503475E-06 | 0.0935042376 | 0.109418871 | 0.0994733049 |
| 24 | 1.53530658E-06 | 0.0931341962 | 0.112035876 | 0.0986138834 |
| 25 | 1.54887686E-06 | 0.094261023 | 0.116575813 | 0.0985165139 |
| 26 | 1.14961416E-06 | 0.0975541734 | 0.12901188 | 0.106662934 |
| 27 | 5.68552528E-07 | 0.0907591924 | 0.135738651 | 0.107457764 |
| 28 | 2.76880094E-07 | 0.0822450455 | 0.144235144 | 0.10845424 |
| 29 | 1.32286809E-07 | 0.0721988665 | 0.15435405 | 0.109631017 |
| 30 | 6.18129812E-08 | 0.0611409669 | 0.165601896 | 0.110927675 |
| 31 | 2.81943467E-08 | 0.0498519025 | 0.177194452 | 0.112252956 |

| | | | | |
|---|---|---|---|---|
| 32 | 1.25518782E-08 | 0.0391694492 | 0.188257075 | 0.113508405 |
| 33 | 5.46310511E-09 | 0.0297569548 | 0.19807259 | 0.114615675 |
| 34 | 2.33156433E-09 | 0.0219672051 | 0.206239714 | 0.11553284 |
| 35 | 9.7924774E-10 | 0.0158461682 | 0.212682635 | 0.11625424 |
| 36 | 4.06186253E-10 | 0.0112286016 | 0.217556092 | 0.116799459 |
| 37 | 1.66920135E-10 | 0.00785091921 | 0.221126015 | 0.117200314 |
| 38 | 6.81313999E-11 | 0.00543533008 | 0.223677647 | 0.117491586 |
| 39 | 2.7674799E-11 | 0.00373546352 | 0.225463308 | 0.117707161 |
| 40 | 1.12030213E-11 | 0.00255274729 | 0.226679499 | 0.117881624 |
| 41 | 4.52401403E-12 | 0.00173626453 | 0.227457008 | 0.118058304 |
| 42 | 1.82351592E-12 | 0.00117555899 | 0.227847043 | 0.118308102 |
| 43 | 7.33795908E-13 | 0.00079175156 | 0.227781994 | 0.118769812 |
| 44 | 2.94677285E-13 | 0.000529404936 | 0.226972452 | 0.119732317 |
| 45 | 1.17908476E-13 | 0.00034994112 | 0.224659822 | 0.121782157 |
| 46 | 4.68113627E-14 | 0.00022666648 | 0.219064045 | 0.125967233 |
| 47 | 1.82496092E-14 | 0.000141222975 | 0.206324298 | 0.13346775 |
| 48 | 6.81788998E-15 | 8.13772288E-05 | 0.179426453 | 0.142659776 |

| | | | | |
|---|---|---|---|---|
| 49 | 2.32109049E-15 | 4.02074817E-05 | 0.131538592 | 0.14093896 |
| 50 | 6.58706761E-16 | 1.5145098E-05 | 0.0707792928 | 0.107730186 |

**Extractive Column composition (contd)**

| Stage | N-BUT-01 | ISOBU-01 | N-PEN-01 | 2-MET-01 |
|---|---|---|---|---|
| 1 | 0.0046994659 | 0.00385225529 | 0.00176153669 | 0.00233136781 |
| 2 | 0.0322699811 | 0.0213303266 | 0.0370786397 | 0.0377690668 |
| 3 | 0.097539013 | 0.0528119655 | 0.30526526 | 0.249625159 |
| 4 | 0.0975908786 | 0.0528518898 | 0.305220218 | 0.249609871 |
| 5 | 0.097657948 | 0.0529038495 | 0.30515603 | 0.249585858 |
| 6 | 0.0977430193 | 0.052970315 | 0.305064585 | 0.249548235 |
| 7 | 0.0978482358 | 0.0530534433 | 0.304934901 | 0.249489853 |
| 8 | 0.0979742852 | 0.053154498 | 0.304753187 | 0.249401081 |
| 9 | 0.0981195189 | 0.0532731476 | 0.304504038 | 0.249270368 |
| 10 | 0.0982793633 | 0.0534068752 | 0.304173447 | 0.249086204 |
| 11 | 0.0984464807 | 0.0535508265 | 0.303753625 | 0.248840621 |
| 12 | 0.0986119182 | 0.0536983471 | 0.303248231 | 0.248533302 |

| | | | | |
|---|---|---|---|---|
| 13 | 0.098766959 | 0.0538421522 | 0.302675257 | 0.248174254 |
| 14 | 0.0989049026 | 0.0539757084 | 0.302065191 | 0.247783086 |
| 15 | 0.099022013 | 0.0540942752 | 0.301454516 | 0.247384669 |
| 16 | 0.0991173888 | 0.0541952704 | 0.300877436 | 0.24700318 |
| 17 | 0.0991920632 | 0.0542779714 | 0.300359492 | 0.246657251 |
| 18 | 0.0992478096 | 0.0543427788 | 0.299915108 | 0.246357828 |
| 19 | 0.0992859044 | 0.0543902329 | 0.299548712 | 0.246108589 |
| 20 | 0.099305659 | 0.0544197345 | 0.299257714 | 0.245907609 |
| 21 | 0.0993019329 | 0.0544275466 | 0.299034939 | 0.245748119 |
| 22 | 0.0992606988 | 0.0544036501 | 0.298865018 | 0.245612027 |
| 23 | 0.09916276 | 0.054333499 | 0.298685973 | 0.245419819 |
| 24 | 0.0991405615 | 0.0542783174 | 0.298125157 | 0.244670473 |
| 25 | 0.10128813 | 0.0552129704 | 0.294638709 | 0.239505292 |
| 26 | 0.123093738 | 0.06461147 | 0.275380257 | 0.203684399 |
| 27 | 0.123153559 | 0.064691548 | 0.274846176 | 0.203352541 |
| 28 | 0.123218185 | 0.0647869756 | 0.274145794 | 0.20291434 |
| 29 | 0.123280215 | 0.0648928337 | 0.273276433 | 0.202366452 |

| | | | | |
|---|---|---|---|---|
| 30 | 0.123331758 | 0.0650014412 | 0.272269052 | 0.201727149 |
| 31 | 0.12336766 | 0.0651044269 | 0.271190259 | 0.201038317 |
| 32 | 0.123387409 | 0.0651951719 | 0.270126689 | 0.200355789 |
| 33 | 0.123394376 | 0.0652702103 | 0.269158273 | 0.199731915 |
| 34 | 0.123393397 | 0.0653291341 | 0.268336626 | 0.199201082 |
| 35 | 0.123388698 | 0.0653735908 | 0.267679189 | 0.198775478 |
| 36 | 0.123383075 | 0.0654061716 | 0.267176803 | 0.198449798 |
| 37 | 0.123378032 | 0.0654296259 | 0.266805928 | 0.198209166 |
| 38 | 0.123374301 | 0.0654464857 | 0.266538828 | 0.198035822 |
| 39 | 0.123372407 | 0.0654590375 | 0.266349536 | 0.197913086 |
| 40 | 0.123373301 | 0.065469616 | 0.266216209 | 0.197827004 |
| 41 | 0.123379357 | 0.0654813777 | 0.266121153 | 0.197766535 |
| 42 | 0.123396608 | 0.0655001512 | 0.266049483 | 0.197723053 |
| 43 | 0.123440527 | 0.0655391771 | 0.265986895 | 0.197689844 |
| 44 | 0.123552615 | 0.0656322402 | 0.265917554 | 0.197663417 |
| 45 | 0.123851916 | 0.0658721222 | 0.26582889 | 0.197655152 |
| 46 | 0.124700063 | 0.066521902 | 0.265763987 | 0.197756104 |

| | | | | |
|---|---|---|---|---|
| 47 | 0.127173263 | 0.0682778566 | 0.266149773 | 0.198465836 |
| 48 | 0.133726991 | 0.0723957263 | 0.269557857 | 0.202151819 |
| 49 | 0.145086833 | 0.0780733017 | 0.287392219 | 0.216929887 |
| 50 | 0.146399296 | 0.0753975753 | 0.345765477 | 0.253913027 |

**Solvent Recovery Column composition**

| Stage | METHA-01 | CARBO-01 | ETHAN-01 | PROPA-01 |
|---|---|---|---|---|
| 1 | 9.95510286E-15 | 0.00022888942 | 0.999614996 | 0.000156111843 |
| 2 | 2.58704473E-15 | 0.000108221721 | 0.999462185 | 0.000429575034 |
| 3 | 9.45468526E-16 | 5.92942948E-05 | 0.998866614 | 0.00107399181 |
| 4 | 5.79494427E-16 | 3.94412016E-05 | 0.997369789 | 0.00259021936 |
| 5 | 4.97169018E-16 | 3.1347562E-05 | 0.993820836 | 0.00614478778 |
| 6 | 4.76864198E-16 | 2.79588351E-05 | 0.985548054 | 0.014407375 |
| 7 | 4.6782329E-16 | 2.63385975E-05 | 0.966645739 | 0.0332376261 |
| 8 | 4.56074651E-16 | 2.51459213E-05 | 0.925237608 | 0.0742586149 |
| 9 | 4.3476496E-16 | 2.36121362E-05 | 0.842337411 | 0.155245224 |
| 10 | 4.00923841E-16 | 2.1298259E-05 | 0.702635291 | 0.28665924 |

| | | | | |
|---|---|---|---|---|
| 11 | 3.59757993E-16 | 1.83308753E-05 | 0.522095699 | 0.4379143 |
| 12 | 3.19450563E-16 | 1.5269887E-05 | 0.348487282 | 0.530341369 |
| 13 | 2.79974593E-16 | 1.23870415E-05 | 0.215276248 | 0.49169602 |
| 14 | 2.42769476E-16 | 9.82972228E-06 | 0.128240295 | 0.33032293 |
| 15 | 2.20514917E-16 | 8.12165855E-06 | 0.0823193016 | 0.163389584 |
| 16 | 9.21309731E-17 | 5.00031307E-06 | 0.0823207154 | 0.163392052 |
| 17 | 3.84917964E-17 | 3.07852809E-06 | 0.0823207573 | 0.163394594 |
| 18 | 1.60815061E-17 | 1.89532517E-06 | 0.0823196005 | 0.163397639 |
| 19 | 6.7186456E-18 | 1.1668613E-06 | 0.0823171945 | 0.163401654 |
| 20 | 2.80693761E-18 | 7.18370921E-07 | 0.082313245 | 0.163407169 |
| 21 | 1.17268003E-18 | 4.42253268E-07 | 0.0823073189 | 0.163414961 |
| 22 | 4.8991437E-19 | 2.72259565E-07 | 0.082298582 | 0.163425978 |
| 23 | 2.04669309E-19 | 1.67602798E-07 | 0.0822859261 | 0.163441611 |
| 24 | 8.55015541E-20 | 1.031715E-07 | 0.0822677244 | 0.163463786 |
| 25 | 3.57173733E-20 | 6.35053839E-08 | 0.0822416706 | 0.163495219 |
| 26 | 1.49197897E-20 | 3.9086088E-08 | 0.0822044968 | 0.163539738 |
| 27 | 6.23181283E-21 | 2.40535185E-08 | 0.0821516092 | 0.163602755 |

| | | | | |
|---|---|---|---|---|
| 28 | 2.60268449E-21 | 1.47998369E-08 | 0.0820765269 | 0.163691905 |
| 29 | 1.08684004E-21 | 9.10384747E-09 | 0.0819701479 | 0.163817953 |
| 30 | 4.5375417E-22 | 5.59805679E-09 | 0.0818196948 | 0.163996037 |
| 31 | 1.89386842E-22 | 3.44056642E-09 | 0.0816073096 | 0.164247363 |
| 32 | 7.90135674E-23 | 2.11306637E-09 | 0.0813081663 | 0.164601493 |
| 33 | 3.29461207E-23 | 1.29646659E-09 | 0.0808880108 | 0.165099314 |
| 34 | 1.37264366E-23 | 7.9432835E-10 | 0.0803001263 | 0.165796777 |
| 35 | 5.71248235E-24 | 4.85723288E-10 | 0.0794818247 | 0.166769255 |
| 36 | 2.37366138E-24 | 2.96210527E-10 | 0.0783509333 | 0.168115984 |
| 37 | 9.84214272E-25 | 1.79968178E-10 | 0.0768032866 | 0.169963205 |
| 38 | 4.06921641E-25 | 1.0879241E-10 | 0.074713211 | 0.172463265 |
| 39 | 1.67597468E-25 | 6.53242923E-11 | 0.0719399729 | 0.175784861 |
| 40 | 6.86835658E-26 | 3.88795202E-11 | 0.0683437205 | 0.180087128 |
| 41 | 2.7969131E-26 | 2.28810828E-11 | 0.0638136759 | 0.185469205 |
| 42 | 1.13006302E-26 | 1.3278754E-11 | 0.0583061563 | 0.191887485 |
| 43 | 4.52340475E-27 | 7.57707222E-12 | 0.0518828874 | 0.199038439 |
| 44 | 1.79110543E-27 | 4.23821587E-12 | 0.0447316947 | 0.206208487 |

| | | | | |
|---|---|---|---|---|
| 45 | 7.00482415E-28 | 2.31582436E-12 | 0.0371531681 | 0.212088315 |
| 46 | 2.70009235E-28 | 1.23034737E-12 | 0.0295115793 | 0.214535342 |
| 47 | 1.02160789E-28 | 6.30492916E-13 | 0.0221710099 | 0.210292805 |
| 48 | 3.75742702E-29 | 3.06829774E-13 | 0.0154515758 | 0.194893495 |
| 49 | 1.31014317E-29 | 1.37222701E-13 | 0.00963068262 | 0.163652137 |
| 50 | 4.01595925E-30 | 5.20268643E-14 | 0.00496557846 | 0.11535247 |

Solvent Recovery Column composition (contd)

| Stage | N-BUT-01 | ISOBU-01 | N-PEN-01 | 2-MET-01 |
|---|---|---|---|---|
| 1 | 5.62026001E-10 | 2.23155183E-09 | 5.3892494E-15 | 3.522305E-14 |
| 2 | 3.99043101E-09 | 1.3800157E-08 | 1.0303633E-13 | 5.610945E-13 |
| 3 | 2.48405783E-08 | 7.50763684E-08 | 1.701851E-12 | 7.73565618E-12 |
| 4 | 1.51480855E-07 | 3.99200345E-07 | 2.783519E-11 | 1.05467759E-10 |
| 5 | 9.18418117E-07 | 2.10829022E-06 | 4.53325393E-10 | 1.432041E-09 |
| 6 | 5.53127124E-06 | 1.10542816E-05 | 7.31790453E-09 | 1.928979E-08 |
| 7 | 3.28370344E-05 | 5.70886524E-05 | 1.15743967E-07 | 2.550924E-07 |

| | | | | |
|---|---|---|---|---|
| 8 | 0.000188697903 | 0.000284949575 | 1.74798789E-06 | 3.235340E-06 |
| 9 | 0.00101057955 | 0.00132176174 | 2.39097058E-05 | 3.750232E-05 |
| 10 | 0.00472110956 | 0.00532632667 | 0.0002709479 | 0.000365786852 |
| 11 | 0.0177460734 | 0.0172026525 | 0.00229844947 | 0.00272449448 |
| 12 | 0.0506705487 | 0.0421055789 | 0.0137919772 | 0.0145879745 |
| 13 | 0.105552143 | 0.0751706587 | 0.057649023 | 0.0546435209 |
| 14 | 0.150837677 | 0.0927177125 | 0.161534265 | 0.13633729 |
| 15 | 0.1479362 | 0.0799268836 | 0.300986351 | 0.225433559 |
| 16 | 0.147936426 | 0.0799271112 | 0.300985591 | 0.225433104 |
| 17 | 0.147936632 | 0.0799273209 | 0.300984918 | 0.225432699 |
| 18 | 0.147936856 | 0.0799275511 | 0.300984197 | 0.225432261 |
| 19 | 0.147937134 | 0.079927841 | 0.300983298 | 0.225431712 |
| 20 | 0.147937514 | 0.0799282339 | 0.300982124 | 0.225430996 |
| 21 | 0.147938049 | 0.0799287886 | 0.300980459 | 0.22542998 |
| 22 | 0.147938827 | 0.0799295827 | 0.300978169 | 0.22542859 |
| 23 | 0.147939953 | 0.0799307225 | 0.300974967 | 0.225426653 |
| 24 | 0.147941581 | 0.0799323564 | 0.300970492 | 0.225423957 |

| | | | | |
|---|---|---|---|---|
| 25 | 0.147943925 | 0.0799346923 | 0.300964232 | 0.225420197 |
| 26 | 0.147947284 | 0.0799380218 | 0.30095547 | 0.22541495 |
| 27 | 0.147952077 | 0.0799427544 | 0.300943177 | 0.225407603 |
| 28 | 0.147958889 | 0.0799494656 | 0.300925905 | 0.225397293 |
| 29 | 0.147968542 | 0.0799589632 | 0.300901592 | 0.225382793 |
| 30 | 0.147982182 | 0.0799723781 | 0.300867335 | 0.225362367 |
| 31 | 0.148001404 | 0.079991288 | 0.300819054 | 0.225333578 |
| 32 | 0.148028411 | 0.0800178799 | 0.300751041 | 0.225293006 |
| 33 | 0.148066222 | 0.0800551603 | 0.300655385 | 0.225235906 |
| 34 | 0.148118917 | 0.0801072155 | 0.300521221 | 0.225155743 |
| 35 | 0.14819192 | 0.0801795152 | 0.300333838 | 0.225043647 |
| 36 | 0.148292293 | 0.0802792434 | 0.300073732 | 0.224887814 |
| 37 | 0.148429016 | 0.0804156243 | 0.299715841 | 0.224673027 |
| 38 | 0.148613269 | 0.0806002322 | 0.299229436 | 0.224380587 |
| 39 | 0.148858933 | 0.0808473882 | 0.298579565 | 0.223989279 |
| 40 | 0.149184052 | 0.0811750522 | 0.297731562 | 0.223478485 |
| 41 | 0.149615084 | 0.0816072899 | 0.296660055 | 0.22283469 |

| | | | | |
|---|---|---|---|---|
| 42 | 0.150197678 | 0.0821802227 | 0.295364793 | 0.222063665 |
| 43 | 0.151019481 | 0.0829535085 | 0.293894819 | 0.221210865 |
| 44 | 0.152249296 | 0.0840258749 | 0.292387327 | 0.220397321 |
| 45 | 0.15418294 | 0.0855397093 | 0.291144525 | 0.219891343 |
| 46 | 0.157235047 | 0.0876243772 | 0.290825383 | 0.220268271 |
| 47 | 0.161676939 | 0.0901565961 | 0.292950815 | 0.222751834 |
| 48 | 0.166663172 | 0.0921373572 | 0.301086916 | 0.229767484 |
| 49 | 0.168086624 | 0.0906710811 | 0.322814389 | 0.245145086 |
| 50 | 0.156772585 | 0.0807399565 | 0.370265085 | 0.271904325 |

# REFERENCESREFERENCES


1. Bullin, K. and P. Krouskop, *Composition Variety Complicates Processing Plans for US Shale Gas.* Oil and Gas Journal, 2009. **107**(10): p. 50-55.

2. Shimekit, B. and H. Mukhtar, *Natural gas purification technologies-major advances for CO2 separation and future directions.* Advances in natural gas technology, 2012.

3. Rufford, T.E., et al., *The removal of CO2 and N2 from natural gas: A review of conventional and emerging process technologies.* Journal of Petroleum Science and Engineering, 2012. **94-95**: p. 123-154.

4. Bindwal, A.B., P.D. Vaidya, and E.Y. Kenig, *Kinetics of carbon dioxide removal by aqueous diamines.* Chemical Engineering Journal, 2011. **169**(1-3): p. 144-150.

5. Kohl, A.L. and R. Nielsen, *Gas Purification* Gulf Publishing Company 1997. **25**: p. 121-129.

6. Penny, D.E. and T.J. Ritter, *Kinetic-Study of the Reaction between Carbon-Dioxide and Primary Amines.* Journal of the Chemical Society-Faraday Transactions I, 1983. **79**: p. 2103-2109.

7. Vaidya, P.D. and E.Y. Kenig, *CO2-alkanolamine reaction kinetics: A review of recent studies.* Chemical Engineering & Technology, 2007. **30**(11): p. 1467-1474.

8. Versteeg, G.F., L.A.J. Van Dijck, and W.P.M. Van Swaaij, *On the kinetics between CO2 and alkanolamines both in aqueous and non-aqueous solutions. An overview.* Chemical Engineering Communications, 1996. **144**: p. 113-158.

9. Energy, E.E.R., *Clean Cities: Alternate Fuel Report*, U.S.D.o. Energy, Editor. 2018. p. 27.

10. Energy, E.E.R., *Alternate Fuel and Advanced Technology Vehicles*, U.S.D.o. Energy, Editor. 2018. p. 18.

11. Ferdinand, H.J.C., *Histoire de la chimie. Vol. 1.* . 1842, Hachette.

12. Kopp, H., *Geschichte der Chemie, 4 vols.* (1843): 1847, Braunschweig.

13. Berthelot, M., *Histoire des sciences: la chimie au moyen âge (Vol. 2).* 1893.

14. Brunschwig, H., *Liber de arte distillandi de simplicibus*. 1500, Strasburg.

15. Brunschwig, H. and J. Grüninger, *Liber de arte distillandi de composition*. 1507, Strasburg.

16. Brunschwig, H. and L. Andrew, *The Vertuose Boke of Distyllacyon of the Waters of All Maner of Herbes: With the Fygures of the Styllatoryes, Fyrst Made and Compyled by the Thyrte Yeres Study and Labour of the Moste Co [n] nynge and Famous Master of Phisyke, Maister Iherom Bruynswyke. And Now Newly Translate Out of Duyche Into Englysshe, Nat Only to the Synguler Helpe and Profyte of the Surgyens, Phisycyens, and Pothecaryes, But Also of All Maner of People, Parfytely and in Dewe Tyme and Ordre to Lerne to Dystyll All Maner of Herbes, to the Profyte, Cure,[and] Remedy of All Maner Dysseases and Infirmytees Apparant and Nat Apparant. And Ye Shall Vndersta [n] de that the Waters be Better Than the Herbes, as Auicenna Testefyeth in His Fourth Canon Saynge that All Maner Medicynes Vsed with Theyr Substance, Febleth and Maketh Aged, and Weke. Cum Gratia Et Priuilegio Regali*. 1973: In the flete strete by me Laurens Andrewe, in the sygne of the golden Crosse.

17. Lonicer, A., *Kunstliche Conterfeytunge*. 1573, Frankfurt.

18. D'Eremita, D., *Dell'Elixir Vitae Di Frà Donato D'Eremita Di Rocca D'Evaandro dell'ord. De Pred*. Libri Quattro. Naples: Secondino Roncagliolo.

19. Hausbrand, E., *Die Wirkungsweise der Rectifier und Distillin Apparate*. 1893, Berlin.

20. Sorel, E., *La rectification de l'alcool*. 1894: Gauthier-Villars et fils.

21. Colburn, A.P., *Simplified calculation of diffusional processes.* Industrial & Engineering Chemistry, 1941. **33**(4): p. 459-467.

22. Underwood, A., *Fractional distillation of multi-component mixtures.* Chem. Eng. Prog., 1948. **44**: p. 603-614.

23. Brown, G.G. and H.Z. Martin, *An empirical relationship between reflux ratio and the number of equilibrium plates in fractionating columns*. 1939: American Institute of chemical engineers.

24. Gilliland, E., *Multicomponent rectification.* Industrial & Engineering Chemistry, 1940. **32**(8): p. 1101-1106.

25. Mayfield, F.D. and J.A. May, Petroleum Refine, 1946. **25**: p. 141.

26. Shiras, R., D. Hanson, and C. Gibson, *Calculation of minimum reflux in distillation columns.* Industrial & Engineering Chemistry, 1950. **42**(5): p. 871-876.

27. Bachelor, J.B., Petrol. Refiner

1957. **36**(6): p. 161.

28. May, J., *Minimum Reflux Ratio for Multicomponent Distillation.* Industrial & Engineering Chemistry, 1949. **41**(12): p. 2775-2782.

29. Holland, C.D., *Multicomponent distillation*. 1963: Prentice-Hall.

30. Lewis, W., *The efficiency and design of rectifying columns for binary mixtures.* Industrial & Engineering Chemistry, 1922. **14**(6): p. 492-496.

31. McCabe, W.L. and E. Thiele, *Graphical design of fractionating columns.* Industrial & Engineering Chemistry, 1925. **17**(6): p. 605-611.

32. Ponchon, M., *Graphical study of distillation.* Tech. Modern, 1921. **13**: p. 20.

33. Savarit, R., *Eléments de distillation.* Arts et métiers, 1922. **75**(65): p. 142.

34. Kirkbride, C.G., *Process design procedure for multicomponent fractionators.* Petroleum Refiner, 1944. **23**(9): p. 321-336.

35. Lewis, W. and G. Matheson, *Studies in distillation.* Industrial & Engineering Chemistry, 1932. **24**(5): p. 494-498.

36. Thiele, E. and R. Geddes, *Computation of distillation apparatus for hydrocarbon mixtures.* Industrial & Engineering Chemistry, 1933. **25**(3): p. 289-295.

37. Hummel, H., Trans. Am. Inst. Chem. Engrs., 1944. **40**: p. 445.

38. Bonner, J.S., Chem. Eng. Progr. Symposium, 1959. **21**(55): p. 87.

39. Bonner, J.S., Petrol. Processing, 1956. **11**(6): p. 64.

40. Newman, J.S., Hydrocarbon Process., 1963. **42**(4): p. 141.

41. Mills, A.K., Chem. Eng. Progr., 1959. **55**(7): p. 93.

42. Greenstadt, J., Y. Bard, and B. Morse, *Multicomponent Distillation Calculation on IBM 704.* Industrial & Engineering Chemistry, 1958. **50**(11): p. 1644-1647.

43. Rose, A., et al., Chem. Eng. Progr. Symposium, 1959. **21**(55): p. 79.

44. Rose, A., R.F. Sweeny, and V.N. Schrodt, *Continuous distillation calculations by relaxation method.* Industrial & Engineering Chemistry, 1958. **50**(5): p. 737-740.

45. Acrivos, A. and N.R. Amundson, *On the steady state fractionation of multicomponent and complex mixtures in an ideal cascade: Part 1—Analytic solution of the equations for general mixtures.* Chemical Engineering Science, 1955. **4**(1): p. 29-38.

46. Amundson, N., A. Pontinen, and J. Tierney, *Multicomponent distillation on a large digital computer: II. Generalization with side-stream stripping.* AIChE Journal, 1959. **5**(3): p. 295-300.

47. Amundson, N.R. and A.J. Pontinen, *Multicomponent distillation calculations on a large digital computer.* Industrial & Engineering Chemistry, 1958. **50**(5): p. 730-736.

48. Baer, R.M., J.D. Seader, and R.D. Crozier, Chem. Eng. Progr. 55, No. 12, 88

1959. **55**(12): p. 88.

49. O'Brien, N.G. and R.G.E. Franks, Chem. Eng. Progr. Symposium 1959. **27**(55): p. 25.

50. Waterman, W.W. and J.P. Frazier, *This Distillation Program Generates Its Own Data*. 1965.

51. Gerster, J., *Distillation—Theory and Fundamentals.* Industrial & Engineering Chemistry, 1960. **52**(8): p. 645-653.

52. Hanson, D.N., J.H. Duffin, and G.F. Somerville, *Computation of multistage separation processes*. 1962: Reinhold New York.

53. Davis, J.A., N. Rodewald, and F. Kurata, *Solid-Liquid-Vapor Phase Behavior of the Methane-Carbon Dioxide System.* Aiche Journal, 1962. **8**(4): p. 537-539.

54. Donnelly, H.G. and D.L. Katz, *Phase Equilibria in the Carbon Dioxide Methane System.* Industrial and Engineering Chemistry, 1954. **46**(3): p. 511-517.

55. Mraw, S.C., S.C. Hwang, and R. Kobayashi, *Vapor-Liquid-Equilibrium of Ch4-Co2 System at Low-Temperatures.* Journal of Chemical and Engineering Data, 1978. **23**(2): p. 135-139.

56. Sterner, C.J., *Phase Equilibria in the CO2 - Methane Systems*, in *Advances in Cryogenic Engineering*. 1961, Springer: Boston, MA.

57. Holmes, A.S., et al. *Pilot tests prove Ryan/Holmes Cryogenic Acid Gas/ Hydrocarbon Seperations*. in *61st Annual GPA Convention*. 1982. Dallas, Texas.

58. Winkle, M.V., *Distillation*. Chemical Engineering Series. 1967: McGraw-Hill.

59. Lastari, F., et al., *Extractive distillation for CO2–ethane azeotrope separation.* Chemical Engineering and Processing: Process Intensification, 2012. **52**: p. 155-161.

60. Colburn, A.P. and E.M. Schoenborn, *The Selection of Separating Agents for Azeotropic and Extractive Distillation and for Liquid-Liquid Extraction.* Transactions of the American Institute of Chemical Engineers, 1945. **41**(4): p. 421-443.

61. Pellegrini, L.A., *Process for the Removal of CO2 from Acid Gas.*, in *WO Patent*. 2014.

62. Lange, S. and L.A. Pellegrini, *Energy Analysis of the New Dual-Pressure Low-Temperature Distillation Process for Natural Gas Purification Integrated with Natural Gas Liquids Recovery.* Industrial & Engineering Chemistry Research, 2016. **55**(28): p. 7742-7767.

63. De Guido, G., M.R. Fogli, and L.A. Pellegrini, *Effect of Heavy Hydrocarbons on CO2 Removal from Natural Gas by Low-Temperature Distillation.* Industrial & Engineering Chemistry Research, 2018. **57**(21): p. 7245-7256.

64. Baccanelli, M., et al., *Low temperature techniques for natural gas purification and LNG production: An energy and exergy analysis.* Applied Energy, 2016. **180**: p. 546-559.

65. Thomson, J., *On the origin of windings of rivers in alluvial plains, with remarks on the flow of water round bends in pipes.* Proceedings of the Royal Society of London, 1876. **25**: p. 171-178.

66. Thomson, J., *Experimental demonstration in respect to the origin of windings of rivers in alluvial plains, and to the mode of flow of water round bends of pipes.* Proceedings of the Royal Society of London, 1877. **26**: p. 356-357.

67. Williams, G.S., *Experiments at Detroit, Mich., on the effect of curvature upon the flow of water in pipes.* Proceedings of the American Society of Civil Engineers, 1902. **27**(5): p. 314-505.

68. Grindley, J.H. and A.H. Gibson, *On the frictional resistances to the flow of air through a pipe.* Proceedings of the Royal Society of London Series a-Containing Papers of a Mathematical and Physical Character, 1908. **80**(536): p. 114-139.

69. Eustice, J., *Flow of water in curved pipes.* Proceedings of the Royal Society of London Series a-Containing Papers of a Mathematical and Physical Character, 1910. **84**(568): p. 107-118.

70. Eustice, J., *Experiments on stream-line motion in curved pipes.* Proceedings of the Royal Society of London Series a-Containing Papers of a Mathematical and Physical Character, 1911. **85**(576): p. 119-131.

71. Grindley, J.H. and A. Gibson, *On the frictional resistances to the flow of air through a pipe.* Proceedings of the Royal Society of London. Series A, Containing Papers of a Mathematical and Physical Character, 1908. **80**(536): p. 114-139.

72. Dean, W.R., *Note on the notion of fluid in a curved pipe.* Philosophical Magazine, 1927. **4**(20): p. 208-223.

73. Dean, W.R., *The stream-line motion of fluid in a curved pipe. (Second paper.).* Philosophical Magazine, 1928. **5**(30): p. 673-695.

74. Ito, H., *Friction factors for turbulent flow in curved pipes.* Trans. ASME, J. Basic Engng, D, 1959. **81**: p. 123-124.

75. Schmidt, E.F., *Heat Transfer and Pressure Loss in Spiral Tubes.* Chemie Ingenieur Technik, 1967. **39**(13): p. 781-789.

76. Srinivasan, P.S., N.S. S., and F.A. Holland, *Pressure Drop and Heat Transfer in Coils.* Transactions of the Institution of Chemical Engineers and the Chemical Engineer, 1968. **46**(4): p. C113-+.

77. Mori, Y. and W. Nakayama, *Study on forced convective heat transfer in curved pipes:(3rd report, theoretical analysis under the condition of uniform wall temperature and practical formulae).* International journal of heat and mass transfer, 1967. **10**(5): p. 681-695.

78. White, C.M., *Streamline flow through curved pipes.* Proceedings of the Royal Society of London Series a-Containing Papers of a Mathematical and Physical Character, 1929. **123**(792): p. 645-663.

79. Srinivasan, P.S., S.S. Nandapurkar, and F.A. Holland, *Friction Factors for Coils.* Transactions of the Institution of Chemical Engineers and the Chemical Engineer, 1970. **48**(4-6): p. T156-+.

80. Mishra, P. and S.N. Gupta, *Momentum-Transfer in Curved Pipes .1. Newtonian Fluids.* Industrial & Engineering Chemistry Process Design and Development, 1979. **18**(1): p. 130-137.

81. Manlapaz, R.L. and S.W. Churchill, *Fully-Developed Laminar-Flow in a Helically Coiled Tube of Finite Pitch.* Chemical Engineering Communications, 1980. **7**(1-3): p. 57-78.

82. Gnielinski, V. *Heat transfer and pressure drop in helically coiled tubes*. in *Proceedings 8th International Heat Transfer Conference*. 1986. San Francisco, Hemisphere, Washington DC.

83. Hart, J., J. Ellenberger, and P.J. Hamersma, *Single-Phase and 2-Phase Flow through Helically Coiled Tubes.* Chemical Engineering Science, 1988. **43**(4): p. 775-783.

84. Ali, S., *Pressure drop correlations for flow through regular helical coil tubes.* Fluid Dynamics Research, 2001. **28**(4): p. 295-310.

85. Downing, R.S. and G. Kojasoy, *Single and two-phase pressure drop characteristics in miniature helical channels.* Experimental Thermal and Fluid Science, 2002. **26**(5): p. 535-546.

86. Coronel, P. and K.P. Sandeep, *Pressure drop and friction factor in helical heat exchangers under nonisothermal and turbulent flow conditions.* Journal of Food Process Engineering, 2003. **26**(3): p. 285-302.

87. Tarbell, J.M. and M.R. Samuels, *Momentum and heat transfer in helical coils.* The Chemical Engineering Journal, 1973. **5**(2): p. 117-127.

88. Wang, C., *On the low-Reynolds-number flow in a helical pipe.* Journal of Fluid Mechanics, 1981. **108**: p. 185-194.

89. Hüttl, T. and R. Friedrich, *Influence of curvature and torsion on turbulent flow in helically coiled pipes.* International Journal of Heat and Fluid Flow, 2000. **21**(3): p. 345-353.

90. Hüttl, T. and R. Friedrich, *Direct numerical simulation of turbulent flows in curved and helically coiled pipes.* Computers & fluids, 2001. **30**(5): p. 591-605.

91. Yamamoto, K., et al., *Experimental study of the flow in a helical circular tube.* Fluid Dynamics Research, 1995. **16**(4): p. 237-249.

92. Yamamoto, K., S. Yanase, and R. Jiang, *Stability of the flow in a helical tube.* Fluid Dynamics Research, 1998. **22**(3): p. 153-170.

93. Yamamoto, K., et al., *Flow through a rotating helical pipe with circular cross-section.* International Journal of Heat and Fluid Flow, 2000. **21**(2): p. 213-220.

94. Grundmann, R., *Friction diagram of the helically coiled tube.* Chemical Engineering and Processing: Process Intensification, 1985. **19**(2): p. 113-115.

95. Mishra, P. and S. Gupta, *Momentum transfer in curved pipes. 1. Newtonian fluids.* Industrial & Engineering Chemistry Process Design and Development, 1979. **18**(1): p. 130-137.

96. Mishra, P. and S. Gupta, *Momentum transfer in curved pipes. 2. Non-Newtonian fluids.* Industrial & Engineering Chemistry Process Design and Development, 1979. **18**(1): p. 137-142.

97. Bolinder, C.J. and B. Sunden, *Flow visualization and LDV measurements of laminar flow in a helical square duct with finite pitch.* Experimental thermal and fluid science, 1995. **11**(4): p. 348-363.

98. Ujhidy, A., J. Nemeth, and J. Szépvölgyi, *Fluid flow in tubes with helical elements.* Chemical Engineering and Processing: Process Intensification, 2003. **42**(1): p. 1-7.

99. Xin, R., et al., *An experimental study of single-phase and two-phase flow pressure drop in annular helicoidal pipes.* International Journal of Heat and Fluid Flow, 1997. **18**(5): p. 482-488.

100. Ju, H., et al., *Hydraulic performance of small bending radius helical coil-pipe.* Journal of Nuclear Science and Technology, 2001. **38**(10): p. 826-831.

101. Guo, L., Z. Feng, and X. Chen, *An experimental investigation of the frictional pressure drop of steam–water two-phase flow in helical coils.* International journal of heat and mass transfer, 2001. **44**(14): p. 2601-2610.

102. Ali, S., *Pressure drop correlations for flow through regular helical coil tubes.* Fluid dynamics research, 2001. **28**(4): p. 295.

103. Kirpikov, A.V., *Heat transfer in helically coiled pipes.* Trudi. Moscov. Inst. Khim. Mashinojtrojenija, 1957. **12**: p. 43-56.

104. Seban, R.A. and E.F. McLaughlin, *Heat transfer in tube coils with laminar and turbulent flow.* International journal of heat and mass transfer, 1963. **6**(5): p. 387-395.

105. Rogers, G.F.C. and Y.R. Mayhew, *Heat transfer and pressure loss in helically coiled tubes with turbulent flow*. International Journal of Heat and Mass Transfer, 1964. **7**(11): p. 1207-1216.

106. Pratt, N.H., *The heat transfer in a reaction tank cooled by means of a coil.* Trans. Inst. Chem. Eng, 1947. **25**: p. 163-180.

107. Orlov, V.K. and P.A. Tselishchev, *Heat exchange in spiral coils with turbulent flow of water*. Thermal Eng, 1964. **11**: p. 97.

108. Yang, G. and M.A. Ebadian, *Turbulent forced convection in a helicoidal pipe with substantial pitch.* International Journal of Heat and Mass Transfer, 1996. **39**(10): p. 2015-2022.

109. Lin, C.X. and M.A. Ebadian, *Developing turbulent convective heat transfer in helical pipes.* International Journal of Heat and Mass Transfer, 1997. **40**(16): p. 3861-3873.

110. Prabhanjan, D.G., G.S.V. Raghavan, and T.J. Rennie, *Comparison of heat transfer rates between a straight tube heat exchanger and a helically coiled heat exchanger.* International Communications in Heat and Mass Transfer, 2002. **29**(2): p. 185-191.

111. Jayakumar, J.S., et al., *Experimental and CFD estimation of heat transfer in helically coiled heat exchangers.* Chemical Engineering Research and Design, 2008. **86**(3): p. 221-232.

112. Di Piazza, I. and M. Ciofalo, *Numerical prediction of turbulent flow and heat transfer in helically coiled pipes.* International Journal of Thermal Sciences, 2010. **49**(4): p. 653-663.

113. Lockhart, R. and R. Martinelli, *Proposed correlation of data for isothermal two-phase, two-component flow in pipes.* Chem. Eng. Prog, 1949. **45**(1): p. 39-48.

114. Ghiaasiaan, S.M., *Two-Phase Flow, Boiling, and Condensation: In Conventional and Miniature Systems*. 2nd ed. 2017: Cambridge University Press.

115. Chisholm, D. and A.D.K. Laird, *Two-phase flow in rough tubes.* Trans. ASME, 1958. **80**(2): p. 276-286.

116. Rippel, G., C. Eidt Jr, and H. Jordan Jr, *Two-Phase Flow in a Coiled Tube. Pressure Drop, Holdup, and Liquid Phase Axial Mixing.* Industrial & Engineering Chemistry Process Design and Development, 1966. **5**(1): p. 32-39.

117. Boyce, B., J. Collier, and J. Levy, *Hold-up and pressure drop measurement in the two-phase flow of air-water mixing tubes in helical coils.* Proc. of Int. Syrup. on Research in Concurrent Gas and Liquid Flow, 1969: p. 203-231.

118. Banerjee, S., E. Rhodes, and D.S. Scott, *Studies on cocurrent gas-liquid flow in helically coiled tubes. I. Flow patterns, pressure drop and holdup.* The Canadian Journal of Chemical Engineering, 1969. **47**(5): p. 445-453.

119. Kasturi, G. and J. Stepanek, *Two phase flow—I. Pressure drop and void fraction measurements in concurrent gas-liquid flow in a coil.* Chemical Engineering Science, 1972. **27**(10): p. 1871-1880.

120. Stepanek, J. and G. Kasturi, *Two phase flow—II. Parameters for void fraction and pressure drop correlations.* Chemical Engineering Science, 1972. **27**(10): p. 1881-1891.

121. Duckler, A., M. Wicks III, and R. Cleveland, *Frictional pressure drop in two-phase flow: A. A comparison of existing correlations for pressure loss and holdup.* AIChE J, 1964. **10**: p. 38-43.

122. Hughmark, G., *Holdup in gas-liquid flow.* Chemical Engineering Progress, 1962. **58**(4): p. 62-65.

123. Rangacharyulu, K. and G. Davies, *Pressure drop and holdup studies of air—liquid flow in helical coils.* The Chemical Engineering Journal, 1984. **29**(1): p. 41-46.

124. Xin, R., et al., *An investigation and comparative study of the pressure drop in air-water two-phase flow in vertical helicoidal pipes.* International journal of heat and mass transfer, 1996. **39**(4): p. 735-743.

125. Awwad, A., et al., *Flow patterns and pressure drop in air/water two-phase flow in horizontal helicoidal pipes.* Journal of fluids engineering, 1995. **117**(4): p. 720-726.

126. Awwad, A., et al., *Measurement and correlation of the pressure drop in air-water two-phase flow in horizontal helicoidal pipes.* International journal of multiphase flow, 1995. **21**(4): p. 607-619.

127. Ruffell, A., *The application of heat transfer and pressure drop data to the design of helical coil once-through boilers.* Multiphase Flow Systems Meet., Glasgow, 1974.

128. Ünal, H., M. Van Gasselt, and P. Van't Verlaat, *Dryout and two-phase flow pressure drop in sodium heated helically coiled steam generator tubes at elevated pressures.* International journal of heat and mass transfer, 1981. **24**(2): p. 285-298.

129. Zhao, L., et al., *Convective boiling heat transfer and two-phase flow characteristics inside a small horizontal helically coiled tubing once-through steam generator.* International Journal of Heat and Mass Transfer, 2003. **46**(25): p. 4779-4788.

130. Colorado, D., et al., *Development and experimental validation of a computational model for a helically coiled steam generator.* International Journal of Thermal Sciences, 2011. **50**(4): p. 569-580.

131. Santini, L., et al., *Two-phase pressure drops in a helically coiled steam generator.* International Journal of Heat and Mass Transfer, 2008. **51**(19-20): p. 4926-4939.

132. Chen, X. and L. Guo, *Flow patterns and pressure drop in oil–air–water three-phase flow through helically coiled tubes.* International Journal of Multiphase Flow, 1999. **25**(6-7): p. 1053-1072.

133. Weinberger, C. and M.-T. Shu, *Helical gas—solids flow I. Pressure drop measurement and prediction.* Powder technology, 1986. **48**(1): p. 13-18.

134. Weinberger, C. and M.-T. Shu, *Helical gas—solids flow II. Effect of bend radius and solids flow rate on transition velocity.* Powder technology, 1986. **48**(1): p. 19-22.

135. Aspen Tech, I., *Aspen Plus Version 9*. 2016: Bedford, Massachesetts

136. Berstad, D., P. Nekså, and R. Anantharaman, *Low-temperature CO2 Removal from Natural Gas.* Energy Procedia, 2012. **26**: p. 41-48.

137. Luyben, W.L., *Control of an Extractive Distillation System for the Separation of CO2 and Ethane in Enhanced Oil Recovery Processes.* Industrial & Engineering Chemistry Research, 2013. **52**(31): p. 10780-10787.

138. Tavan, Y., S. Shahhosseini, and S.H. Hosseini, *Feed-splitting technique in the extractive distillation of CO2–ethane azeotropic process.* Separation and Purification Technology, 2014. **122**: p. 47-53.

139. Robinson, D., *The Characterization of the Heaptanes and Heavier Fraction for the GPA Programs. Gas Processors Association. Report RR-28 1978.(b) Robinson, DB; Peng, D.-Y. and Chung, SY-K. The development of the Peng-Robinson Equation and its Application to Phase Equilibrium in a System Containing Methanol.* Fluid Phase Equilibria, 1985. **24**: p. 25-41.

140. Soave, G., *Equilibrium constants from a modified Redlich-Kwong equation of state.* Chemical engineering science, 1972. **27**(6): p. 1197-1203.

141. Smith, R., H. Inomata, and C. Peters, *Equations of State and Formulations for Mixtures*, in *Supercritical Fluid Science and Technology*. 2013, Elsevier. p. 333-480.

142. Peng, D.-Y. and D.B. Robinson, *A new two-constant equation of state.* Industrial & Engineering Chemistry Fundamentals, 1976. **15**(1): p. 59-64.

143. Eggeman, T. and S. Chafin, *Beware the pitfalls of CO2 freezing prediction.* Chemical Engineering Progress, 2005. **101**(3): p. 39-44.

144. Hong, J.H. and R. Kobayashi, *To Break an Azeotrope - the Use of Normal-Pentane to Break the Co2-Ethane Azeotrope, for Co2 Eor Gas Processing.* Industrial & Engineering Chemistry Process Design and Development, 1986. **25**(3): p. 736-741.

145. Flynn, T.M., *Cryogenic Engineering*. 2nd ed. 2005: Marcel Dekker, New York.

146. Laroche, L., et al., *The curious behavior of homogeneous azeotropic distillation—implications for entrainer selection.* AIChE journal, 1992. **38**(9): p. 1309-1328.

147. Ghiaasiaan, S.M., *Convective heat and mass transfer*. 2018: CRC Press.

148. Mills, A. and B. Chang, *Error analysis of experiments: a manual for engineering students.* University of California, 2004: p. 1-49.

149. Pratt, N., *The heat transfer in a reaction tank cooled by means of a coil.* Trans. Inst. Chem. Eng, 1947. **25**: p. 163-180.

150. Orlov, V. and P. Tselishchev, *Heat exchange in spiral coils with turbulent flow of water.* Thermal Eng, 1964. **11**: p. 97.

151. *Sinda: Advanced Thermal Simulation Solution*. 2017, MSC Software Corporation: New Port Beach, California.

152. *Thermal Desktop*. 2017, Cullimore and Ring Technologies Inc.